AFRL-RV-PS-
TR-2016-0130
Vol. II

AFRL-RV-PS-
TR-2016-0130
Vol. II

A DESIGNER FLUID FOR ALUMINUM PHASE CHANGE DEVICES

Volume II of III
Aluminum Inorganic Aqueous Solutions (IAS) Chemistry and Experiments

Qi Yao and Ivan Catton

University of California, Los Angeles
420 Westwood Plaza, Room 43-132
Los Angeles, CA 90095-1597

17 Nov 2016

Final Report

AIR FORCE RESEARCH LABORATORY
Space Vehicles Directorate
3550 Aberdeen Ave SE
AIR FORCE MATERIEL COMMAND
KIRTLAND AIR FORCE BASE, NM 87117-5776

DTIC COPY
NOTICE AND SIGNATURE PAGE

This report is the result of contracted fundamental research deemed exempt from public affairs security and policy review in accordance with SAF/AQR memorandum dated 10 Dec 08 and AFRL/CA policy clarification memorandum dated 16 Jan 09. This report is available to the general public, including foreign nationals. Copies may be obtained from the Defense Technical Information Center (DTIC) (http://www.dtic.mil).

AFRL-RV-PS-TR-2016-0130, Vol. II HAS BEEN REVIEWED AND IS APPROVED FOR PUBLICATION IN ACCORDANCE WITH ASSIGNED DISTRIBUTION STATEMENT.

//SIGNED//   //SIGNED//
ANDREW WILLIAMS   PAUL HAUSGEN, Ph.D.
Program Manager   Technical Advisor, Spacecraft Component Technology

//SIGNED//
JOHN BEAUCHEMIN
Chief Engineer, Spacecraft Technology Division
Space Vehicles Directorate

Approved for public release; distribution is unlimited.

REPORT DOCUMENTATION PAGE

Form Approved
OMB No. 0704-0188

Public reporting burden for this collection of information is estimated to average 1 hour per response, including the time for reviewing instructions, searching existing data sources, gathering and maintaining the data needed, and completing and reviewing this collection of information. Send comments regarding this burden estimate or any other aspect of this collection of information, including suggestions for reducing this burden to Department of Defense, Washington Headquarters Services, Directorate for Information Operations and Reports (0704-0188), 1215 Jefferson Davis Highway, Suite 1204, Arlington, VA 22202-4302. Respondents should be aware that notwithstanding any other provision of law, no person shall be subject to any penalty for failing to comply with a collection of information if it does not display a currently valid OMB control number. **PLEASE DO NOT RETURN YOUR FORM TO THE ABOVE ADDRESS.**

1. REPORT DATE	2. REPORT TYPE	3. DATES COVERED
17-11-16	Final Report	29 Jun 2015 - 26 Sep 2016

4. TITLE AND SUBTITLE

A DESIGNER FLUID FOR ALUMINUM PHASE CHANGE DEVICES,
Vol II of III
Aluminum Inorganic Aqueous Solutions (IAS) Chemistry
and Experiments

5a. CONTRACT NUMBER
FA9453-15-1-0318

5b. GRANT NUMBER

5c. PROGRAM ELEMENT NUMBER
62601F

6. AUTHOR(S)

Michael J. Subblebine and Ivan Catton

5d. PROJECT NUMBER
8809

5e. TASK NUMBER
PPM00020770

5f. WORK UNIT NUMBER
EF126504

7. PERFORMING ORGANIZATION NAME(S) AND ADDRESS(ES)

University of California, Los Angeles
420 Westwood Plaza, Room 43-132
Los Angeles, CA 90095-1597

8. PERFORMING ORGANIZATION REPORT NUMBER

9. SPONSORING / MONITORING AGENCY NAME(S) AND ADDRESS(ES)
Air Force Research Laboratory
Space Vehicles Directorate
3550 Aberdeen Ave SE Kirtland
AFB, NM 87117-5776

10. SPONSOR/MONITOR'S ACRONYM(S)
AFRL/RVSV

11. SPONSOR/MONITOR'S REPORT NUMBER(S)

AFRL-RV-PS-TR-2016-0130, Vol. II

12. DISTRIBUTION / AVAILABILITY STATEMENT
Approved for public release; distribution is unlimited.

13. SUPPLEMENTARY NOTES

14. ABSTRACT
Aluminum thermo-syphon and heat pipes were explored theoretically and tested experimentally to verify efficacy of various inhibitor solutions in different thermo-syphon geometries tested under different test conditions. Simple corrosion tests were also carried out within a vacuumed chamber to determine relative amounts of hydrogen generated when an aluminum sample is in direct, static contact with a test fluid. The results demonstrate that while there is good evidence that inorganic inhibitors can significantly reduce the production of NCG in an aluminum-water heat pipe, the complex nature of two phase fluid circulation in such devices still presents serious challenges to the reliability and adoption of inhibitor fluids for critical thermal management needs.

15. SUBJECT TERMS
inorganic aqueous solution <and> heat pipe, spacecraft, satellites, thermal control, two-phase, heat transfer

16. SECURITY CLASSIFICATION OF:			17. LIMITATION OF ABSTRACT	18. NUMBER OF PAGES	19a. NAME OF RESPONSIBLE PERSON
			Unlimited	190	Andrew Williams
a. REPORT Unclassified	**b. ABSTRACT** Unclassified	**c. THIS PAGE** Unclassified			**19b. TELEPHONE NUMBER** *(include area code)*

Standard Form 298 (Rev. 8-98)
Prescribed by ANSI Std. Z39.18

(This page intentionally left blank)

Table of Contents

Approved for public release: distribution is unlimited.

Approved for public release: distribution is unlimited.

List of Figures

Approved for public release: distribution is unlimited.

List of Tables

ACKNOWLEDGMENTS

DISCLAIMER

The views and conclusions contained herein are those of the authors and should not be interpreted as necessarily representing the official policies or endorsements, either expressed or implied, of Air Force Research Laboratory or the U.S. Government.

(This page intentionally left blank)

1 Summary

Water is one of the most capable and widely used working fluids in heat pipes and thermosyphons. Aluminum is a high conductivity, lightweight, and high strength choice for heat pipe casing material. However, aluminum and water are a heat pipe combination that is not considered viable due to the rapid generation of hydrogen, a noncondensable gas (NCG), resulting from chemical reactions between water and aluminum. A great deal of past research has been done evaluating the compatibility of many pure fluids with different metal heat pipe casings, yielding a large volume of lifetime tests demonstrating success or failure of various combinations. On the other hand, very little research was found analyzing what, if any, progress can be made to take low compatibility combinations and make them more compatible through the use of chemical inhibitors. This is particularly true for the combination of water and aluminum. Recently, inorganic chemicals in an aqueous solution, with the proper concentrations and pH range, have been shown to suppress the unwanted reactions and subsequent hydrogen formation rates in a manner that could prove useful enough to allow aluminum heat pipe casings to operate with aqueous based solutions as a working fluid.

The goal of this report is to produce, understand, and experimentally show the robustness of using inorganic inhibitors in aqueous heat pipe fluids for aluminum devices. Thermodynamic predictions were made to estimate conditions in which a stable oxide layer of the base metal, as well as the oxidizing inhibitors, will form within the pipe, thus giving a better chance at preventing NCG generation. $E - pH$, or Pourbaix, diagrams will be generated as a function of temperature to allow for prediction at any given heat pipe operating temperature range. Chemical reactions and processes responsible for NCG suppression will be explained. Inhibitor species' concentrations

will be investigated as an independent variable to determine recommended inhibitor amounts. Aluminum thermo-syphons and heat pipes will be experimentally tested to verify efficacy of various inhibitor solutions in different thermo-syphon geometries tested under different test conditions. Simple corrosion tests will also be carried out within a vacuumed chamber to determine relative amounts of hydrogen generated when an aluminum sample is in direct, static contact with a test fluid. The results of this report will show that while there is good evidence that inorganic inhibitors can significantly reduce the production of NCG in an aluminum-water heat pipe, the complex nature of two phase fluid circulation in such devices still presents serious challenges to the reliability and adoption of inhibitor fluids for critical thermal management needs. Reasons behind this phenomenon will be presented along with pathways for future research. These future work paths are believed to provide great opportunities for overcoming the challenges found in this work as well as potentially expanding the application of inhibiting heat pipe fluids to other active metals such as steel devices. The creation of a dilute aqueous solution which maintains the high latent heat of water but is also compatible with aluminum heat pipes would allow for significantly higher heat transport per device unit mass than currently used aluminum and ammonia heat pipes and provide another option for intermediate temperature heat pipes at low cost.

2 Introduction

Heat pipes and thermo-syphons are a highly effective means of managing heat generated by electronics and other sources because they are able to transfer heat under near isothermal conditions across the device. The use of two-phase heat transfer devices such as heat pipes is now a common means to passively transfer heat from a source, where the working fluid is evaporated, to a sink, where vapor is carried by buoyancy forces and heat is rejected as it recondenses. Broad

summaries of applications and implementations are covered extensively in texts such as Chi [1] or Reay and Kew [2]; while specific examples of heat pipe applications are also common in the literature. Examples include everything from early uses of heat pipes on the Trans-Alaska pipeline by Heuer [3] to high heat flux, biporous wick studies by Semenic and Catton [4]. A great review article has also been recently penned by Faghri [5]. One common use today is for electronics cooling or thermal control of electronics. These heat pipes are used in most laptops and are often of the sintered copper variety as shown below in Figure 1.
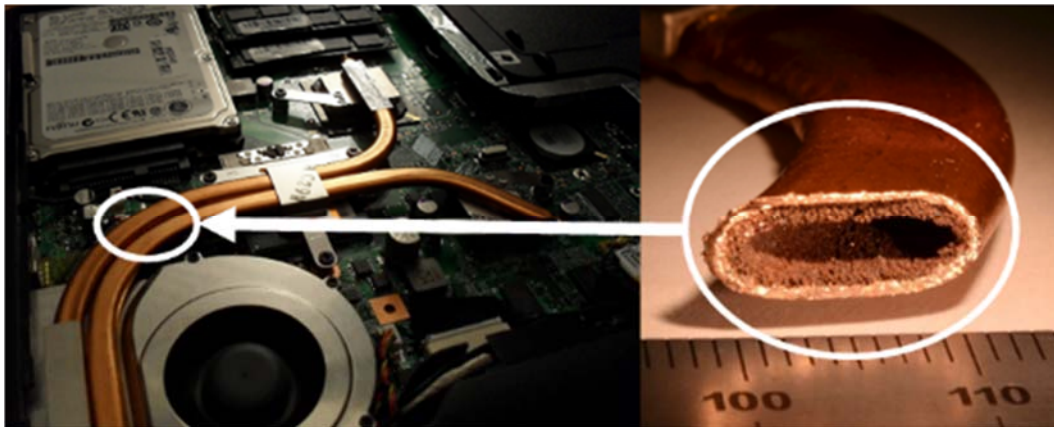
Figure 1: Sintered copper heat pipes used in a laptop [6]

Fluid is returned from the condenser to the evaporator by a variety of methods. In the simplest implementation of a heat pipe, a thermo-syphon, the walls of the tube are smooth and the condensed liquid is returned by gravity forces. Below in Figure 2 a basic schematic of a thermo-syphon is shown.

3
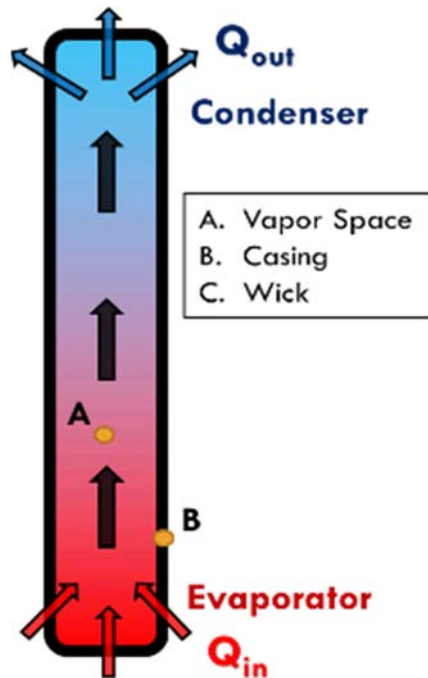
Figure 2: Schematic of a basic thermo-syphon

The first thermo-syphons were patented by Ludlow Perkins in 1936 and were referred to at that time as Perkins tubes [7]. However, the first uses of similar devices predate this patent by a large margin. Ludlow Perkins' father, A. M. Perkins began work on the Perkins tube in the early 1800s.

As compared to a thermo-syphon, a heat pipe returns liquid to the evaporator by capillary pressure differences created by a wicking structure rather than gravity as shown in Figure 3.
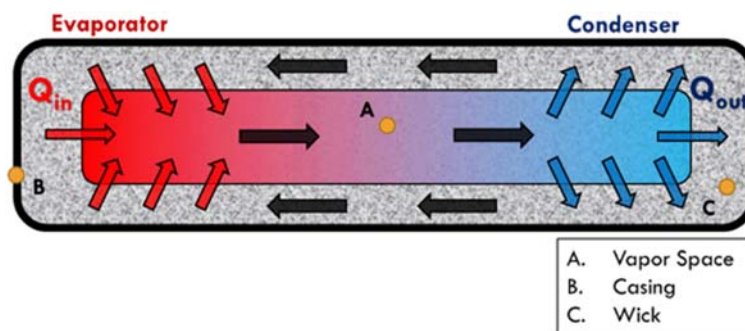
Figure 3: Schematic of basic heat pipe

Since thermo-syphons take advantage of gravitational forces alone, the heat source must be beneath the location of heat rejection in a vertical orientation. However, in a heat pipe with a wick

Approved for public release: distribution is unlimited.

structure, such as grooves or sintered material, the orientation can be with or against gravity and the heater can be located above the condenser. Both thermo-syphons and heat pipes alike are most often created by taking a hollow metal casing and, under partial vacuum, charging a small amount of liquid into the void before sealing both ends.

For terrestrial heat pipes, copper is the most commonly used casing material due to its high thermal conductivity, excellent compatibility with water, and wide availability. Copper heat pipes are commonly paired with water as the working fluid and there is a large amount of literature describing various implementations. However, for space applications, such as heat pipes employed in satellite cooling systems, copper is an unwise choice due to its high density [2]. Aluminum is widely used in these situations as its density is more than three times less than copper and it also has higher strength properties. Examples of aluminum heat pipes are shown below in Figure 4.

Figure 4: Aluminum heat pipes [8]

In many heat pipes, protecting the device from a harmful environment is of paramount importance in increasing the device lifetime. Environmental concerns can degrade, destroy, or form harmful materials that interfere with normal operation. For instance, in a heat pipe, the use of pure, deionized (DI) water in conjunction with aluminum is an incompatible combination as

water will oxidize the surface of bare aluminum, forming aluminum oxide and hydrogen gas as products through the following reaction in equation (1).

$$2Al_{(s)} + 3H_2O_{(l)} \rightarrow Al_2O_{3(s)} \downarrow + 3H_{2(g)} \uparrow \tag{1}$$
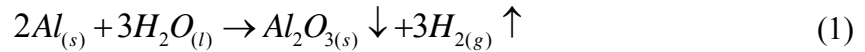
Near room temperature this reaction is quite slow and NCG production may not be noticeable. This is especially true in open air systems or closed systems at pressures near or above atmospheric pressure. However, the high temperatures and low pressures inside a heat pipe accelerate the reaction and also cause accumulated NCG to expand and cover a larger portion of the tube than if it were not under vacuum.

Hydrogen is known as NCG because it does not change phases and will remain a gas except under extremely low temperatures (hydrogen $BP \approx 20K$ for atmospheric pressure). NCGs such as hydrogen can continually generate and build up in the condenser, thus creating a large thermal resistance. This large gas thermal resistance effectively blocks the area available for condensation by preventing vapor from reaching the condenser surface. This leads to a break in the thermal circuit which catastrophically decreases the effective thermal performance and often leads quickly to outright failure as shown in aluminum and water tests done by Terdtoon et al. [9]. A diagram demonstrating how NCG inhibits heat rejection is shown below in Figure 5.
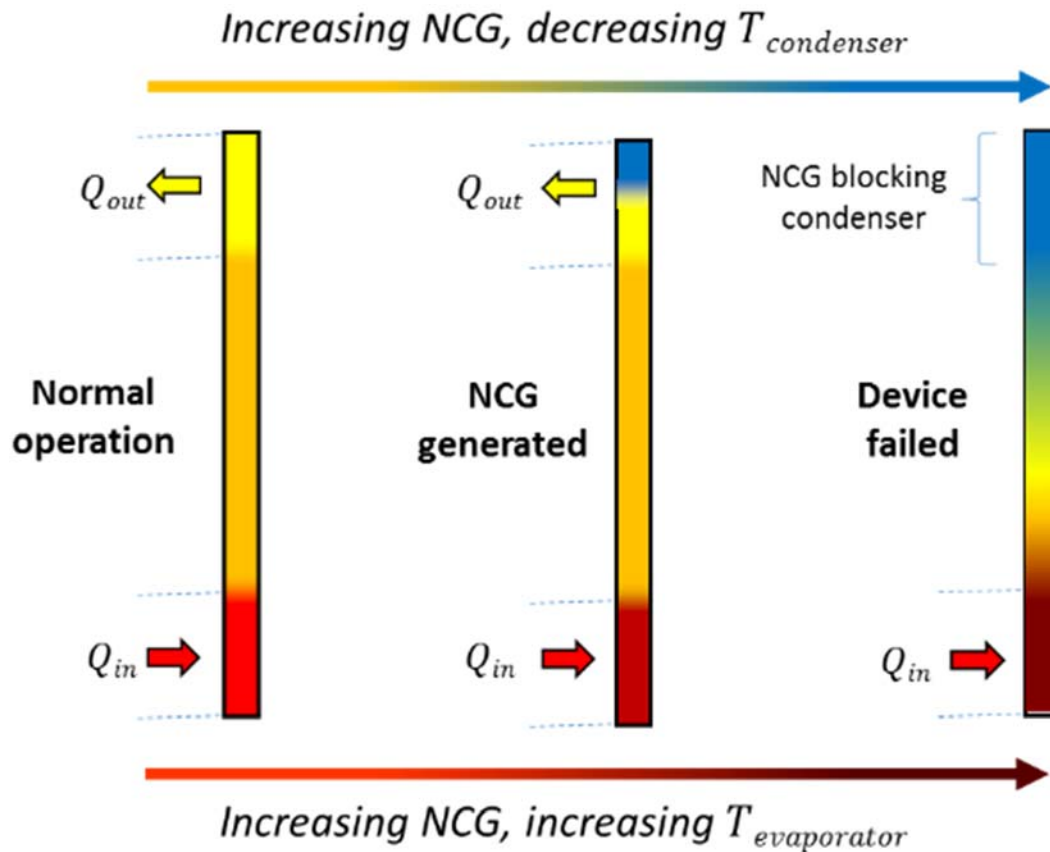
Figure 5: Negative effects of NCG generation on heat pipe performance

In corrosion engineering, the term passivation refers to the ability of an oxide layer to form a protective barrier on the metal surface, thus greatly diminishing the reaction rate between bare metal and fluid by up to many orders of magnitude. Protection can be achieved by anodizing or chemically reacting the surface to build a protective oxide coating. However, the current state of the art method for avoiding NCG production in aluminum heat pipes is simply to use a different working fluid than water. Typically, fluids such as ammonia or even acetone are used as the working fluid in aluminum heat pipes to avoid NCGs. While this practice allows one to easily make use of aluminum's light weight and high strength relative to copper, it can negatively impact heat transfer for intermediate temperature ranges because the thermophysical properties of ammonia and acetone (namely latent heat of vaporization) are significantly lower. The operating

temperature ranges for ammonia and acetone are significantly lower than for water as well, making it difficult to use for some electronics cooling applications above room temperature. Consequently, to take advantage of the structural and reduced weight advantages of an aluminum heat pipe, one is forced to use working fluids with inferior thermophysical properties compared to those of water. Additionally, water is commonly available and an excellent fluid for intermediate temperature heat pipe applications.

Some key fluid properties when considering two-phase heat transfer devices, such as heat pipes, are the latent heat of vaporization (h_{fg}), surface tension (σ), and liquid kinetic viscosity (v). These properties are commonly grouped into a heat pipe figure of merit or liquid transport factor. This merit number is a parameter that measures relative performance among different working fluids. The equation for the merit number can be seen below in equation (2) [2].

$$M_{wf} = \frac{\sigma_l h_{fg}}{v_l} \quad \left[\frac{W}{m^2} \right]$$
(2)

This measures the theoretical maximum heat transport, due to the capillary limit, by a particular fluid considering simple assumptions of negligible gravitational forces and vapor pressure losses.

From merit number data in Figure 6, it can be seen that water has a much higher Merit number than ammonia over the working fluid temperature range the two fluids share [8].
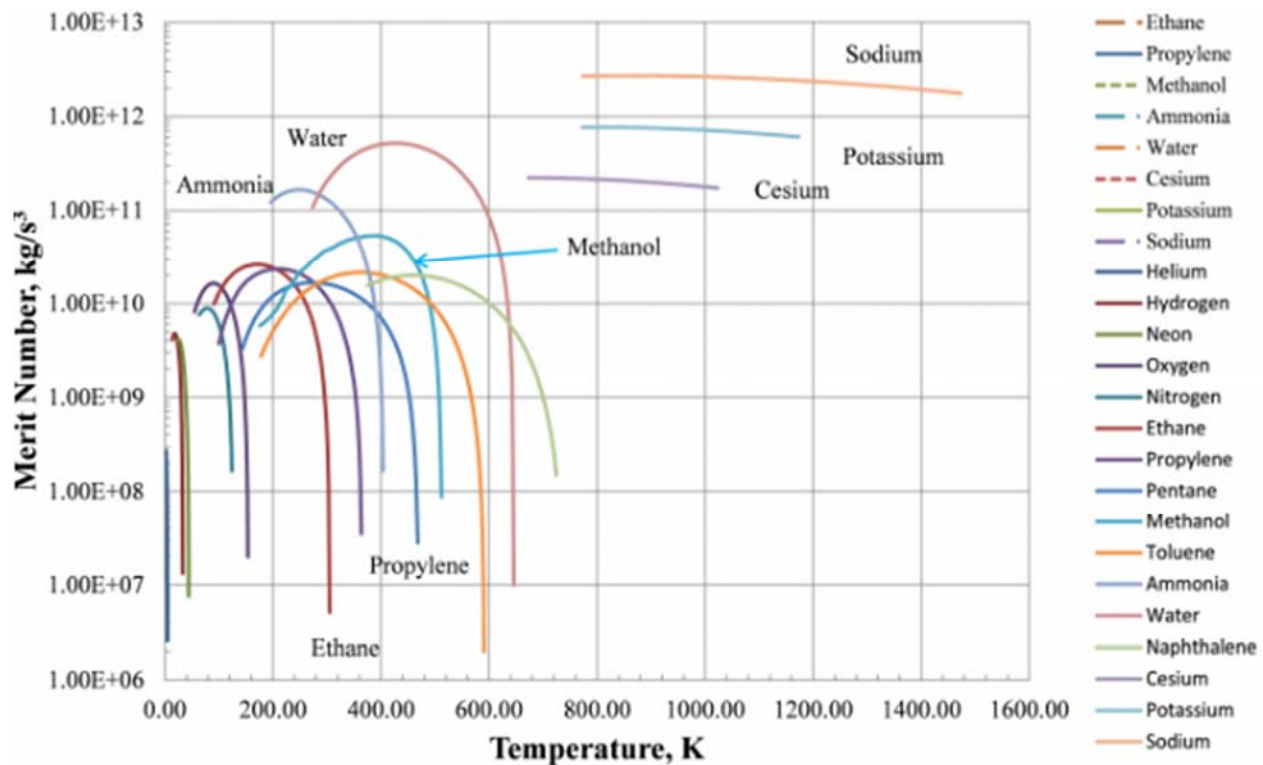
Figure 6: Merit numbers for various fluids [8]

Furthermore, the use of water could expand the usable range of aluminum heat pipes to higher operating temperatures than capable with ammonia or acetone. Ammonia heat pipes have a useful range of about $-60\ to\ 100°C$ while water-based devices typically operate in a range of $30\ to\ 200°C$ [2] and have more favorable thermophysical properties than ammonia. The data suggest that developing a method by which water could be used in an aluminum heat pipe would be extremely valuable, not just for increasing device limits but also for cost as water is widely available and very low cost relative to many heat transfer fluids. The goal of this report is to investigate the plausibility of aluminum heat pipe passivation. This will be achieved through inhibitor selection via past literature and thermodynamic modeling followed by experimentally testing selected aqueous solutions and assessing NCG generation or lack thereof.

3 Literature Review

3.1 Heat Pipe Casing/Fluid Compatibility

In general, heat pipe compatibility is established by performing compatibility tests which simulate intended operation. Often these are referred to as lifetime tests. These test programs consist of testing desired casing and fluid combinations under conditions representative of real world conditions for extended periods of time. Results of such tests can be sensitive to a variety of factors including tube preparation, cleaning, sealing, charging, etc. Although theoretical data regarding chemical or fluid compatibility with various metals may be available in the literature for general use cases, due to the large number of complexities involved in heat pipes it has become common for lifetime tests to be performed again by the end user to verify these estimations experimentally for their specific application even if that combination has been implemented previously with some level of success. For less understood materials or applications this is even more critical. Analysis of the tube contents and inner tube surface after testing via microscope imaging and/or chemical analysis are sometimes performed to shed more light on what reaction products may be present and understand what took place inside a representative device during operation. A series of compatibility tests performed by Van Oost and Aalders with the European Space Agency [10] demonstrate the difficulty in pinpointing the source of tube failures. They concluded that some noted incompatibilities were actually the result of the heat pipe tube sealing method and not incompatibility between casing and fluid. They speculated that the stainless steel alloy 304L tubes (with stainless steel alloy 316 wick) they sealed by hard-brazing, instead of oxygen or nitrogen TIG-welding, failed due to this change and not the fluid used inside.

Table 1: Compatibility data for low to moderate temperature working fluids [11]

Wick Material	Working Fluid					
	Water	Acetone	Ammonia	Methanol	Dow-A	Dow-E
Copper	RU	RU	NR	RU	RU	RU
Aluminum	GNC	RL	RU	NR	UK	NR
Stainless steel	GNT	PC	RU	GNT	RU	RU
Nickel	PC	PC	RU	RL	RU	RL

RU	recommended by past successful use
RL	recommended by literature
PC	probably compatible
NR	not recommended
UK	unknown
GNC	generation of gas at all temperatures
GNT	generation of gas at high temperatures in presence of oxide

Other compatibility testing focuses on qualifying new fluids whose compatibility for use in heat pipes is largely unknown. For example, a large number of mostly organic, intermediate temperature fluids have been tested by Basiulis and Filler [11] with various casing materials. Condensed results of their study can be found above in Table 1. Note the strongly referenced incompatibility of aluminum/water devices in all circumstances, and nuanced compatibility recommendations regarding steel/water devices which were observed to fail at high temperatures and when oxygen is present in the system. Copper/water combinations were found to be one of the most resilient. Aluminum/ammonia heat pipes achieved lifetimes of 8,000 hours and were recommended. Basiulis and Prager [12] conducted an even more impressive array of lifetime tests a few years later at Hughes Aircraft; summarization of selected results can be seen in Table 2 below.

Approved for public release: distribution is unlimited.

Table 2: Compatibility recommendations [12]

Working Fluid	Casing Material	
	Recommended	Not Recommended
Ammonia	Aluminum	Copper
	Carbon steel	
	Nickel	
	Stainless steel	
Acetone	Copper	
	Silica	
	Aluminum	
	Stainless steel	
Methanol	Copper	Aluminum
	Stainless steel	
	Silica	
Water	Copper	Stainless steel
	Monel	Aluminum
	347 Stainless steel	Silica
		Inconel
		Nickel
		Carbon Steel

Other lifetime tests by Kreeb et. al. [13] also indicated very long lifetimes of copper/water heat pipes of more than 20,000 hours without degradation. However, these researchers reported considerable NCG generation with stainless steel/water (alloy 316) heat pipes. More stainless steel tests conducted by Busse et. al. [14] concluded that above vapor temperatures of 250°C there were no changes in tube preparation or operation conditions which resulted in acceptable levels of hydrogen gas production. The authors noted that the effects of hydrogen gas were often observable within only two hours of operation from start-up. It can be seen that NCG generation can be an immediate threat to heat pipe operation.

Garrels and Larson [15] conducted lifetime tests on aluminum alloy 6062 and stainless steel 321 with a wide variety of charge fluids. Their intended device application was for satellite

thermal management with a required device lifetime of five years. The authors reported ammonia as a recommended fluid for both casing materials, although it was stressed that the water content must be kept to only a few parts per million otherwise NCG formation would occur. Regarding aluminum, Garrels and Larson concluded that ammonia and butane were acceptable for operating tempeartures below $65°C$, while benzene, heptane, and pentane were acceptable for more intermediate temperatures below $150°C$. In this study, water was only tested with the stainless steel and found to be incompatible.

3.2 Passivation of Heat Pipes with Aqueous Fluids

As previously discussed, water is a nearly ideal heat transfer fluid for heat pipes due to its abundance, favorable thermophysical properties, and generally broad compatibility with various casing materials. Steel/water heat pipes are a partial exception to this rule. The first two-phase thermo-syphon devices from Perkins and Buck [16] and King [17] were made of iron casings charged with water and often displayed acceptable device lifetimes despite the fact that gas generation was noted to occur, as summarized by Reay and Kew [2]. Modern applications with more demanding performance requirements and device longevity have driven attempts to prevent NCG generation within steel/water heat pipes. Additionally, in the case of satellite cooling, heat pipes are likely unable to be serviced at any point within the operation cycle. This creates a need for relative certainty regarding the behavior of any heat pipes on board the system.

In a steel heat pipe, similarly to aluminum, hydrogen is generated by a reaction between the iron surface and water creating iron hydroxide and hydrogen gas. This iron hydroxide decomposes to an iron oxide, Fe_3O_4, which can protect mild steels from further reactions. However, if hydrogen is generated after the tube is sealed, the damage may already be done. Some

early work related to the passivation of mild steels, such as the common austenitic grades 304 or 316, has been done by Novotna et al. [18] in 1988. Novotna et al. considered several possibiilities for preventing the release of hydrogen gas were considered: use of an inhibitor in the working fluid itself, pre-processing the heat pipe casing to create a passivating oxide layer, and the use of both methods simultaneously. Tests were run for 6,000 hours with a small array of methods covering these practices. The inhibitor used was K_2CrO_4, potassium chromate, along with a range of fluid pH from neutral to basic. Preoxidation alone (with high temperature steam) and the use of an inhibitor alone were each found to suppress hydrogen generation to a degree. Results showed that oxidizing the tube inner surface with high temperature steam before filling alongside a small inhibitor concentration with initial fluid $pH = 9.05$, resulted in no measurable amount of hydrogen gas and the lowest heat pipe temperature difference along the condenser. Post-test pH measurements demonstrated the fluid pH became considerably more alkaline during the test period. Ultimately, moderately alkaline initial solutions were recommended with a range of pH from 6 to 11. Their results indicated that the best results (longest lifetimes, lowest hydrogen gas content, and smallest device ΔT) resulted when a passivating oxide layer of $3 - 5$ μm and a slightly alkaline solution with chromate inhibitors were used. Similar results were obtained by Zhang and Zhuang [19].

Similar results were also found by Rassamakin et al. [20] demonstrating further the utility of chromate inhibitors for passivation of mild steel heat pipes. Tests by Rassamakin demonstrated minimal increase in heat pipe thermal resistance over a period of 35,000 hours. Studies in France which nearly mirrored those of Novotna et al. were done more recently by Bricard et al. [21] and similar results were obtained.

Methods not involving chromates have also been investigated for more general passivation of mild steels. For example, Wu et al. [22] recently found success in passivating mild steel using an electrodeposited superhydrophobic silica film. However, this method was not applied to heat pipes and due to the negative evaporative heat transfer consequences of the hydrophobic surface might not even be a good candidate for future work in phase change devices.

Table 1 and Table 2 show compatibilities between not only iron based tubes but also aluminum. The work of Basiulis and Filler [11], Basiulis and Prager [12], and Rassamakin et al. [20] have all consistently found incompatibilities between pure water and aluminum heat pipes. Terdtoon et al. [9] performed an array of thermo-syphon lifetime tests with the goal of studying internal tube corrosion. The researchers used tubes made of aluminum, copper, iron, and stainless steel with water as the working fluid. Disodium hydrogen phosphate (Na_2HPO_4) was added in varying concentrations to some tests and it was found that these additives reduced both internal tube corrosion as well as hydrogen generation in the iron tubes. However, the researchers found that the aluminum tubes tested with water and any level of the same additives still produced hydrogen. The hydrogen generation rates were found to be too high for the tubes to withstand the generated pressure and test data for aluminum and any of the solutions were unable to be obtained. The importance of their work is not just the experimental results but also the quantification of tube corrosion over time using an Arrhenius model for hydrogen generation. Terdtoon et al. used tube weight before and after the testing to determine the level of corrosion accumulated over different test lengths and fit the results to an Arrhenius model. The following relationships in equations (3) and (4) were used for the corrosion rate as a function of time and temperature, respectively.

$$Cr = At^B \tag{3}$$

$$Cr = Ct^{D/T} \tag{4}$$

In these equations, Cr represents the corrosion rate and t is test time. The constants A, B, C, and D are coefficients that will be different depending on the tube material used, fluid charged into that tube, and any method used to affect compatibility such as corrosion inhibitors. Similar Arrhenius relationships were reported using measurements of hydrogen gas mass accumulation, although no information on how this data was collected was provided and reported errors were as high as $\pm 28\%$.

Analyzing corrosion rates of thermo-syphons based on accumulated tube mass may be useful for determining fouling resistances of the tubes and thus the impact on thermal resistance of a thermo-syphon over time. However, this method has less value when assessing the relative utility of different inhibitors when attempting to passivate a thermo-syphon and prevent hydrogen gas generation. Monitoring tube mass after different operating periods does not consider the possibility that an internal oxide layer was generated over a short period of time at the start of testing from oxidizing inhibitors introduced for such a purpose. Also, tube corrosion could take place externally, potentially affecting results. A single Arrhenius model may not have the ability to capture the behavior of a tube with inhibitors because there are likely different relationships between mass accumulation and time depending on the amount of inhibitors consumed. If there are multiple inhibitors present this becomes even more difficult to capture. More importantly, the accumulation of mass in the form of surface oxides does not necessitate the release of NCG.

A series of papers written by Anderson et al. [23-25] tested heat pipe working fluids in an intermediate temperature range ($450K$ to $750K$) including halides, organics, and elemental (sulphur, iodine, mercury) working fluids paired with casings made of titanium, Monel, aluminum,

Approved for public release: distribution is unlimited.

and steel alloys. Their results indicated that titanium and $TiBr_4$ (Br is bromine) were compatible at $653K$ while Hastelloy B-3, C-22, and C-2000 were compatible with $AlBr_3$ at $673K$. No halide working fluids were found to be compatible with aluminum casings. Sulphur was found to be compatible with aluminum at $873K$ in a short duration test and a sulphur iodine mixture was used with success in a 304 SS casing at $623K$ in a 1000 hour test. Organic working fluids were found to decompose at elevated temperatures and it was found that NCG generation accompanied their use in many casings. Napthalene and toluene were found to be compatible in all tests but at lower temperatures. Anderson et al. also reported scanning electron microscope (SEM) images and energy dispersive spectroscopy (EDS) data for destructed heat pipes once they had either failed or reached the end of the life test cycle. This information is important because it gives an indication of what reaction processes may be at work within the heat pipe.

Methods used by Terdtoon et al. and Anderson et al. represent highly useful data for analyzing heat pipe and working fluid compatibility. However, a common thread among many previous works, including these, is that they spent little if any time analyzing the chemical interactions between the fluid and casing material. For the use of inhibitors, this is even more important since identifying the correct inhibitor(s) is the first step and knowing the concentration required likely requires more detailed optimization for different cases. The primary means of testing the utility of a particular inhibitor or inhibitor concentration has typically relied upon measurements of performance metrics such as ΔT, internal tube pressure, or NCG slug detection via condenser temperature tracking. Additional data regarding the fluid potential and pH before and after testing would allow for the calculation of how much oxidizers are consumed and the likely products. This would help other researchers to extrapolate the results for different size

thermo-syphons and potentially heat pipes with simple wicks. The action of NCG inhibitors for heat pipes is rooted in the chemical reactions at work; therefore, their consideration should be addressed in any work attempting to passivate a particular thermo-syphon casing material for use with a typically incompatible fluid.

Depending on volume, charge amount, and operating temperature, pure water charged aluminum devices typically fail within an hour or two, sometimes sooner. This is based upon both previous literature, such as that done by Terdtoon et al. [9], as well as other tests with grooved aluminum heat pipes performed performed by Stubblebine et al. [26, 27].

3.3 Aluminum Corrosion Prevention

While there are few examples of researchers studying aluminum and water compatibility for heat transfer fluids [2], there has been a great deal of research done on aluminum corrosion protection, or passivation, for other use cases. While reviewing these methods, an important differentiation between aluminum/water compatibility for heat pipes versus many other corrosion environments is that heat pipes are hermetically sealed and air has been evacuated. This means that hydrogen or other NCG generation is more of a concern than in an open system. Another important point to make is that while steel and aluminum passivation is similar, aluminum is a more highly reactive metal as shown below in the abbreviated half-reaction chart of Table 3.

Approved for public release: distribution is unlimited.

Table 3: Half-reaction chart comparing aluminum and steel (iron)

Half-cell reaction	φ^θ/V
$Al^{3+} + 3e^- \rightarrow Al$	-1.677
$Fe^{2+} + 2e^- \rightarrow Fe$	-0.44
$Fe^{3+} + 3e^- \rightarrow Fe$	-0.04
$2H^+ + 2e^- \rightarrow H_2$	0
$Cu^{2+} + 2e^- \rightarrow Cu$	0.339
$Fe^{3+} + e^- \rightarrow Fe^{2+}$	0.771

One common class of passivation schemes uses strong chromate oxidizers in aqueous solution. Chromate passivation schemes are a common method of protecting aluminum surfaces of everyday objects or machine parts. The general principle is to use hexavalent chromium as an oxidizer to build a protective, passivating oxide layer on the metal part. In addition to being alloyed with chromium directly, alumium alloys used in aircraft construction are commonly treated with chromic acid solutions to protect them against corrosion and wear, thus increasing part lifetime.

Kendig and Buchheit [28] reviewed existing chromate conversion coatings (CCC) used to prevent corrosion and pitting of various aluminum alloys. Their work summarized recent studies showing that the inhibition of aluminum surface corrosion is a result of the CCC inhibiting oxygen reduction reactions at the surface. These CCC treatments were found to be excellent at preventing oxygen reduction in solutions with near-neutral pH. Furthermore, Kendig and Buchheit explored the successful use of CCC's ability to actively repair defects in the passivation coating. Rocco et al. [29] compared two different methods of chromate coatings on Al/Zn alloys which were designed to discourage corrosion and allow increased adherence of paints. The research done by Kendig and Buchheit and Rocco et al. did not look at the use of CCC's for aluminum passivation

in heat pipes; however, their work serves as a solid basis upon which to begin an attempt at this goal while keeping in mind that hydrogen generation is an additional concern.

3.4 Inorganic Aqueous Solutions (IAS)

Recently, there has been increased interest in a specific water-based fluid with inorganic aqueous oxidizers (IAS) first created in China. This working fluid contains chromate and other oxidizers similar to those used to passivate steels and for chromate conversion coatings. However, initial applications of this fluid were actually for performance enhancement of copper heat pipes, not aluminum passivation. Some early experiments on the IAS fluid were conducted by Blackmon [30] at University of Huntsville, AL and summarized in a NASA brief. The tubes he tested were run with a China produced mix known as IAS Mix 2.5. His results demonstrated that the copper heat pipes had high thermal conductivity; however, these were early results and the tubes that were obtained from the Chinese manufacturer appeared to be of inconsistent quality and, while the data were promising, the tests ultimately yielded inconsistent performance results. Broad investigations into the IAS fluid were performed by Rao [31] in his Master's report and increased heat transfer capabilities in copper heat pipes were again reported. Reilly and Catton [32] found that IAS leaves wick-like hydrophilic deposits in sintered biporous copper wicks in the evaporator area and that the use of IAS led to significant performance enhancement. Their research indicated that both the passivation and heat transfer enhancement of devices by IAS is likely impacted by the surface area to be passivated, i.e. the internal surface area of the heat pipe. IAS deposits can be found mainly in the evaporator section of thermo-syphons and wicked heat pipes as demonstrated by the copper sintered wick in Figure 7. Depending upon the material used for the heat transfer device casing, the deposits formed are different in amount as a result of the chemistry.
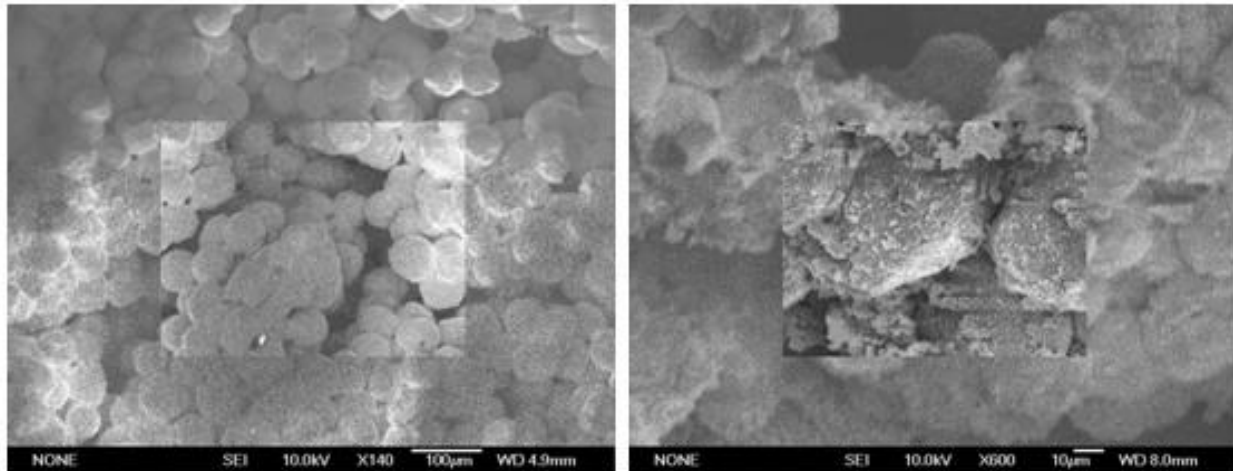
Figure 7: Effect of IAS on sintered copper wick [32]

Stubblebine and Catton [33] looked at using IAS fluids in aluminum flat heat pipes which had grooved wicks. A schematic of the test layout can be found below in Figure 8.
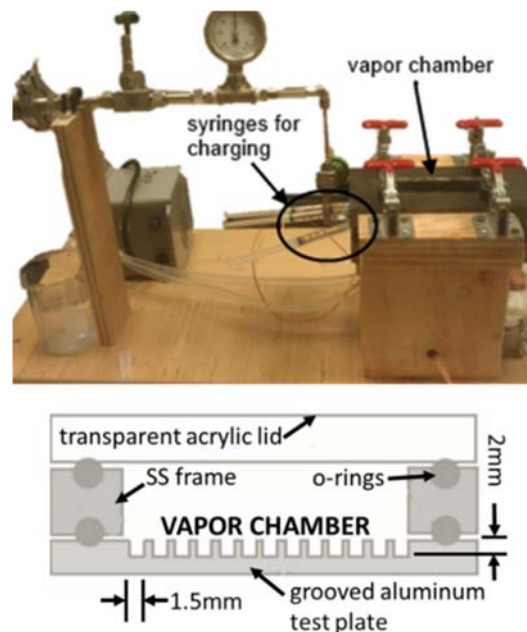
Figure 8: Flat heat pipe test setup (top), vapor chamber schematic (bottom); (representation, not actual scale)

When pure water was tested with aluminum grooved plates, there was obvious and rapid NCG generation which failed the test. This can be observed below in Figure 9 which shows performance data for a test inclination of 1°.
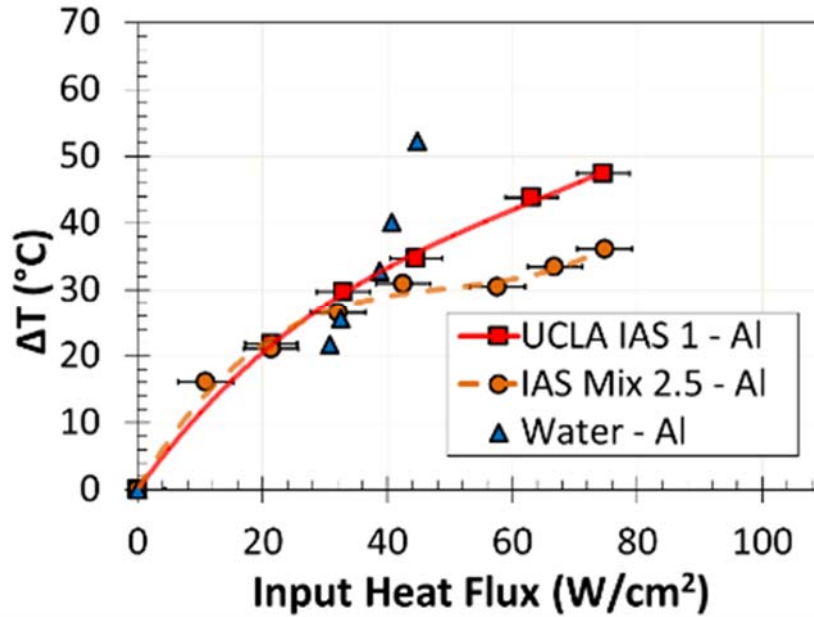
Figure 9: 1° Data: heat flux vs. *ΔT*, all aluminum plates (water, UCLA IAS 1, and IAS Mix 2.5)

The $\Delta T = T_{heater} - T_{condenser}$ for water increases rapidly at low heat fluxes while the IAS fluids had only gradual increases in ΔT as input power increased. Additional tests at a steeper inclination angle of 3° were also ran. At this angle, water ΔT increased so rapidly, even at a constant input power, that data was not able to be obtained. However, data for IAS fluids is shown below in Figure 10.
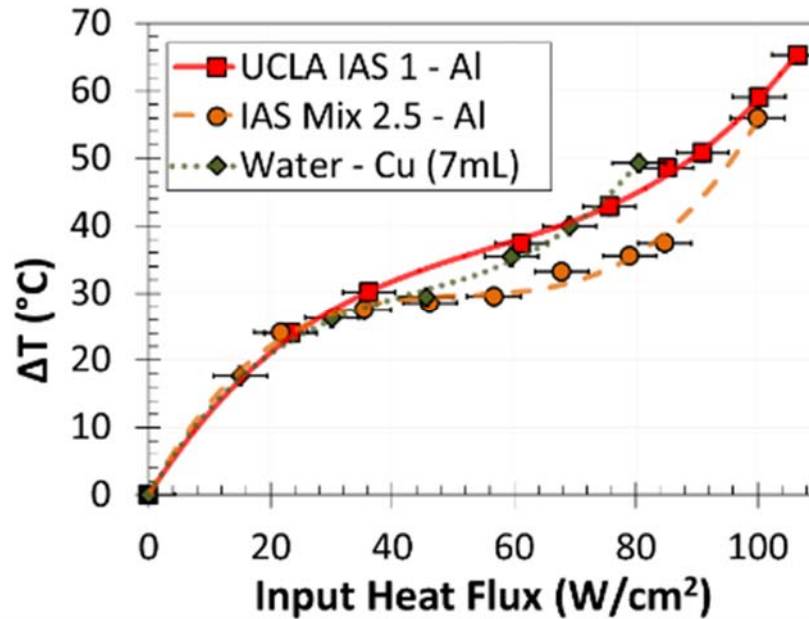
Figure 10: 3° Data: heat flux vs. *ΔT*; UCLA IAS 1-aluminum, IAS Mix 2.5-aluminum, water-copper

Dryout was able to be observed for each test and performance data was similar to that of a copper grooved plate ran in the same setup. The results were encouraging due to the stark contrast between the IAS fluid performance and pure water performance with aluminum grooved plates. However, the large vapor space design and initial purpose of testing performance and not compatibility made these experiments ill-suited for sensitive detection of NCG. In summary, NCG was certainly suppressed but a quantitative, long-term estimate of IAS fluid compatibility with aluminum was not obtained.

The IAS fluids were also shown in tests by Stubblebine et al. [27] to both passivate aluminum phase change heat transfer (PHCT) devices and also decrease device thermal resistance. Experiments performed by Reilly et al. [34] also showed that IAS was able to actively passivate an aluminum surface in such a way that the fluid may be charged and used in aluminum heat pipes with an obvious suppression of NCG. IAS fluids are a complex mix of dilute chemical constituents

in aqueous solution, including strong chromate oxidizers such as those used in chromate conversion coatings. Yao's report work [35] demonstrated both chromates and permanganate strong oxidizers were likely responsible for the passivation effects seen. A table showing a list of the ions present in Yao's report work [35] can be found in Table 4.

Table 4: Ions present in Yao [35]

Positive ions	Negative ions
K^+	MnO_4^-
Na^+	$HCrO_4^-$
Ca^{2+}	$Cr_2O_7^{2-}$
Sr^{2+}	CrO_4^{2-}

Yao also hypothesized that stronger, permanganate oxidizer was useful in perfecting an initial aluminum oxide passivation layer and chromate oxidizers were useful for backup protection because they react slower and remain in solution to repair potential defects throughout device lifetime.

Thermophysical properties of IAS have been measured by Yao [35] and it was found that the bulk properties of IAS vary negligibly from water due to the very small overall molarities of the chemicals. Surface tension for UCLA IAS 1 was reported as 69 mN/m vs. 71 mN/m for water, both at $25°C$; this represented a small 2.8% difference. Contact angle was measured for both IAS and water on a smooth copper surface and values of 100° and 98°, respectively were reported; representing a small 2% difference. All other thermophysical properties exhibited only slight differences from water with density being the next largest discrepency. Density of IAS was only 0.78% lower than water. While a generic IAS solution is still produced in China, the

Approved for public release: distribution is unlimited.

consistency of product is poor and the creators do not actually know or understand how the fluid works. Therefore they are incapable of insuring consistant results and confidence in their product. Furthermore, the intended use of the fluid in China is marketed as a performance enhancement fluid, not aluminum passivation.

Yao [35] and Yao et al. [36] have also published on more fundamental studies of the chemistry theory allowing IAS fluids to passivate and enhance heat transfer, focusing primarily on copper applications. This report will investigate the effects of oxidizers and their concentrations only on NCG suppression in aluminum thermo-syphons. The starting point will be new solutions mixed with oxidizers only using the oxidizer concentrations used in Yao's report as well as a balanced pH.

3.5 Summary

This goal of this report is to investigate, through modeling and experiments, the effects and limits of using inorganic oxidizers in aqueous solutions charged in aluminum PCHT (phase change heat transfer) devices such as heat pipes or thermo-syphons. Starting with an overview of the chemical reactions and thermodynamics of active metal passivation, a MATLAB code was developed to calculate and draw Pourbaix diagrams as a function of temperature so that past and future experimental results could be compared. Pourbaix diagrams use chemical and electrochemical reactions along with thermodynamics to predict the most stable species for a given solution electrode potential (E) and pH. Using these tools, new inhibitor fluids were formulated, mixed, and tested in a corrosion test chamber built specifically to test fluid compatibility with metal samples in a low vacuum environment at constant temperature for extended time. Next, the

25

same fluids were again tested in thermo-syphon experiments with different methods of heating and cooling. Heater block tests were done with natural convection cooling first so that an IR camera could be used to visualize the growth of any potential NCG slug within the pipe. Constant temperature heating using a silicon oil bath was performed next in an effort to run longer tests that required less active observation, all while keeping the infrared (IR) camera to visualize NCG growth over time. Finally, a heater block and condenser block setup were used to test thermo-syphons using a more powerful, localized condenser to investigate the role of the form and rate of liquid back flow condensation as compared to that with natural convection cooling spread over the entire exposed pipe.

The use of an aluminum heat transfer device, in combination with a water-based charge solution, would present an important step forward in heat pipe technology, especially for applications where low weight and/or cost is important. Understanding the limits and reliability of such a device are essential if this technology is to be adopted and benefited by industry.

4 Methods, Assumptions, and Procedures (Thermodynamics and Corrosion Prediction)

Following the previous experimental work with lifetime tests, flat heat pipe tests, and Yao's report using IAS fluids and aluminum devices, a "back to basics" approach was taken with regard to the aluminum/water NCG problem. The experimental results presented thus far demonstrate there are benefits to using inorganic inhibitors in aqueous solution; however, they lacked rigor and strong conclusions. A simple thermodynamic model was seen as a helpful step in confirming initial suppositions of why and how passivation could be achieved. This report will consider the effects and limits of strong oxidizers, solution pH, and temperature on passivation of aluminum thermosyphons. This section starts by reexaming the aluminum/water NCG problem before building $E - pH$ diagrams for aluminum and the two IAS oxidizers, manganese and chromium.

4.1 Summary of Aluminum/Water NCG Problem

There are many situations where water and aluminum are in contact where hydrogen generation is acceptable, such as an open system at atmospheric pressure. In some corrosion prevention literature aluminum is referred to as compatible with water and little corrosion is expected. Aluminum as a structural material is often found in contact with aqueous environments. Whether submersed entirely or in outdoor environments where rain or other water contamination is likely, aluminum appears to have little problem resisting the corroding effects of water. Aluminum has a natural oxide layer which protects it. This aluminum oxide layer protects aluminum very well in neutral waters. For these instances metal degradation is often the primary concern and to this end aluminum can persist in natural water environments for long lifetimes. The oxide may wash off but it is instantly replenished with a small amount of hydrogen generation. In

open systems this is hardly a concern. Even if the water starts out neutral it will likely wash some of the oxide off at some point and require repair to the coating. In the case of pure water this will increase the pH and eventually move the water E and pH outside of the passivation region, leading to further corrosion. Additionally, the oxide repairing reaction between bare aluminum and pure water will release hydrogen gas as a byproduct. In the case of a heat pipe, not only is the system closed but it is typically brought to partial vacuum before sealing. While it depends on the specific application and desired vapor temperature, most heat pipes are evacuated to at least medium vacuum around 10^{-2} $Torr$ and can be pumped down to high vacuum levels which can reach 10^{-5} $Torr$ or more. Even at a medium vacuum the pressure is approximately four orders of magnitude less than atmospheric pressure. A simple ideal gas analysis shows this corresponds to an increase in hydrogen gas volume, relative to atmospheric pressure, of the same four orders of magnitude. The low pressure environment within a heat pipe demands more strict requirements on corrosion and the specific corrosion products than many open air uses of aluminum in water.

4.2 Thermodynamic Modeling for Passivation

The prevention of hydrogen gas generation using inhibitors in aluminum heat pipes can be investigated by modeling the thermodynamic stability of a multi-component, aqueous solution. Initial screening using thermodynamics can help determine what solution conditions are necessary to both resist corrosion and hydrogen generation. $E - pH$ diagrams are used to predict the most thermodynamically stable species at a given fluid pH and potential when equilibrium has been reached. Both pH and potential are dependent upon the specific chemicals and their concentrations existing in solution as well as temperature. An example of an $E - pH$ diagram can be found for a representative aluminum/water system in Figure 11.

Approved for public release: distribution is unlimited.
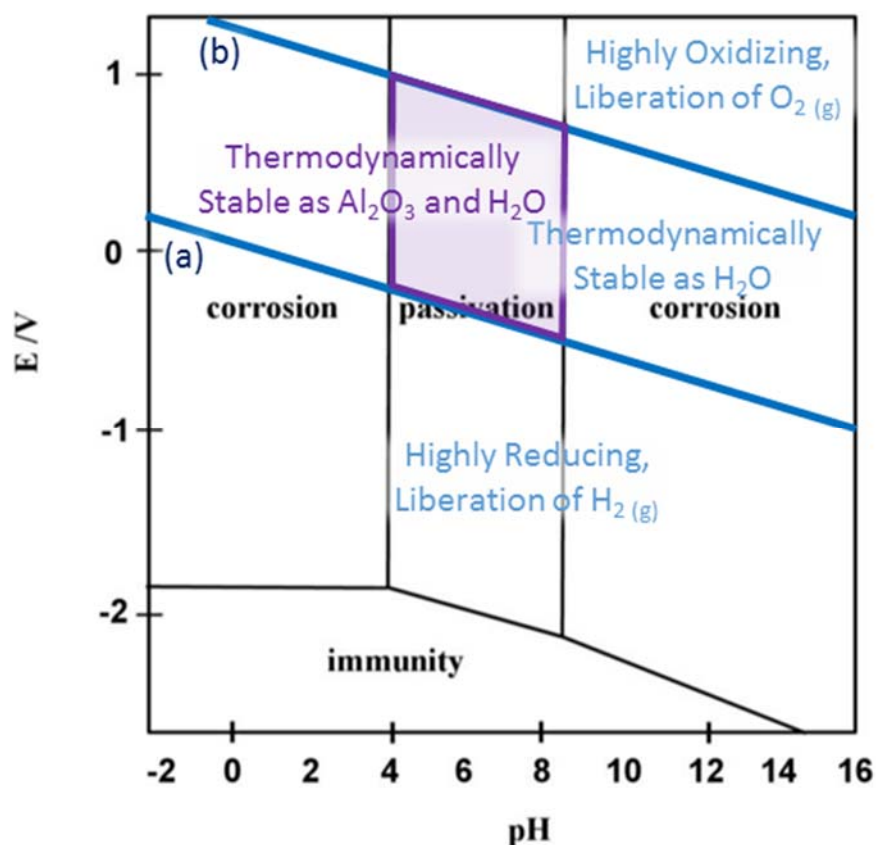
Figure 11: E-pH diagram for water at 25°C [37]

There are three main types of regions in these diagrams. The first region is immunity.

Within the immunity region atomic aluminum metal is the most thermodynamically stable species

and it will be non reactive. Within the corrosion region a soluble, ionic species will be most stable,

such as Al^{3+} ions. This indicates corrosion is occuring. Within the passivation region, an oxide

film of the metal species is most stable. The diagram cannot determine if that film is protective.

The blue lines correspond to water stability. A highly reducing solution will exist below the bottom

diagonal line (a) in Figure 11 where hydrogen gas will be liberated from ionization of water itself.

Hydrogen gas can also be generated via chemical reactions with a metal electrode. The reason

unprotected aluminum metal produces hydrogen gas when contacting water is because the

immunity region exists entirely below the (a) line in Figure 11 over the entire pH range. This

hydrogen evolution can be prevented or diminished substantially by establishing a protective oxide barrier on the metal surface.

Solutions containing strong oxidizers can act to maintain the system equilibrium within the passivation zone for the metal and within the thermodynamically stable zone for water. Conditions where both water and a protective oxide coating are thermodynamically stable and gas generation rates are substantially lowered are shown within the purple region of Figure 11. Although not used in the previous Figure 11, normal convention dictates that short dashed lines represent equilibrium between an ionic species and a solid species, long dashed lines show boundaries between two soluble ionic species, and solid lines represent equilibrium between two solid species. These conventions will be adopted throughout from this point forward. By measuring the E and pH of a system, one can plot the point on the diagram and determine the thermodynamically favored species for each component.

Typically, the resulting reactions from metals in aqueous solution will release either oxygen or hydrogen gas. For metals with a large immunity region encompassing standard pure water conditions, such as copper, this rate is extremely low and often neglected. However, it is important to note that there is no situation in which a metal electrode in aqueous solution will not liberate either oxygen or hydrogen gas. This applies to copper electrodes as well even though it is commonly considered to be "NCG free" when used with water. In copper phase change heat transfer (PCHT) devices, the corrosion and NCG generation rates are so small under most operating conditions that we often refer to it in practice as an inert combination.

4.3 Building a Pourbaix ($E - pH$) Diagram as a Function of Temperature

For electrochemical reactions involving the transferrance of electrons, Pourbaix diagram lines are drawn from the Nernst equation,

$$E(T) = E^{\circ}(T) - 2.303 \frac{RT}{nF} \log Q \qquad (5)$$

where the standard reduction potential is written as,

$$E^{\circ}(T) = -\frac{\Delta G_r^{\circ}(T)}{nF} \qquad (6)$$

Purely chemical reactions are evaluated using the Van't Hoff equation,

$$\Delta G_r^{\circ} = -2.303 \log K \qquad (7)$$

Note that equation (5) uses Q, the reaction quotient, while equation (7) makes use of K, the equilibrium constant. At equilibrium conditions, such as those necessary for $E - pH$ stability diagrams, the two are equivalent ($Q = K$) and there is no discrepancy. The "not" or "°" superscript on some variables indicates it is referenced to standard conditions of $1\ atm$ pressure and 1 molar solution concentration. The definition of K is,

$$K = \frac{[C]^c [D]^d}{[A]^a [B]^b} \qquad (8)$$

where the lowercase letters are species coefficients in the representative chemical reaction in equation (9). The capital letters are the species themselves. Bracketed capital letters in equation (8) represent the individual species molar concentration or activity, which, at dilute concentrations that will be used in this work are essentially equivalent.

$$aA + bB \leftrightarrows cC + dD \qquad (9)$$

The fluid pH enters the equation through the concentration, or activity, of the aqueous hydrogen ion through the following definition for pH,

$$pH = -\log_{10}\left[H^+_{(aq)}\right] \tag{10}$$

When drawing lines for the equilibrium diagrams, all other aqueous ion species concentrations are known in that we assume a small value below which that species' existence is defined as negligible. In adherence with standard corrosion science and geochemical research convention, these ion concentrations in solution are often assumed to be equal to $10^{-6}\ M$. This is practical because it denotes a line which distinguishes the boundary between corrosion and no corrosion. Pure liquids and gases, such as water, and solids are assumed to be equal to 1.

For both chemical and electrochemical situations, the standard Gibbs free energy change of reaction, ΔG_r°, can be found in most thermodynamic tables at $25°C$. $E - pH$ diagrams based on this temperature are also readily available for a multitude of systems. However, if one wants to construct diagrams at any given temperature $\Delta G_r^\circ(T)$, the standard Gibbs free energy as a function of temperature must be found. This requires more calculation steps and data is less readily available in a convenient form, particularly for aqueous, ionic species.

Starting with the definition of Gibbs free energy, enthalpy, and the changes in each we have,

$$G = H - TS \tag{11}$$

$$dG = dH - TdS - SdT \tag{12}$$

$$H = U + PV \tag{13}$$

$$dH = dU + PdV + VdP \tag{14}$$

Approved for public release: distribution is unlimited.

Substituting in the change of enthalpy into the equation for Gibbs free energy and canceling terms we get the following,

$$dG = VdP - SdT \tag{15}$$

where relations for volume, V, and entropy, S, are obtained by recognizing that, as a state function, Gibbs free energy in equation (15) can be represented in the following way,

$$dG = \left(\frac{\partial G}{\partial P}\right)_T dP + \left(\frac{\partial G}{\partial T}\right)_P dT \tag{16}$$

$$\left(\frac{\partial G}{\partial P}\right)_T = V \tag{17}$$

$$\left(\frac{\partial G}{\partial T}\right)_P = -S \tag{18}$$

Similarly, the Gibbs free energy at any given temperature and pressure, $G(T,P)$, can be assumed to be a composite sum of $G(T,P_r)$, the Gibbs energy at any temperature and a reference pressure of 1 atm, and the second term in equation (19). This second term represents the change in Gibbs energy from the reference pressure to any given pressure while temperature is held constant.

$$G(T,P) = G(T,P_r) + \int_{P_r}^{P} \left(\frac{\partial G}{\partial P}\right)_T dP \tag{19}$$

The first term to the right of the equality in equation (19) is obtained from the definition of Gibbs free energy as follows in equation (20),

$$G(T,P_r) = H(T,P_r) - TS(T,P_r) \tag{20}$$

Substituting this term back into equation (19) and removing the partial derivative for G in the pressure term by substituting V back in we get equation (21),

$$G(T,P) = H(T,P_r) - TS(T,P_r) + \int_{P_r}^{P} V dP \qquad (21)$$

The $\int_{P_r}^{P} V dP$ term can be assumed negligible. Uhlig's corrosion handbook [38] suggests this term is negligible for $P < 100\ atm$, giving,

$$G(T,P_r) = H(T,P_r) - TS(T,P_r) \qquad (22)$$

Our equation now looks similar to the original definition of Gibbs energy, however, we have eliminated the pressure dependence and learned that the temperature dependence is stronger and can be decoupled from the pressure. Furthermore, we have rewritten our equation for Gibbs free energy such that it is referenced to standard pressure at $P_r = 1\ atm$.

Using the well-known relationships for temperature dependent enthalpy and entropy equations,

$$H(T,P_r) = H(T_r,P_r) + \int_{T_r}^{T} C_p(T) dT \qquad (23)$$

$$S(T,P_r) = S(T_r,P_r) + \int_{T_r}^{T} \frac{C_p(T)}{T} dT \qquad (24)$$

where the first term right of the equality in each are equivalent to standard enthalpy of formation and absolute standard entropy as seen in equations (25) and (26),

$$H(T_r,P_r) = \Delta H_f^{\circ} \qquad (25)$$

$$S(T_r,P_r) = S^{\circ} \qquad (26)$$

After substituting these expressions into equation (22), the final equation is obtained,

$$G^{\circ}(T) = \Delta H_f^{\circ}(T_r) + \int_{T_r}^{T} C_p(T) dT - T\left[S^{\circ}(T_r) + \int_{T_r}^{T} \frac{C_p(T)}{T} dT \right] \tag{27}$$

This is a pseudo "absolute" Gibbs energy in that it is used as an intermediate step in the following equation (28). True Gibbs energies cannot be absolute in nature.

$$\Delta G_r^{\circ}(T) = \sum_{products} \left[G^{\circ}(T) \right] - \sum_{reactants} \left[G^{\circ}(T) \right] \tag{28}$$

The result in equation (27) is calculated for each species in a given chemical or electrochemical reaction and substituted into equation (28) to determine the Gibbs free energy of that particular reaction. It is this value that is used in the Nernst or Van't Hoff equations to determine $E - pH$ relationships which can be plotted on a Pourbaix diagram.

4.4 High Temperature Thermodynamic Properties for Aqueous Species

The thermodynamic properties of aqueous species are not as readily available in the literature as many solid or liquid materials. The Helgeson-Kirkham-Flowers (HKF) method for determining high temperature thermodynamic properties as a function of temperature was used when experimental correlations were unavailable. This method was first published by Helgeson and Kirkham [39] and has since been updated and revised as newer experimental data becomes available [40-42].

The basic equation given by Shock and Helgeson [41] for standard partial molal specific heat is,

$$\begin{aligned}
\overline{C}_P^{\circ}(T) &= c_1 + \frac{c_2}{(T-\theta)^2} - \left(\frac{2T}{(T-\theta)^3} \right)\left[a_3(P-P_r) + a_4 \ln\left(\frac{\psi+P}{\psi+P_r} \right) \right] + \omega TX \\
&+ 2TY\left(\frac{\partial \omega}{\partial T} \right)_P - T\left(\frac{1}{\varepsilon} - 1 \right)\left(\frac{\partial^2 \omega}{\partial T^2} \right)_P
\end{aligned} \tag{29}$$

where c_1, c_2, a_3, and a_4 are all species-specific constants which are independent of both temperature and pressure, T is temperature, and P is pressure. The variable ω is a temperature and pressure dependent Born coefficient. There are two global constants in this equation, $\Theta = 228\ K$ and $\psi = 2600\ bars$. This specific heat equation gives the value for standard state, taken as 1 molal solutions, and is valid for variable temperature and pressure. The variable X is the Born parameter and is a function of ε, the temperature dependent dielectric constant of water, data for which is taken from Shock et al. [43]. Similarly, Y is also a function only of the temperature dependency of water's dielectric constant.

$$X = \frac{1}{\varepsilon}\left[\left(\frac{\partial^2 \ln \varepsilon}{dT^2}\right)_P - \left(\frac{\partial \ln \varepsilon}{dT}\right)_P^2\right] \tag{30}$$

Using the previous assumption that the pressure dependency of aqueous species properties is negligible this equation can be simplified and the terms containing a_3 and a_4 can be neglected. Additionally, Shock and Helgeson report that ω can be taken as a constant for temperatures below 170°C and for pressures near the vapor-liquid saturation curve of water. This allows all partial derivative terms involving ω to be neglected. The result is,

$$\overline{C}_P^{\circ}(T) = c_1 + \frac{c_2}{(T-\theta)^2} + \omega TX \tag{31}$$

where X is given previously in equation (30) and the remaining constants for most species relevent to this work are tabulated in Shock et al. [43].

4.5 Pourbaix Diagram for the Aluminum/Water System

Corrosion of aluminum at high and low pH levels are both unwanted for heat pipe applications as they will both evolve hydrogen gas.

$$2Al_{(s)} + 6H_{(aq)}^+ \rightarrow Al_{(aq)}^{3+} + 3H_{2(g)} \tag{32}$$

$$2Al_{(s)} + 6H_2O_{(l)} + 2OH_{(aq)}^- \rightarrow 2Al(OH)_{4(aq)}^- + 3H_{2(g)} \tag{33}$$
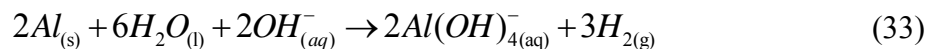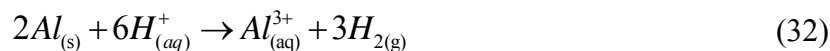
Equation (32) represents the equation for aluminum in acidic media while equation (33) represents an alkaline medium.

The first step in the creation of $E - pH$ diagrams is to identify the chemical and electrochemical equations which will be considered for the application. There may be a large number of reactions which can occur; however, the relevant equations will likely not include all of these. Considering all species possible is not only impractical but also unrealistic. A number of factors were considered when the species and chemical equations were selected. Aluminum is amphoteric meaning that its oxides prefer neutral pH conditions. Therefore, aluminum oxide will dissolve into solution at both high and low pH numbers and exist as ionic species (i.e. corrosion) alongside the release of hydrogen gas. At high pH aluminum oxide will dissolve into $Al(OH)_4^-$ and at low pH into Al^{3+}. The neutral pH range of $4 - 9$ can be considered a starting region within which aluminum oxides are most stable for a wide temperature range [38, 44]. Diagrams will therefore be constructed for the pH range just outside of this for pH from $2\ to\ 11$ and species which exist primarily outside or near the boundaries of this region will be neglected. Thermodynamic data for aluminum and water was reviewed from a number of sources [37, 43, 45-52] before selecting the data found in Table 5. A full review of all literature reviewed can be found in the Appendix in Table 20 for water and Table 21 for aluminum.

Table 5: Thermodynamic data used

	Compound	[kJ/mol]		[J/mol*K]	T = 298.15 K, P = 1 bar
		$\Delta_f H°$	$\Delta_f G°$	S°	Reference
Water	$H_2O_{(l)}$	-285.830	-237.141	69.950	CRC Handbook, 93rd Ed. (2012)
	$H_{2\,(g)}$	0.0	0.0	130.680	CRC Handbook, 93rd Ed. (2012)
	$O_{2\,(g)}$	0.0	0.0	205.148	CRC Handbook, 93rd Ed. (2012)
	$H^+_{(aq)}$	0.0	0.0	0.0	CRC Handbook, 93rd Ed. (2012)
	$OH^-_{(aq)}$	-230.0	-157.2	-10.8	CRC Handbook, 93rd Ed. (2012)
	e^-	0.0	-19.5	0.0	Revie (2011)
Aluminum	$Al_{(s)}$	0.0	0.0	28.3	CRC Handbook, 93rd Ed. (2012)
	$Al_2O_3\text{-}\alpha_{(s)}$	-1675.7	-1582.3	50.9	CRC Handbook, 93rd Ed. (2012)
	$Al^{3+}_{(aq)}$	-531.0	-485.0	-321.7	CRC Handbook, 93rd Ed. (2012)
	$AlO_2^-_{(aq)}$	-930.9	-830.9	-36.8	CRC Handbook, 93rd Ed. (2012)
	$Al(OH)_4^-_{(aq)}$	-1502.5	-1305.3	102.9	CRC Handbook, 93rd Ed. (2012)
Manganese	$Mn_{(s)}$	0.0	0.0	32.0	CRC Handbook, 93rd Ed. (2012)
	$MnO_{2\,(s)}$ (IV)	-520.0	-465.1	53.1	CRC Handbook, 93rd Ed. (2012)
	$Mn_2O_{3\,(s)}$ (III)	-959.0	-881.1	110.5	CRC Handbook, 93rd Ed. (2012)
	$Mn^{2+}_{(aq)}$	-220.8	228.1	-73.6	CRC Handbook, 93rd Ed. (2012)
	$MnO_4^-_{(aq)}$	-541.4	-447.2	191.2	CRC Handbook, 93rd Ed. (2012)
Chromium	$Cr_{(s)}$	0.0	0.0	23.7	Bard et al. (1985)
	$Cr_2O_{3\,(s)}$ (III)	-1139.7	-1058.1	81.7	Bard et al. (1985)
	$Cr^{2+}_{(aq)}$	-172.0	-174.0	-100.0	Bard et al. (1985)
	$Cr^{3+}_{(aq)}$	-251.0	-215.0	-293.0	Bard et al. (1985)
	$CrO_4^{2-}_{(aq)}$	-881.2	-727.8	50.2	Bard et al. (1985)
	$HCrO_4^-_{(aq)}$	-878.2	-764.8	184.1	Bard et al. (1985)
	$Cr(OH)^{2+}_{(aq)}$	-495.0	-430.0	-156.0	Bard et al. (1985)

The species and equations considered for aluminum were selected to be consistent with those used in Ghali [44]. The water reactions must also be considered to discover information

about the stability of water itself and if hydrogen gas or oxygen gas might be potentially released.

For the aluminum/water system, the following reactions are the ones selected for this study.

4.5.1 Aluminum Reactions Considered

$$Al^{3+}_{(aq)} + 3e^- \rightarrow Al_{(s)} \tag{34}$$

$$Al_2O_{3(s)} + 6H^+_{(aq)} + 6e^- \rightarrow 2Al_{(s)} + 3H_2O_{(l)} \tag{35}$$

$$Al(OH)^-_{4(aq)} + 4H^+_{(aq)} + 3e^- \rightarrow Al_{(s)} + 4H_2O_{(l)} \tag{36}$$

$$Al_2O_{3(s)} + 6H^+_{(aq)} \rightarrow 2Al^{3+}_{(aq)} + 3H_2O_{(l)} \tag{37}$$

$$2Al(OH)^-_{4(aq)} + 2H^+_{(aq)} \rightarrow Al_2O_{3(s)} + 5H_2O_{(l)} \tag{38}$$
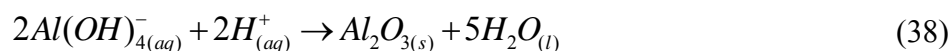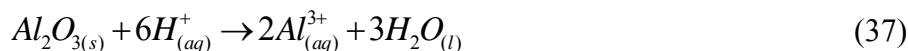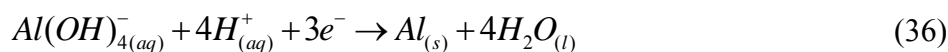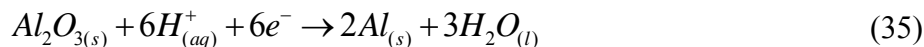
4.5.2 Water Reactions Considered

$$\frac{1}{2}O_{2(g)} + 2H^+_{(aq)} + 2e^- \rightarrow H_2O_{(l)} \tag{39}$$

$$2H^+_{(aq)} + 2e^- \rightarrow H_{2(g)} \tag{40}$$

4.5.3 Aluminum/Water Pourbaix Diagrams at $T = 25°C$

Figure 12 shows the results of a Matlab code (see Appendices) which computes the Gibbs free energy as a function of temperature for each species and then the results of each of the above reactions, see equations (34) through (40) resulting in a Pourbaix diagram for aluminum.
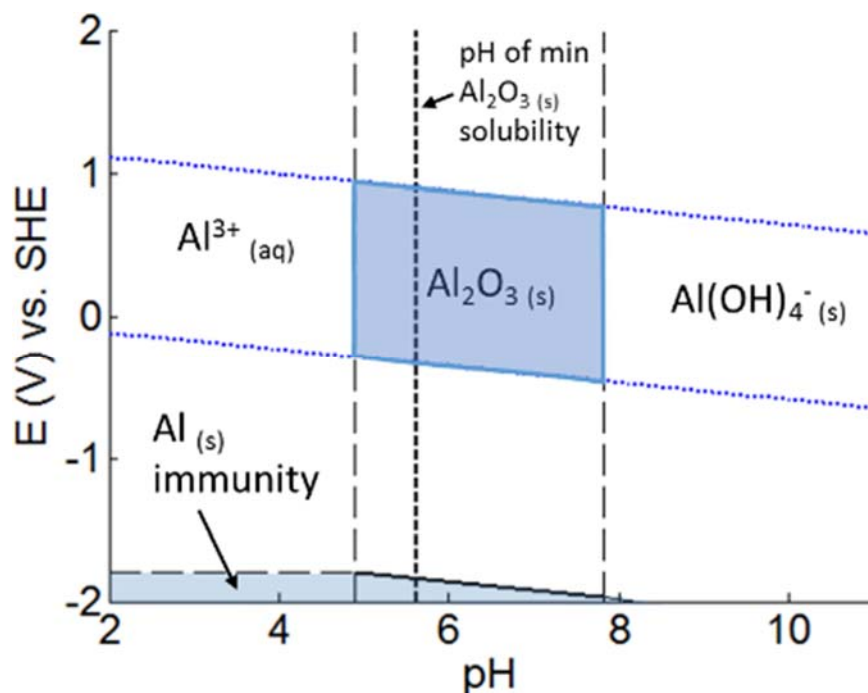
Figure 12: $E - pH$ **diagram for** $Al - H_2O$ **at 25°C,** $C_{tot}[Al] = 10^{-6} \; mol/L$

The plot, Figure 12, was made at a standard temperature of $25°C$ to show as a reference. Temperature effects will be explored in a later section.

      The initial pH of a designed fluid can be selected and then measured experimentally. An important consideration to remember is that the geometry of a heat pipe or thermo-syphon is itself representative of the amount of casing material available for reaction. Therefore, the same fluid with same initial E and pH might have different measurements after testing since there are different amounts of available aluminum (potentially the limiting reagent) in each situation. Both before and after points can be plotted on a diagram to visually see the effect of using a solution with a given amount of inhibitors in different devices with different surface areas. However, post-test measurements are the only essential points to plot. Additional tests and data should be gathered about the expected protectiveness of the oxides created such as simple compatibility experiments using thermo-syphons and a number of temperature measurements throughout the condenser.

4.6 Pourbaix Diagrams for Oxidizing Inhibitors

Pourbaix diagrams for the oxidizers being considered, chromates and permanganate, were constructed in the same manner as was done for aluminum for both the manganese and chromium metal-water systems. In addition to basing their selection on the prior work of Yao [35], these inhibitors were also selected based on those used in past literature discussed in the review [18, 20, 27, 33, 36, 53]. Chromium is well known for its protective oxides for aluminum and mild steels. Thermodynamic data used for chromium and related compounds can be found in Table 5 and was selected from a wide review of multiple sources [43, 45, 47, 54-59] summarized in Table 23, found in the appendix. Final data selected for manganese can also be found in Table 5 and review of existing data [37, 43, 45, 60-65] can be found in the appendix in Table 22.

Chemical and electrochemical equations selected for the manganase metal system are shown in the following equations,

$$Mn^{2+}_{(aq)} + 2e^- \rightarrow Mn_{(s)} \tag{41}$$

$$MnO_{2(s)} + 4H^+_{(aq)} + 2e^- \rightarrow Mn^{2+}_{(aq)} + H_2O_{(l)} \tag{42}$$

$$Mn_2O_{3(s)} + 6H^+_{(aq)} + e^- \rightarrow 2Mn^{2+}_{(aq)} + 3H_2O_{(l)} \tag{43}$$

$$MnO^-_{4\,(aq)} + 4H^+_{(aq)} + 3e^- \rightarrow MnO_{2(s)} + 2H_2O_{(l)} \tag{44}$$

$$2MnO_{2(s)} + H_2O_{(l)} + 2e^- \rightarrow Mn_2O_{3(s)} + 2OH^-_{(aq)} \tag{45}$$
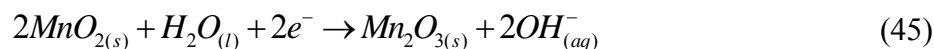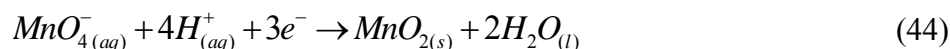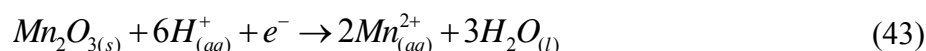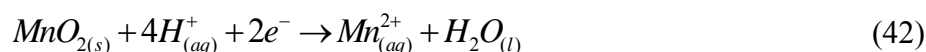
while the chemical and electrochemical equations considered for the chromium metal system are,

$$Cr^{3+}_{(aq)} + e^- \rightarrow Cr^{2+}_{(aq)} \tag{46}$$

$$HCrO_{4(aq)}^- + 7H_{(aq)}^+ + 3e^- \rightarrow Cr_{(aq)}^{3+} + 4H_2O_{(l)} \tag{47}$$

$$Cr_{(aq)}^{2+} + 2e^- \rightarrow Cr_{(s)} \tag{48}$$

$$2CrO_{4(aq)}^{2-} + 10H_{(aq)}^+ + 6e^- \rightarrow Cr_2O_{3(s)}^{3+} + 5H_2O_{(l)} \tag{49}$$

$$Cr_2O_{3(s)} + 6H_{(aq)}^+ + 6e^- \rightarrow 2Cr_{(s)} + 3H_2O_{(l)} \tag{50}$$

$$Cr_2O_{3(s)} + 6H_{(aq)}^+ + 2e^- \rightarrow 2Cr_{(aq)}^{2+} + 3H_2O_{(l)} \tag{51}$$

$$HCrO_{4(aq)}^- + 6H_{(aq)}^+ + 3e^- \rightarrow Cr(OH)_{(aq)}^{2+} + 3H_2O_{(l)} \tag{52}$$

$$Cr_2O_{3(s)} + 4H_{(aq)}^+ \rightarrow 2Cr(OH)_{(aq)}^{2+} + H_2O_{(l)} \tag{53}$$

$$HCrO_{4(aq)}^- \rightarrow CrO_{4(aq)}^{2-} + H_{(aq)}^+ \tag{54}$$

$$Cr(OH)_{(aq)}^{2+} + H_{(aq)}^+ + e^- \rightarrow Cr_{(aq)}^{2+} + H_2O_{(l)} \tag{55}$$

$$Cr_{(aq)}^{3+} + H_2O_{(l)} \rightarrow Cr(OH)_{(aq)}^{2+} + H_{(aq)}^+ \tag{56}$$

$$2HCrO_{4(aq)}^- + 8H_{(aq)}^+ + 6e^- \rightarrow Cr_2O_{3(s)} + 5H_2O_{(l)} \tag{57}$$
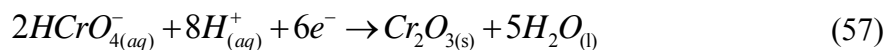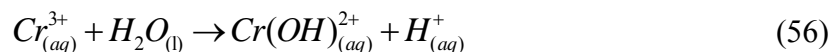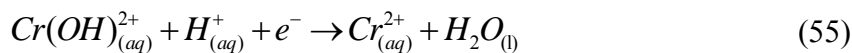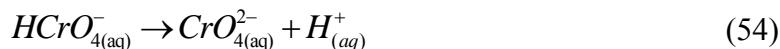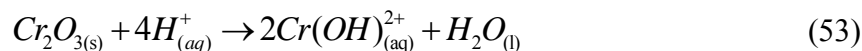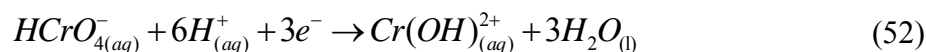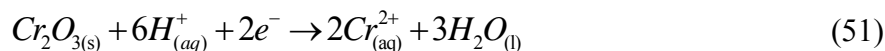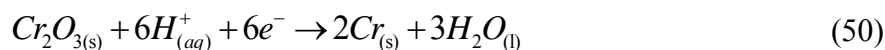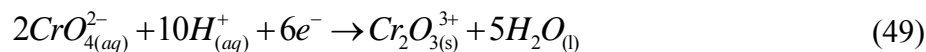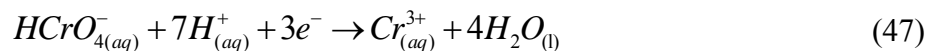
Oxidizer Pourbaix Diagrams at $T = 25°C$

Figure 13 and Figure 15 represent Pourbaix diagrams generated using the Matlab code developed using the aforementioned method and electrochemical equations for manganese-water and chromium-water systems, respectively. Example diagrams from existing software available from FACTsage [66] for both chromium and manganese systems, respectively, are shown in Figure 14 and Figure 16 for soluble species concentrations of $10^{-6}\ mol/L$ at 25°C. It can be seen that the figures generated from this MATLAB code match well with existing data at standard

Approved for public release: distribution is unlimited.

conditions and temperature. The manganese diagram made with the MATLAB code is slightly different in that it neglects the existence of Mn_3O_4 and $MnOH^+$ since they exist largely above pH levels considered in the inhibitor solutions considered for aluminum. For the purposes of comparison to existing diagrams for accuracy, this will be adopted for this section and the need for changing it for a more specific heat pipe environment will be discussed later. In general, more dilute concentrations used will expand the window size of soluble species stability. Below this limit of metal ion concentration there is considered to be no corrosion.
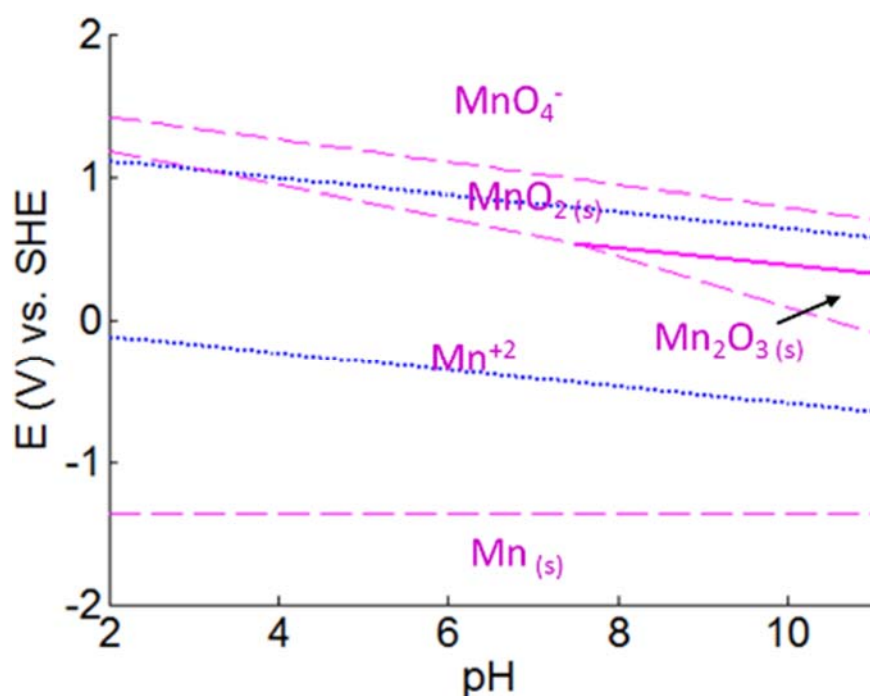
Figure 13: $E - pH$ diagram for $Mn - H_2O$ at 25°C, $C_{tot}[Mn] = 10^{-6} \ mol/L$
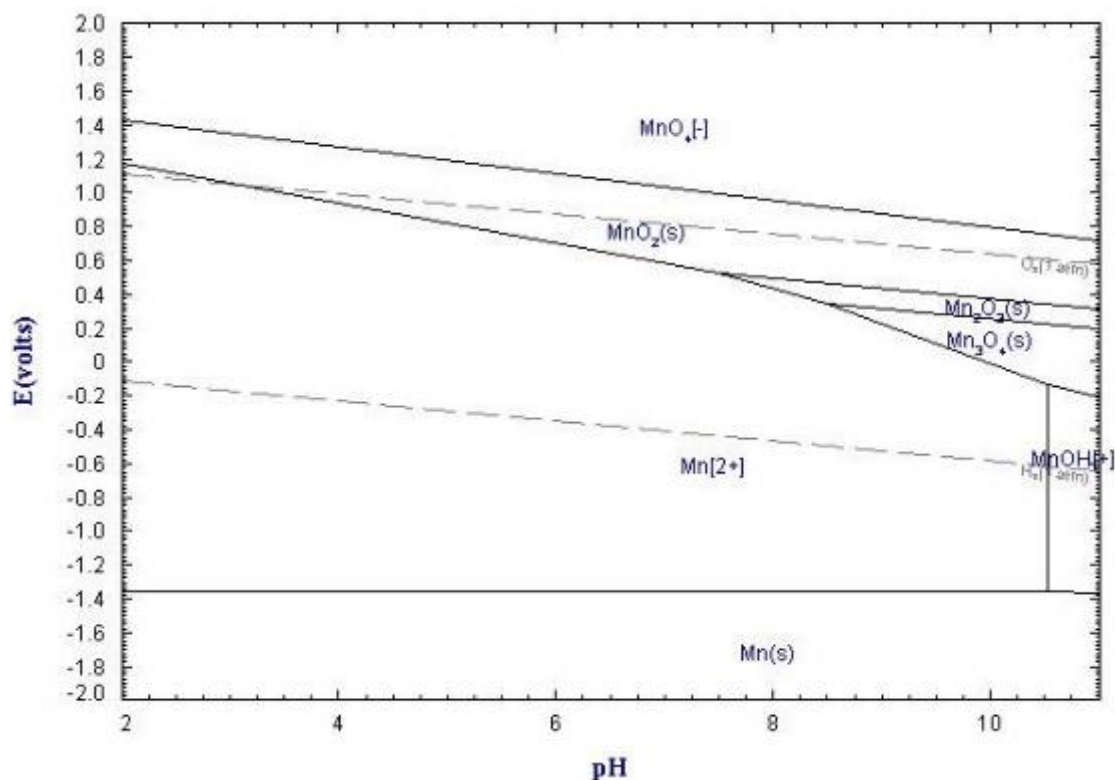
Figure 14: FACT Sage $E - pH$ diagram for $Mn - H_2O$ at 25°C, $C_{tot}[Mn] = 10^{-6} \, mol/L$
[66]
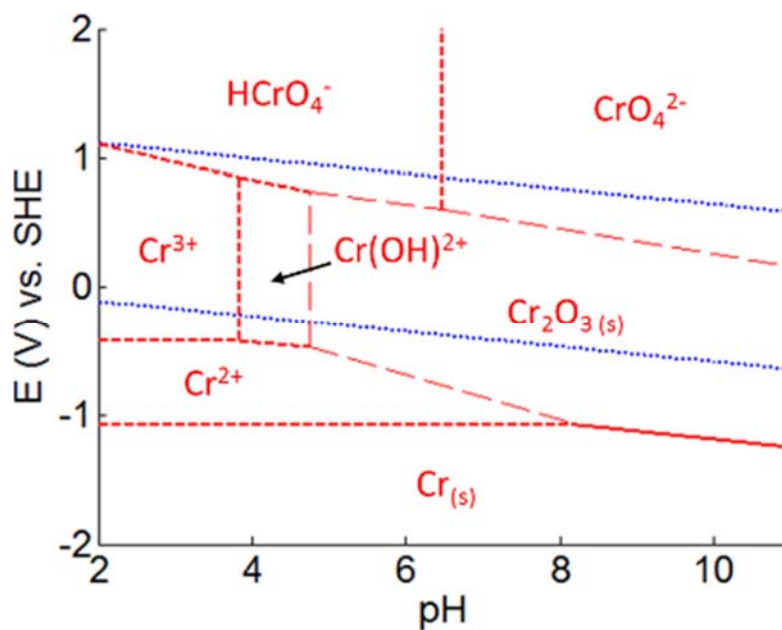
Figure 15: $E - pH$ diagram for $Cr - H_2O$ at 25°C, $C_{tot}[Cr] = 10^{-6} \, mol/L$
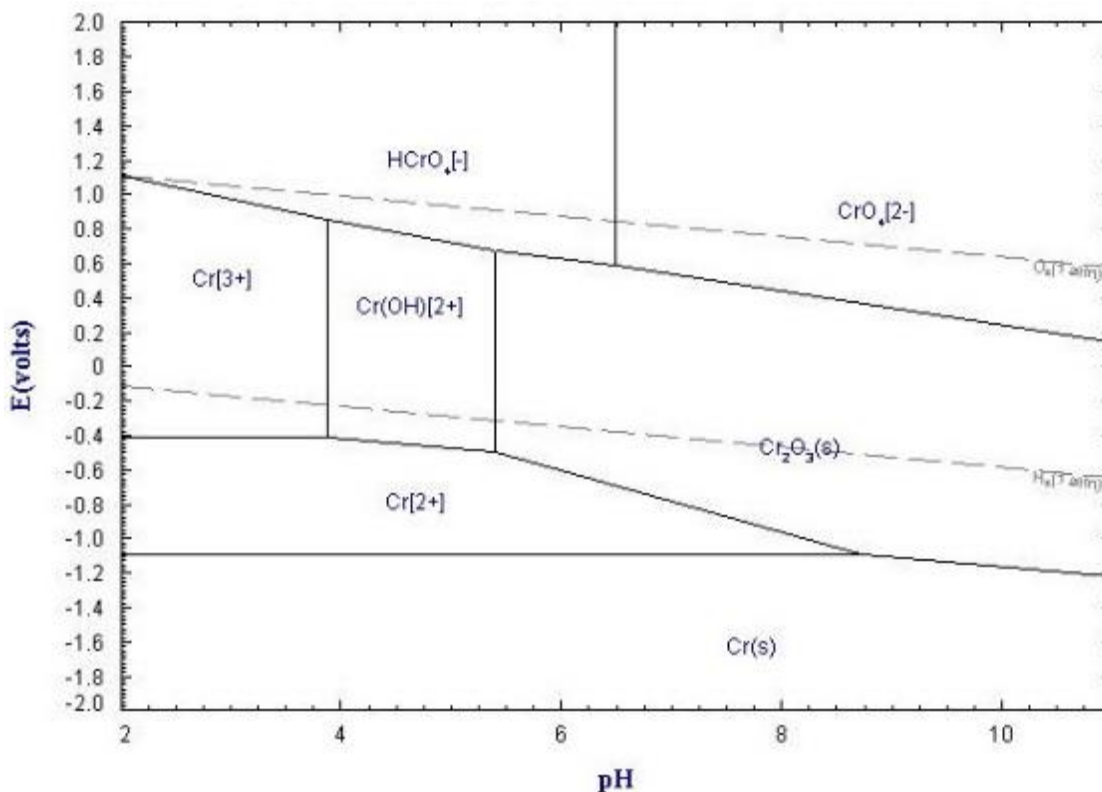
Figure 16: FACT Sage $E - pH$ diagram for $Cr - H_2O$ at $25°C$, $C_{tot}[Cr] = 10^{-6} \, mol/L$
[66]

There are some generalizations to be dissected from these diagrams. For example, all three metal-water solutions analyzed show that the solid metal "immunity" region is below the hydrogen stability diagonal line. Assuming there is no protective oxide layer, this indicates that these are active metals that will corrode and generate hydrogen gas as a product. Another comparison shows that permanganate is a much stronger oxidizer than chromate due to its larger, higher position on the Pourbaix diagram. Finally, there is a wide region in neutral pH and E range where chromium oxide and aluminum oxide, both known protective layers, overlap within the water stability region. This is the area targeted for passivating the aluminum heat pipes. Manganese, on the other hand, does not have a large oxide stability region here. However, it is important to remember that these

Approved for public release: distribution is unlimited.

assessments are made from diagrams where the inhibitor amounts are set at the standard 10^{-6} molar at 25°C.

4.7 Water Equilibrium Changes for Heat Pipe Analysis

As mentioned previously the standard $P = 1\ atm$ assumption used for both $O_{2\ (g)}$ and $H_{2\ (g)}$ when drawing the water equilibrium lines is not a good representation of the conditions within a heat pipe or thermo-syphon device which has been thoroughly degassed. Therefore, a simple calculation was performed to determine what more accurate values should be used. These values were determined by starting with the assumption that the device is thoroughly degassed. At room temperature the partial pressures within are only the vapor pressure and air pressure, which is represented by the vacuum ability of the pump used. The Agilent DS302 pump used is capable of pumping to a pressure of $2\ \mu bar$. At 25°C, the vapor pressure is approximately $0.0317\ bar$. In a system open to atmospheric pressure, which the $P = 1\ atm$ convention is based on, the system pressure will remain at $1\ atm$ and vapor pressure changes due to temperature will be largely negligible until high temperatures are reached. However, in a closed system like a heat pipe the system pressure is assumed to largely track the vapor pressure, which is as a function of temperature, added to the pump's very small vacuum pressure limit. Therefore, rather than using $P = 1\ atm$ for the water equilibrium lines, the following equation will be used,

$$
\begin{aligned}
P &= P_{pump} + P_v\left(T\right) \\
P_{pump} &= 0.002 mbar
\end{aligned}
\tag{58}
$$

From here on, this is the method used to draw the water equilibrium lines in all diagrams.

4.8 Pourbaix Diagram Temperature Effects

The temperature dependency of the diagrams allows for the selection of inhibitors and pH which remain within the desired stable regions throughout the anticipated temperature range the device will see in its lifetime. Two temperatures, 25°C and 100°C, were chosen and plotted on the same figure to demonstrate the trends associated with changing system temperature for Pourbaix diagrams. Figure 17 below shows a Pourbaix diagram for an aluminum-water system.
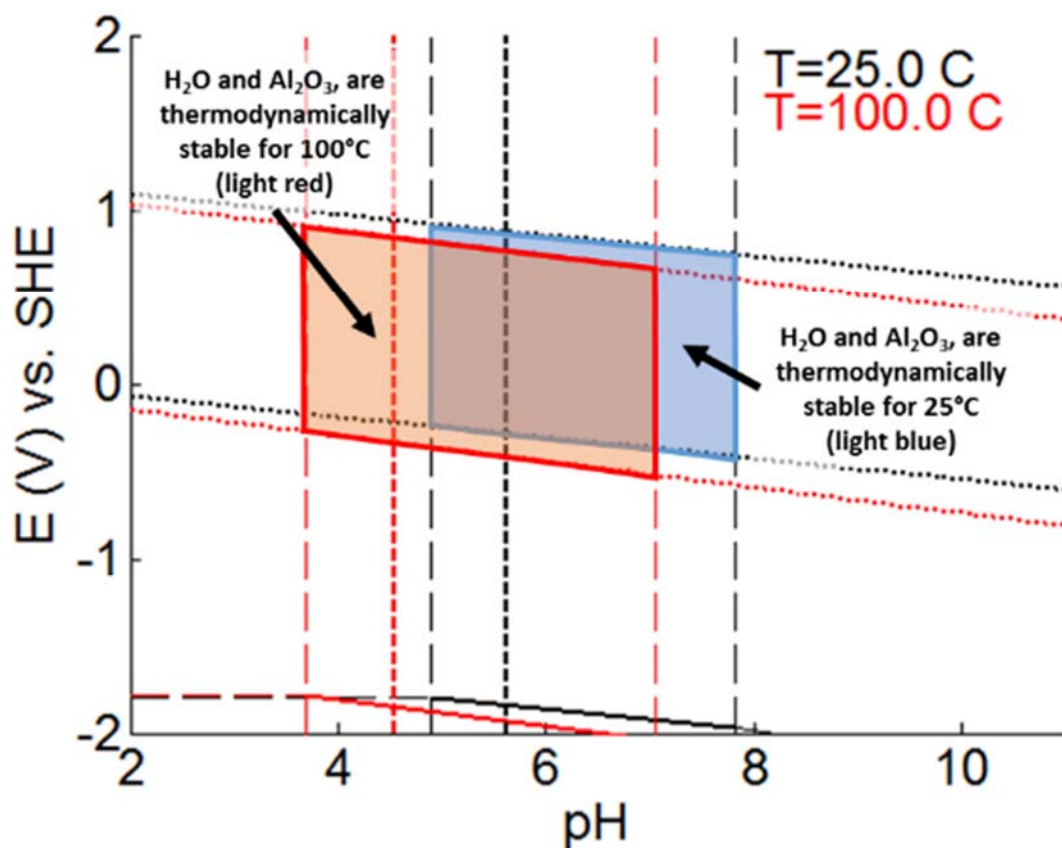
Figure 17: $E - p\,H$ diagram for $Al - H_2O$ at 25°C and 100°C $C_{tot}[Al] = 10^{-6}\,mol/L$

The shaded blue zone is where aluminum oxide and water are both stable at 25°C and the red zone is where they are stable at 100°C. With increasing temperature the safe zone shifts down and to the left on the Pourbaix diagrams with increasing temperature. This corresponds to a less

Approved for public release: distribution is unlimited.

strongly oxidizing solution and more acidic conditions. However, it is not yet known how the solution E and pH will change with temperature. If they move in the same direction and with the same rate as the safe window then there will not be an additional temperature limit associated with maintaining the aluminum oxide stablility window. There will be a limit if the window moves faster than the solution E and pH or if the solution moves in the opposite direction.

4.9   Conclusions

A method for evaluating heat pipe casing and fluid compatibility has been introduced which can be used to help screen for appropriate inhibitors in aqueous solution and determine what fluid E and pH are desired to maintain a protective oxide coating to resist NCG. Using aluminum heat pipes with Mn and Cr based inhibitors as a case study, chemical equations were selected and used to generate $E - pH$ equilibrium diagrams showing the most thermodynamically stable forms of the constituents for a range of conditions. This was done for aluminum, water, manganese, and chromium for any temperature. It may be the case that a temperature limit exists depending upon the behavior of the system E and pH measurements. This will be determined through experiment in a later chapter.

The utility of other oxidizing agents could be investigated in the future by generating similar thermodynamic data and diagrams for those metal-water systems. Therefore, the approach used is not limited in application to aluminum casings; other materials such as steels can be investigated as well by replacing the base metal aluminum with the desired material.

5 Fluid Design

The typical reaction occurring between pure water and an aluminum surface is

$$2Al_{(s)} + 3H_2O_{(l)} \rightarrow Al_2O_{3(s)} \downarrow + 3H_{2(g)} \uparrow \qquad (59)$$
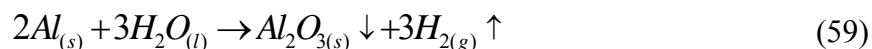
This equation represents the worst case scenario since it generates hydrogen, an NCG. It will be demonstrated that this reaction can be replaced by one which is more preferable and does not yield a hydrogen product with the introduction of strong oxidizers into solution and careful buffering of the fluid pH. The above reaction (59) is not only dwarfed by the preferable reaction with inhibiting strong oxidizers, but the inhibitors also help maintain the system conditions within a favorable range of E and pH for a protective aluminum oxide barrier coating. The oxidizers considered will be limited to permanganate and chromium-based oxidizers. The relative strengths of these oxidizers compared to a reference hydrogen half-cell and common metal half-cells can be found below in Figure 18.

Figure 18: Half-cell reaction chart demonstrating relative oxidizer strengths

Chromium-based oxidizers include chromate (CrO_4^{2-}), dichromate ($Cr_2O_7^{2-}$), and hydrogen chromate ($HCrO_4^-$). All three have similar oxidizing potential and are often referred to collectively as "chromates" since they exist in a complicated equilibrium with one another. This naming convention will be adopted here as well. Figure 18 also demonstrates that the potassium (K^+) and sodium (Na^+) ions are stable, spectator ions that will not be reduced or oxidized by the metals or oxidizers being used in solution. These ions are present because ions themselves are not added to water to form solutions; actual solid chemicals containing these must be used. Chromates are added to solution using potassium dichromate ($K_2Cr_2O_7$) and permanganates are added using potassium permanganate ($KMnO_4$). Sodium ions come from the use of sodium hydroxide ($NaOH$) to adjust pH level.

5.1 Effect of Fluid pH on Oxidization Ability

IAS fluids have a number of ions in solution each with its own solubility and equilibrium constant. Fluid pH has a strong effect on both variables. Each species' half-reaction is affected by solution pH. In other words, the initial pH of the solution will affect both the relative concentrations of different ions in solution (particularly the oxidizing cations) as well as the rates of reactions once the fluid is charged inside an aluminum device. Clearly, this could have an impact on the oxidizing potential of permanganate and chromate in IAS and the effect of initial pH must be investigated before optimizing the concentrations of each of these constituents. The Pourbaix diagrams from the previous section in Figure 13 and Figure 15 show that both permanganate and chromium-based oxidizers increase in oxidizing power as the pH decreases. The relationship between the initial chromium concentration, pH, and the resulting chromate (CrO_4^{2-})/dichromate ($Cr_2O_7^{2-}$)/hydrogen chromate ($HCrO_4^-$) ion concentrations can be seen below in Figure 19 [67].
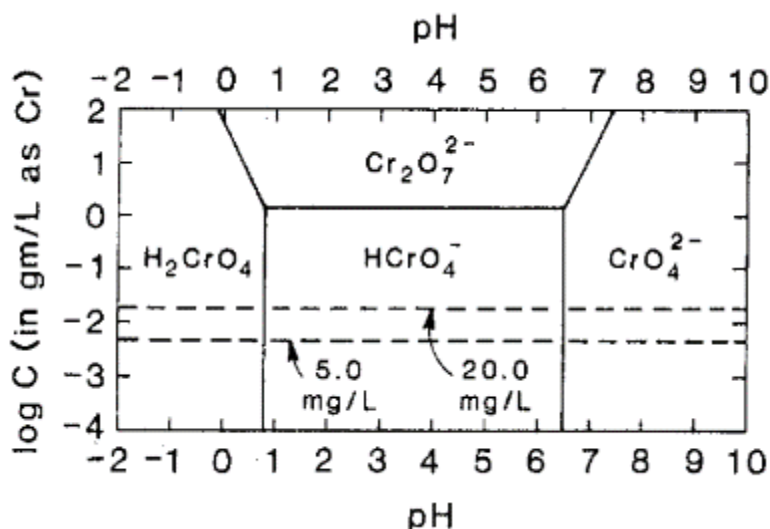
Figure 19: Predominance diagram for different $Cr(VI)$ species in aqueous solution [67]

The different chromium species that can arise each have different but similar oxidizing abilities and therefore different pH levels have the potential to affect the passivation of a device.

However, the problem is simplified by noticing that (referring back to the Pourbaix diagram of Figure 12) $Al_2O_3{}_{(s)}$ is only stable between a pH of 4 and 9 [68].
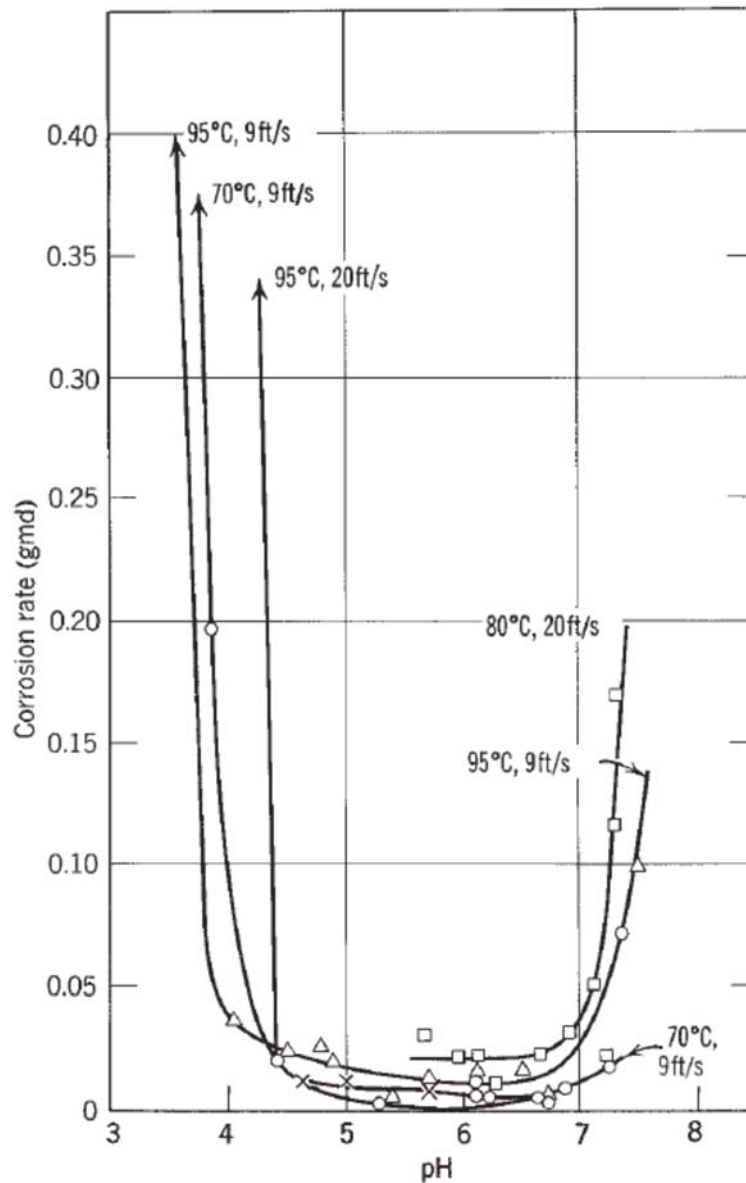
Figure 20: *pH* effect on corrosion rates for aluminum alloy 1100 [69]

Further simplifying the problem, one can reduce the pH range to $5 - 7$ by neglecting pH ranges which increase general aluminum corrosion rates as indicated by the data in Figure 20. This estimate is confirmed by Kendig and Buchheit [28] who recommend near-neutral pH levels for

similar passivation schemes. For a temperature range of 25°C to 150°C, Figure 12 shows a similar range of pH from $5 - 7$ where aluminum oxide passivation coating is expected to be stable.

5.2 Effect of Permanganate Concentration

The reaction between the permanganate oxidizers in IAS and aluminum generates a compact coating which protects and insulates the aluminum surface from further unwanted reactions such as those which produce hydrogen. The aluminum oxide generating reaction, which takes place at the aluminum surface, is demonstrated by

$$2Al_{(s)} + 2MnO_{4(aq)}^{-} + 2H^{+}_{(aq)} \rightarrow Al_2O_{3(s)} \downarrow + 2MnO_{2(s)} \downarrow + H_2O_{(l)} \qquad (60)$$
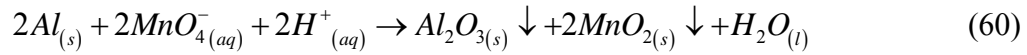
Note that hydrogen ions are consumed and not released as a gaseous hydrogen product as they are with pure water reactions with aluminum. The half reactions contributing to the above full reaction in equation (60) for the oxidization of aluminum by water is,

$$2Al_{(s)} + 3H_2O_{(l)} - 6e^{-} \rightarrow Al_2O_{3(s)} \downarrow + 6H^{+}_{(aq)} \qquad (61)$$
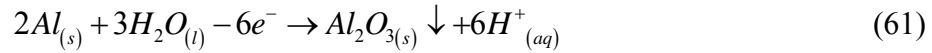
and the half reaction for the reduction of permanganate oxidizers in the evaporator is,

$$MnO_{4(aq)}^{-} + 4H^{+}_{(aq)} + 3e^{-} \rightarrow MnO_{2(s)} \downarrow + 2H_2O_{(l)} \qquad (62)$$
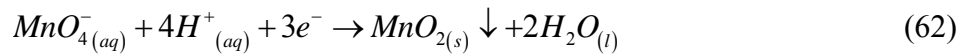
Permanganate is a stronger oxidizer than chromate and reacts more quickly as well. This means that permanganate is expected to contribute primarily to initial passivation of the device when it is first started. Post-test fluids from the experiments performed by Stubblebine and Catton [33], Stubblebine et al. [27], and others were found to be bright yellow in color and lack any purple or red pigmentation. This indicates a lack of permanganate ions in solution since their presence in even miniscule concentrations will result in a marked color change of the solution and lends strong

support to the idea that permanganate reacts quickly and completely within the heat pipe or thermo-syphon device.

Aluminum oxide is a basic oxide, which means that it will dissolve back into solution in an acidic solution. A more basic solution, to an extent, facilitates better coating stability by promoting conditions in which the oxide protection layer will remain precipitated and not dissolve back into solution. The permanganate reaction with the aluminum casing not only helps produce the passivating aluminum oxide coating but also results in a more basic solution by consuming hydrogen ions.

There are problems, as alluded to previously, with maintaining concentrations of permanganate which are orders of magnitude larger than necessary. Adding more permanganate into the solution can produce a thicker coating. Manganese oxide has a thermal conductivity of compared to that of a thermo-syphon or heat pipe casing (which in this case is aluminum), so the generation of a thicker coating also means having a larger thermal resistance throughout the tube. This resistance would work against heat transfer into the evaporator section.

Excess permanganate also has the potential to slowly disassociate into manganese oxide and oxygen gas, characterized by the following chemical reaction,

$$MnO_{4\,(aq)}^{-} + 4H_{(aq)}^{+} \rightarrow 4MnO_{2(s)} \downarrow + 3O_{2(g)} \uparrow + 2H_2O_{(l)} \tag{63}$$
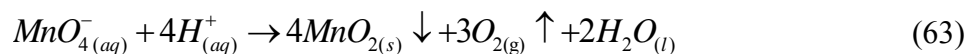
The above reaction (63) is catalyzed by higher temperatures and the existing presence of manganese oxide, creating the potential for a runaway effect and release of oxygen which is also a NCG like hydrogen. As long as ther eis aluminum to react with the permanganate the chemical reaction (60) will occur instead and oxygen gas will not be released. Additionally, depending on

the wick type and geometry used, additional coating thickness could potentially clog the wick, thus reducing capillarity of the heat pipe and limiting the ability to pump liquid back to the evaporator.

Determining the necessity of permanganate in the NCG inhibition process and correct required concentration will be important so that excess is not charged into a thermo-syphon or heat pipe. This may prove difficult since there is likely to be micro-level surface variability in oxide coatings and thus the required initial passivation of each device even if they are manufactured identically on a macro scale.

5.3 Effect of Chromium Concentration

Chromates also work as a strong oxidizer in IAS solutions. Chromates are slower reacting and slightly less powerful oxidizers than permanganate and therefore may not be as useful in initial passivation. However, they offer a number of other benefits. Chromates produce an insoluble oxide passivating layer within similar E and pH boundaries to aluminum. They also do not disassociate into oxygen gas on their own and can remain in solution as strong backup oxidizers. Finally, chromates are a powerful pH and E buffering compound which acts to maintain the solution pH and E within the passivation range even after the reaction of some chromate ions to repair oxide defects. The reaction taking place between the chromates in IAS and the aluminum surface, resulting in the formation of the oxide coatings, are shown by

$$2Al_{(s)} + 2CrO_4^{2-}{}_{(aq)} + 4H^+{}_{(aq)} \rightarrow Al_2O_{3(s)} \downarrow + Cr_2O_{3(s)} \downarrow + 2H_2O_{(l)} \tag{64}$$
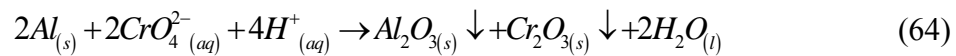
The Cr^{6+} (in the form of chromate, CrO_4^{2-}) used in solution has a role similar to that of permanganate. The chromate reaction with the aluminum casing will also result in a more basic

solution by consuming hydrogen ions. The half reaction for the oxidation of aluminum in the evaporator is

$$2Al_{(s)} + 3H_2O_{(l)} - 6e^- \rightarrow Al_2O_{3(s)} \downarrow + 6H^+_{(aq)} \tag{65}$$
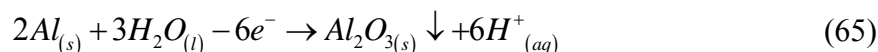
and the reduction of chromate oxidizers in the evaporator is

$$2CrO_4^{2-}{}_{(aq)} + 10H^+{}_{(aq)} + 6e^- \rightarrow Cr_2O_{3(s)} \downarrow + 5H_2O_{(l)} \tag{66}$$
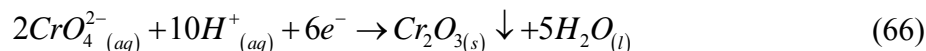
Theoretically, permanganate and chromate, which are strong oxidizers, react with most metals resulting in production of $Mn(IV)$ and $Cr(III)$ compounds. However, some parts of the reactions are only theoretically possible. Practically, some of these reactions take place too slowly to be accounted for. For example, based on the measured pH number of the yellow fluid (effluent) collected from several heat transfer experiments, it was concluded that permanganate was reduced to $Mn(IV)$ oxide [35], while chromate played a varied role as oxidizer reflecting its backup nature. It will need to be determined through experiment if chromates can act as both the primary initial oxidizer and backup oxidizer and allow for the elimination of permanganates in solution altogether or vice versa. The first tests will determine the behavior of aluminum samples when in direct contact with oxidizer solutions with near neutral pH.

6 Corrosion Tests

Given the promising but incomplete results of the early passivation tests using a thermo-syphon [27], flat heat pipe [33], and Yao's report [35], corrosion tests were designed to investigate aluminum passivation representing a simpler case where the metal is fully submersed in the inhibiting solution. The goal was to two-fold: 1) determine if chromium only is enough to passivate aluminum fully submersed in solution, 2) will the use of excess permanganate result in NCG due to oxygen gas release? These tests used square aluminum coupons with the same exposed surface area submersed in three different fluids and run at 100℃ for 24 hours. Sample mass and system pressure at a fixed baseline temperature were recorded to determine mass gained through corrosion and the amount of NCG generated.

6.1 Test Setup

A corrosion test chamber was built in order to study aluminum sample corrosion in inhibitor solutions at elevated temperatures in a vacuumed system. This chamber was built using a $500\ mL$ volume cylindrical shaped reaction vessel from Chemglass with a flat flange on top with an o-ring groove formed on the sealing surface. The OD of the cylindrical chamber was $105\ mm$ and the reaction vessel was $135\ mm$ tall. The flange opening was $100\ mm$ in diameter. It was sealed using a quick-release, Teflon-coated, screw down clamp to fix a 5.5″ diameter, 3/8″ thick heat-resistant borosilicate glass piece to the top opening. A chemical resistant o-ring coated in vacuum grease was sandwiched in between the two glass pieces within a groove to create a vacuum resistant seal. The aluminum coupons used for testing were alloy 6061-T6 and cut to be

Approved for public release: distribution is unlimited.

$50\ mm\ x\ 50\ mm$ square samples, each $0.040''$ ($1.016\ mm$) thick. Dimensions for the reaction

vessel, lid, and aluminum coupon can be found below in Figure 21.
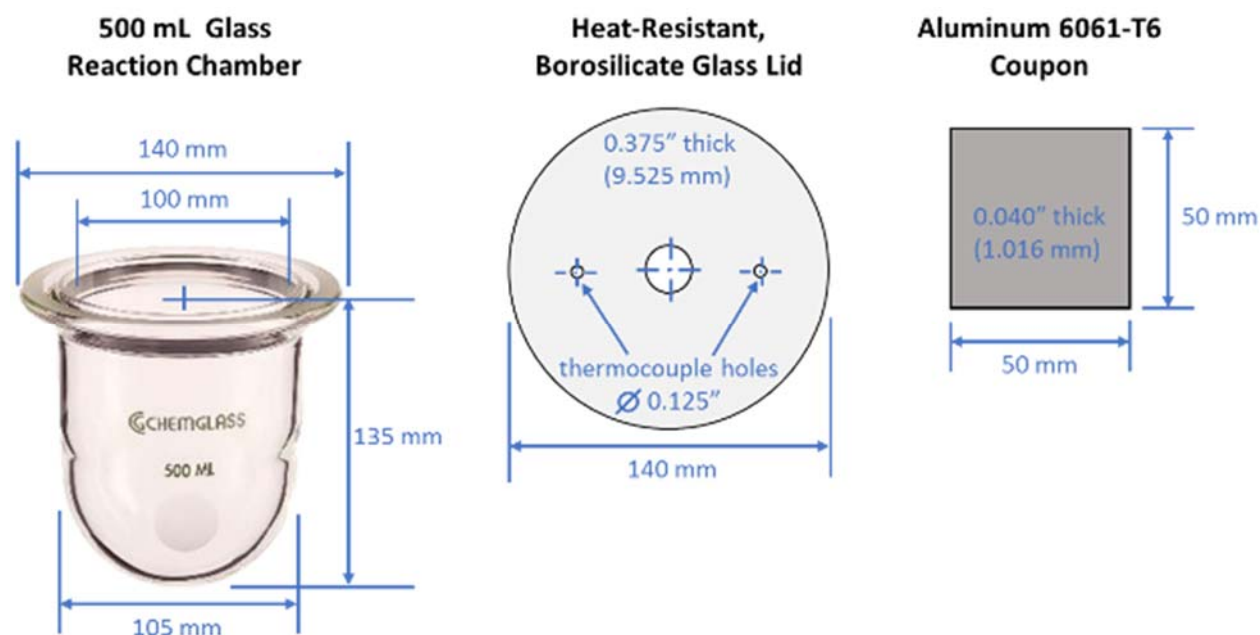
Figure 21: Dimensions for corrosion test reaction vessel, lid with instrumentation through-holes, and aluminum test sample

Three holes were carefully drilled into the glass lid using special drill bits made for glass

and ceramic materials to allow for insertion of instrumentation. A schematic of the through-hole

placement, which was not needed to be exact and is shown roughly to scale, can also be found in

Figure 21. The center hole was made to connect vacuum line made of 316L stainless steel leading

to a pressure transducer and finally a Swagelok needle valve and $1/8''$ OD outer tube diameter

connector to hook up to a Agilent DS302 vacuum pump. The pressure transducer used was an

Omega PX409-005AUSBH high accuracy pressure transducer capable of $0-5\ psi$ absolute

range. It connected to a laptop via universal serial bus (USB) for data logging. All fittings were

covered in marine-grade, high temperature JB weld epoxy to ensure a leak tight seal. The mating

point of the stainless steel line to the glass lid was also covered in multiple layers of the same

epoxy on both sides over the course of several days to ensure a good vacuum seal. Both pieces were also roughened in the area epoxy was applied to promote further cohesion. The two smaller, 1/8″ diameter holes were drilled to allow for insertion of Omega K-type S.L.E. (special limits of error) thermocouple probes. One was inserted straight down to measure liquid temperature and the other was coiled to measure the vapor temperature inside the reaction vessel. These probes were also carefully sealed using JB weld in the same manner as the vacuum line. A picture showing an assembled corrosion chamber during test (left) and fully assembled without insulation (right) can be seen in Figure 22.
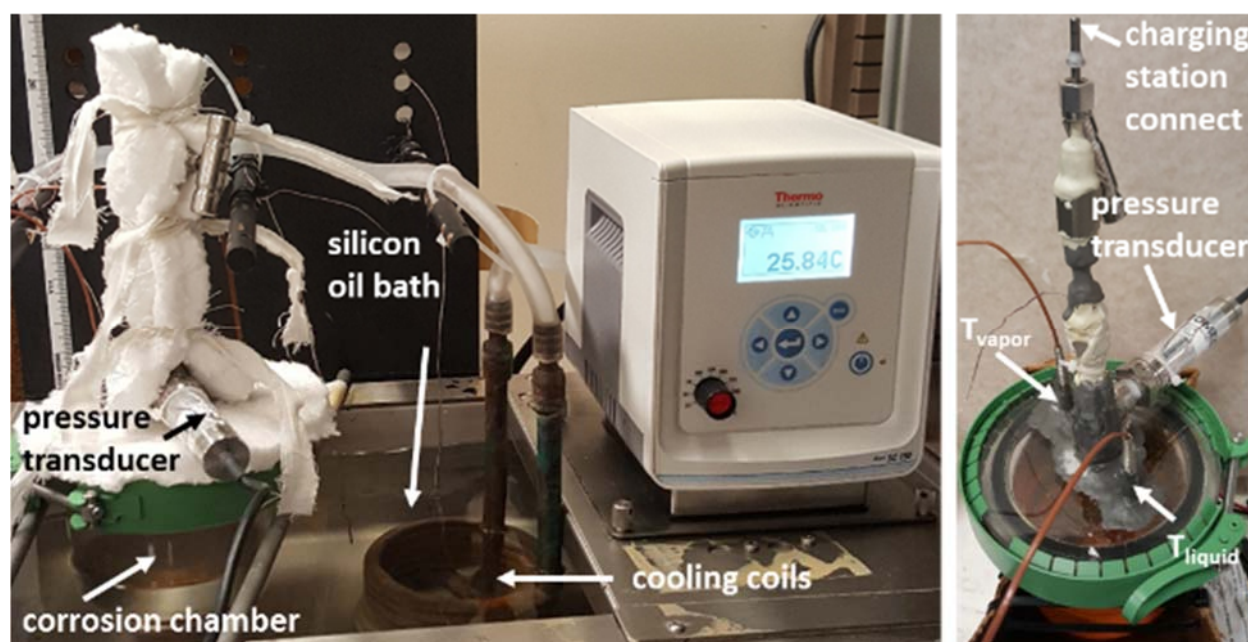
Figure 22: Corrosion test chamber and constant temperature bath experimental setup

In Figure 22, the constant temperature bath setup (left) can also be seen. To maintain a constant temperature a Thermo-Scientific SC150-S21 heated bath with temperature controller was used. The bath was filled with Sil 180 silicon oil fluid and is capable of maintaining temperature stability within $\pm0.02°C$. However, this bath does not have a cooling component and so in order to quickly lower the temperature to room temperature from the high set point used during the test

Approved for public release: distribution is unlimited.

a cooling coil was used. The cooling coil was made of copper pipe and inserted into the silicon bath. Water lines ran to a bucket of ice water and was circulated by an external pump.

6.2 Test Procedure

Corrosion tests were conducted by first cleaning out the glass reaction vessel and drying it. Next, $200\ mL$ of the fluid being tested were poured into the vessel. A plastic-coated magnetic stirring rod was also placed into the fluid at the bottom of the vessel. An aluminum 6061-T6 sample was then weighed and placed in the fluid. The o-ring was recoated in vacuum grease and placed into its groove on top of the flange before the lid was set on it and the clamp carefully tightened. The entire assembly was then placed on a magnetic stirring plate turned to high and connected to the charging station. The vacuum pump was turned on for about $90\ mins$ to make sure the vessel and fluid were sufficiently degassed. The stirring rod circulated the fluid and made sure air bubbles did not adhere to the aluminum sample. This promoted fluid degassing and greatly speeds the process.

Once the fluid and chamber were degassed and vacuumed, the needle valve was tightened and the assembly was disconnected. Thick fiberglass insulation was wrapped around the exposed portions of the assembly to maintain an isothermal test and help prevent condensation in the upper parts of the apparatus. The thermocouples were next attached to a (personal data acquisition) PDAQ56 data acquisition board and the pressure transducer was plugged into the same computer.

Once everything was double checked, the assembly was lowered into the constant temperature bath set to 30°C. This temperature was chosen because a low temperature was required as a set point where pressure readings could be taken both before and after the test. Without a constant temperature to measure the pressure, the readings would be meaningless since they would

Approved for public release: distribution is unlimited.

track the vapor pressure and not reveal if additional NCG from chemical reactions was present. Room temperature was not used because the stability of the bath set point was poor at 20°C. The corrosion test was typically left at 30°C for about one hour before the temperatures within the corrosion test reached steady state. Pressure was then recorded. The "set point" temperatures used refer to the temperature of the bath fluid and not the temperatures within the reaction vessel. Due to the small conduction resistance across the glass thickness these temperatures were typically a degree to a few degrees lower than the bath set point but still constant at steady state.

The next set point used was 100°C. This was the actual test temperature. It typically took about 60 $mins$ for the test itself to reach steady state. A high temperature was used to accelerate any corrosion which may occur and shorten test time. Also, previous experiments showed that even pure water and aluminum reacted very slowly below 60°C. The test was left at 100°C for 24 hours before the temperature was reduced to 30°C to measure pressure again. The ice bath cooling loop was turned on to assist in bringing the bath temperature back down to near room temperatures. This process took about 60 $mins$ before steady state was again reached. Finally, the corrosion test was removed from the bath, the test fluid was collected, the sample was cleaned and weighed again, and the entire assembly was cleaned for reuse.

6.3 Results and Discussion

Fluids tested with aluminum samples were pure DI water, $Mn - 0$ (chromium only), and $Mn - 4$. Pure DI water was also tested on its own, without any metal sample, several times to check the test for large leaks and determine baseline pressure change that might occur due to unavoidable micro-leaks, incomplete degassing, or other sources of constant test error. A summary of the fluids used can be found below in Table 6.

Approved for public release: distribution is unlimited.

Table 6: Fluids used in corrosion tests

Metal/Fluid	Charge (mL)	Initial pH	Initial E (mV SHE)	$[Mn^{+7}]$ (mmol/L)	$[Cr^{+6}]$ (mmol/L)	Mn^{+7} (μmol/cm^2)	Cr^{+6} (μmol/cm^2)
Aluminum Mn-0,Cr-1	200	6.33	524	0.00	79.56	0.00	318.25
Aluminum Mn-4,Cr-1	200	5.92	984	9.96	79.55	39.86	318.19

DI Water was tested without aluminum four times to understand the new corrosion test that had been designed. The results indicate the test holds a vacuum well and is repeatable. The average pressure change from start to end of the water only tests was $0.0089\ psia$, very close to the uncertainty of the ΔP measurements which was $0.0057\ psia$. The tests were highly repeatable. Corrosion test results for the water only baseline studies and other fluids tested can be found in Table 7.

Table 7: Corrosion test results summary

Metal/Fluid	Test #	m_1 (g)	m_2 (g)	Δm (g)	%m change	P_1 (psia)	T_{v1} (°C)	P_2 (psia)	T_{v2} (°C)	ΔP (psia)
Water Only	1	0.0000	0.0000	0.0000	N/A	0.5698	28.9	0.5835	28.9	0.0137
	2	0.0000	0.0000	0.0000	N/A	0.5625	28.7	0.5718	28.5	0.0093
	3	0.0000	0.0000	0.0000	N/A	0.5763	28.5	0.5822	28.6	0.0060
	4	0.0000	0.0000	0.0000	N/A	0.5846	28.6	0.5911	28.6	0.0065
Al/Water	1	6.6208	6.6261	0.0053	0.080%	0.5404	28.4	0.6447	28.4	0.1043
	2	6.6025	6.6086	0.0061	0.092%	0.5657	28.7	0.6584	29.0	0.0927
	3	6.6164	6.6221	0.0057	0.086%	0.5789	28.9	0.6730	28.8	0.0941
Al/Mn-0,Cr-1	1	6.5880	6.5883	0.0003	0.005%	0.6013	29.4	0.6078	29.3	0.0065
	2	5.3213	5.3214	0.0001	0.002%	0.5691	28.5	0.5783	28.5	0.0092
Al/Mn-4,Cr-1	1	6.5877	6.6245	0.0368	0.559%	0.5821	29.0	0.8026	29.0	0.2205

When aluminum was tested in water the ΔP was much higher than the baseline tests. The average pressure increase was $0.0970\ psia$. The pressure increase was roughly an order of magnitude greater than the measurement uncertainty or baseline measurements, showing it is significant. This pressure increase corresponds to $\sim 0.1\ psia$ of hydrogen gas NCG generated over

the 24 hour test at 100℃, indicating a relatively large amount of metal corrosion and NCG formed. The mass change of the aluminum sample was 5 or $6\ mg$ for each water/aluminum test. This also indicates corrosion was taking place on the sample surface.

When the chromium only fluid ($Mn - 0$) was tested, the tests were essentially the same as water only. In other words, the results showed pressure increases and sample mass increases within, or very near to, the accuracy of the measurement. This indicates a statistically insignificant amount of NCG generated and surface corrosion occurring over the test period. Longer tests or tests at even higher temperature would be needed to determine the very low corrosion rate for this combination. The primary purpose of these tests was to determine if chromium could act as a lone oxidizer if in direct contact with the aluminum surface; the results indicate this to be true. Other considerations such as remote passivation may place additional resistance burdens on the electrochemical cycle and require stronger oxidizers such as permanganate to overcome it.

Another test was also performed using the $Mn - 4$ solution. This test performed very differently than the others. After 24 hours, the ending fluid looked like a dirty suspension of murky black particles and the aluminum sample was dark purple to black in color and had noticeable pitting and other signs of large-scale corrosion. Below, in is an image showing the aluminum sample after exposure to $Mn - 4$ fluid.
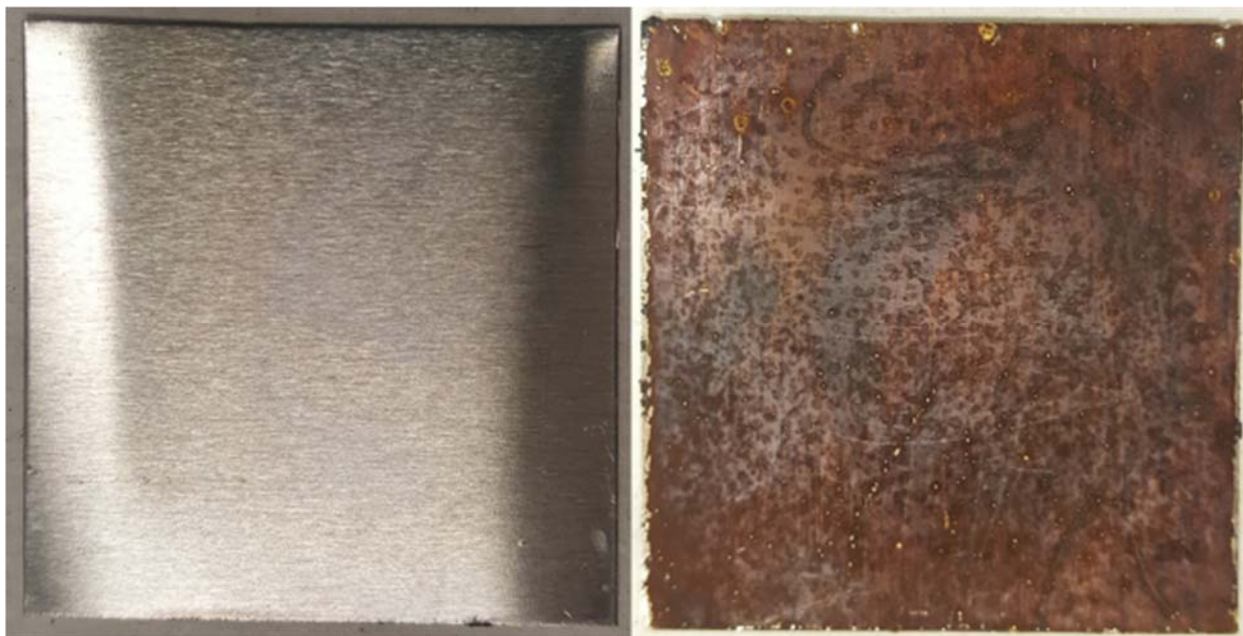
Figure 23: Aluminum corrosion sample (left) before and (right) after exposure to $Mn - 4$ fluid

The mass increase was $\sim 37\ mg$, roughly $7x$ more than that for aluminum and water. The pressure increase was considerable as well at $0.2205\ psia$, more than double the highest ΔP for water-aluminum tests. One explanation for this is that with such a large amount of permanganate relative to the available aluminum for reacting, the excess permanganate began to disassociate into $MnO_{2\ (s)}$ and O_2 gas, another NCG. Without being able to fully react out of solution, the permanganate was still in excess and at high temperature led to a runaway effect forming NCG and surface corrosion.

6.4 Uncertainty Analysis

The 95% confidence uncertainty of a single temperature measurement using the Omega type-K thermocouple probes was found to be $\pm 1.56°C$ as shown in Table 8, below.

Table 8: PDAQ56, Omega type-K thermocouple probe error

PDAQ 56: Type-K Thermocouple Error				
Source	Value (+/-)	Shape	Divisor	Std Unc (°C)
Resolution	0.005	Uniform	1.73	0.0029
DAQ+CJ	1.1	Normal	2	0.55
TC Probe (SLE)	1.1	Normal	2	0.55
T Combined Standard Uncertainty =				0.78
T Expanded Uncertainty (95%, std. dist.) =				1.56

The high accuracy pressure transducer used had a reported accuracy of $\pm0.08\%$ of the full scale range, which was $0-5\ psia$. The 95% confidence uncertainty of a single pressure measurement was found to be $\pm0.0040\ psia$. The uncertainty of a pressure difference calculation was $\pm0.0057\ psia$. These calculations are shown below in Table 9.

Table 9: Omega PX409 $0-5\ psia$ USB, high accuracy pressure transducer error

Omega PX409-005A USB-H: High Accuracy Pressure Transducer				
Source	Value (+/-)	Shape	Divisor	Std Unc (psia)
Resolution	0.00005	Uniform	1.73	2.89E-05
0.08% FS Accuracy	0.0040	Normal	2	0.0020
P Combined Standard Uncertainty =				0.0020
P Expanded Uncertainty (95%, std. dist.) =				0.0040
ΔP Standard Uncertainty =				0.0028
ΔP Expanded Uncertainty (95%, std. dist.) =				0.0057

The accuracy of the gram mass scale was very low, $\pm0.0002\ g$.

6.5   Conclusions

Three fluids were tested with identical aluminum 6061-T6 alloy samples. These corrosion tests were ran within a vacuumed reaction vessel and kept at a temperature of 100°C for 24 hours. Mass changes of the sample from corrosion and pressure changes of the system due to NCG formation were measured. The results indicate that the chromium only solution was capable of

inhibiting corrosion over the course of the test due to negligible mass increases in the sample and pressure increases equal to both the uncertainty of the pressure transducer and identical to the results observed when no aluminum sample was present in the chamber. Water tests run with aluminum samples produced significant hydrogen gas NCG release accompanied by a small but repeatable increase in sample mass. The $Mn-4$, high permanganate concentration fluid (also containing chromium in the same concentration as the chromium only fluid) released more than $2x$ the pressure of NCG compared to water only and aluminum. The mass increase for $Mn-4$ fluid was also high, rougly $37x$ higher than that of aluminum and water only. After the test this fluid had a large amount of black suspension particles, a sign of $MnO_{2\,(s)}$ formation. Such a large amount of both $MnO_{2\,(s)}$ and NCG released suggests that O_2 gas was released in this case due to a highly catalyzed disassociation of permanganate.

This information is useful for future thermo-syphon and heat pipe experiments because it indicates that chromium in moderate quantities is likely adequate for PCHT device applications where the fluid is in direct contact with much of the metal device surface. Examples of this include TGPs (thermal ground planes) and thin flat heat pipes or micro-channeled grooves. Another useful conclusion is that there is at least some danger in the use of permanganate due to oxygen gas release and a large amount of $MnO_{2\,(s)}$ product. This may be mitigated if the amount of permanganate is not in excess compared to available metal surface area. In the case of this test, experimental design forced the use of a large volume of solution. Future tests may want to redesign around this limitation and also look at different concentrations of both permanganate and chromates. Longer tests and higher temperatures (which were not possible due to a trade-off between pressure transducer accuracy and max pressure when equipment was being purchased)

should also be investigated but more expensive, sensitive equipment than was available would be necessary to perform these measurements.

Thermo-syphon tests will be performed next to determine how well the proposed oxidizer inhibitor scheme works for actual thermo-syphon devices. NCG slugs will be visualized using an IR camera and changes in performance using thermocouples will also be measured over time.

7 Natural Convection, Heater Block Thermo-syphon Experiments

Thermodynamics and corrosion tests have shown that direct contact between a fluid containing chromium and aluminum metal can result in successful passivation and NCG suppression over a relatively short period of time. Vertical thermo-syphons were constructed to more fully investigate the passivation of PCHT devices. The goal of these tests was to see of, like the fully submersed tests of Chapter 6, chromium only was enough to passivate aluminum thermo-syphons, and if not how much, if any, permanganate was necessary to assist in preventing NCG generation. Test setup details, results, and discussion follow in this chapter.

7.1 Test Setup

Vertical thermo-syphons measuring $45\ cm$ in length were constructed out of 6061-T6 alloy aluminum tubes with an OD of $0.375''$ and inner tube diameter (ID) of $0.305''$. Tubes were cut to length and fitted with 6061-T6 alloy aluminum end caps which were press fit and then secured for vacuum by applying high-temperature and corrosion-resistant, marine grade JB Weld epoxy around the joint. Heater blocks $5\ cm$ in length with embedded cartridge heaters were used as evaporator and natural convection over the remaining $40\ cm$ of tube length was the method of condensation. Natural convection was chosen to allow for easy visualization using an infrared camera. Figure 24 shows details of the construction and dimensions of each element.
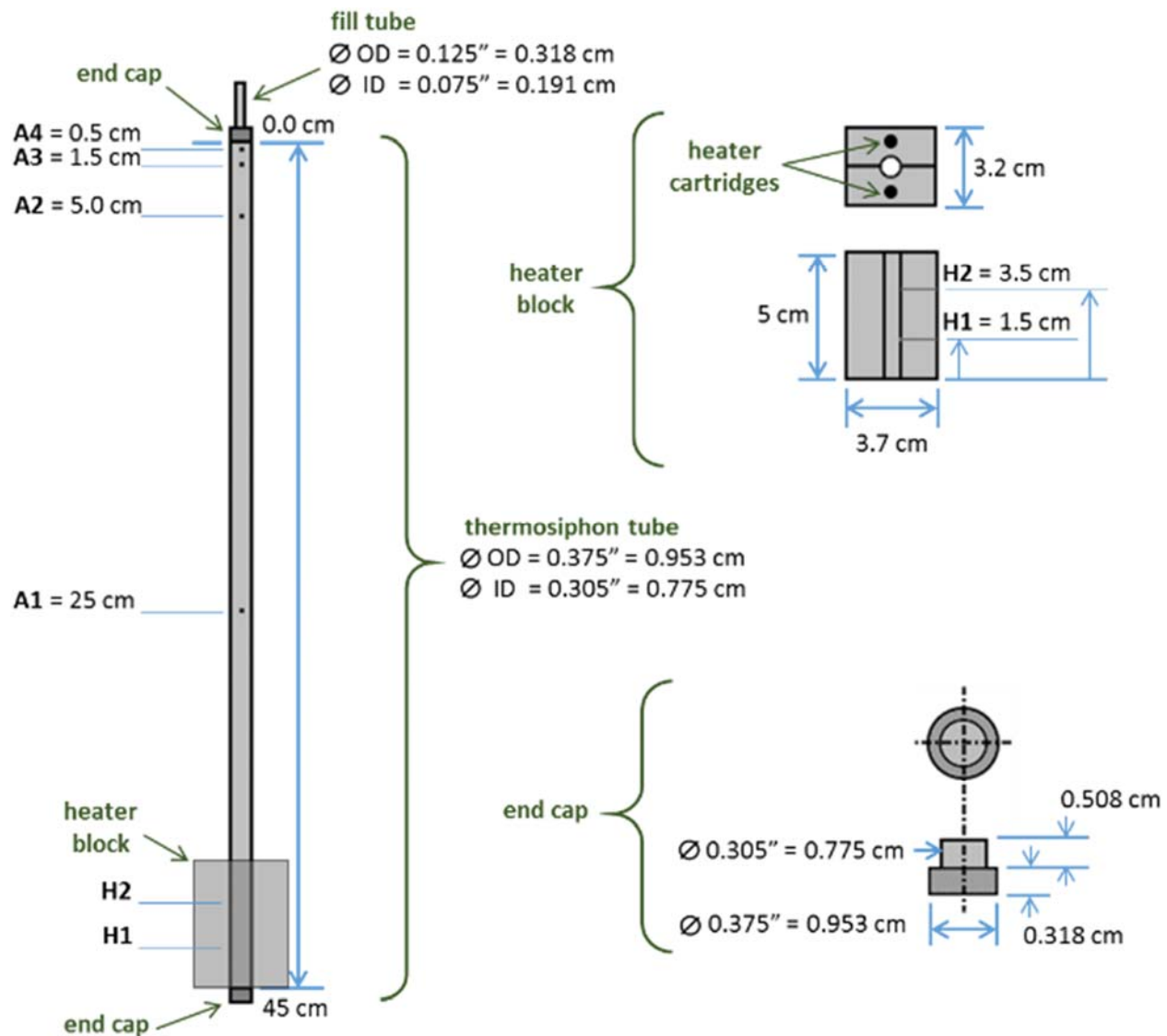
Figure 24: Thermo-syphon and heater block dimensions with thermocouple map

Fill tubes made from aluminum alloy 3003 having 0.125″ OD and 0.075″ ID were cut approximately 5 *cm* long each and inserted in a through a 1/8″ hole in one of the tube's end caps. The same JB Weld epoxy was used to further secure and seal this joint. The JB Welded joints were then all allowed to fully cure overnight. Once cured, each thermo-syphon assembly was painted with a thin layer of flat black spray paint and allowed to dry for a short time, usually 30 *mins* was enough. The black paint serves two purposes. First, it provides a consistent surface for the thermo-

syphon condensation section via mixed natural convection and radiation exchange with the ambient room temperature, air environment. More importantly, the black surface is required to accurately use the IR camera in this study to visualize the growth of possible NCG slugs.

Four type-T thermocouples were then attached to the tube body according to the thermocouple map in Figure 24. The small area where the thermocouple weld contacts the tube was carefully sanded to remove the paint and ensure thermocouples were attached directly to the metal body of the tube. Thermocouple attachment was done using Arctic Alumina Thermal Adhesive. This high thermal conductivity, white adhesive was used for attaching thermocouples due to its 5 min cure time, high strength, and good conductivity.

With the tube assembled, painted, and instrumented, the working fluid can then be charged. Using a vacuum charging station, the tubes were evacuated to dry out any small amount of water which might have found its way inside the device. This process typically took about $2 - 5$ $hours$ depending on the water content of that particular tube. This was essential because tube weight before and after was used to accurately determine liquid charge amount within the thermo-syphon. Any pre-existing liquid inside the tube would cause the measured liquid charge to inaccurately indicate the tube was charged with less liquid than was actually present and could furthermore affect the concentration of oxidizers inside by adding excess pure water to solution.

Once dry, tube assemblies were weighed and reattached to the charging station. Now ready for their final vacuum, tubes were vacuumed for 1 $hour$ to ensure they reached the 0.002 $mbar$ max vacuum pressure of the Varian DS302 Dual Stage Rotary Vane Vacuum Pump. A vacuum pressure transducer was also part of the charging station assembly to check for consistent and stable final vacuum pressure before charging. Degassed working fluid was then introduced into

the vacuumed thermo-syphon. Charge amount was initially measured using a graduated cylinder in the station assembly but the mass difference of the tube, once disconnected and re-weighed, was considered the real charge amount. Once charged and still attached to the station, thermo-syphons were disconnected and sealed using a cold weld device to fuse the small diameter fill tube walls together. JB Weld was again used to cover the cold weld joint as a caution against vacuum leaks during future device testing. Due to the difficulty of welding or soldering aluminum and the unknown role the high temperature process and/or solder material might have on material compatibility with the tested inhibitor fluids, JB weld was used in tube construction and sealing against vacuum leaks. This removes solder material, heat-affected zone, or sealing procedure as another complicated variable to consider for device passivation.

The fully built thermo-syphon was next fitted with a heater block using thermal paste to fill micro air gaps between the block faces and tube wall to minimize thermal resistances between heat source and test device. Two more type-T thermocouples were inserted in small $1\ mm$ diameter holes in the heater block such that they contacted the tube wall perpendicularly. The assembly was then wrapped in fiberglass insulation and mounted in a vice clamp vertically, using a digital angle meter to confirm vertical orientation to $\pm 0.1°$ in both axes. Next, the heater cartridges were wired to a variac power supply and a multimeter in line to measure input voltage. Joule heating Input power to the thermo-syphon was calculated using equation (67).

$$P = \frac{V^2}{R} \tag{67}$$

Power was set at 10 W at the start for all tests in this study and not changed during testing. Another thermocouple was also used to record ambient air temperature since the thermo-syphons were cooled via natural convection. Thermocouple readings were recorded using an IOTech DAQ56

Approved for public release: distribution is unlimited.

data acquisition board and DasyLab software. Infrared images were also recorded using a forward looking infrared (FLIR) A310 IR camera. The IR images make it easy to visually see the formation of NCG slugs over time.

Previous testing performed has also shown that an evaporator fill ratio, V', of 60% provides optimal heat transfer results for aqueous based solutions in vertical thermo-syphons. Therefore, $V' = 60\%$ will be used for all tests in this chapter, corresponding to a liquid charge volume of $\sim 1.45 \ mL$ for the dimensions of these thermo-syphons. Figure 25, below, shows a test for aluminum and DI water fully assembled and ready to begin the experiment.
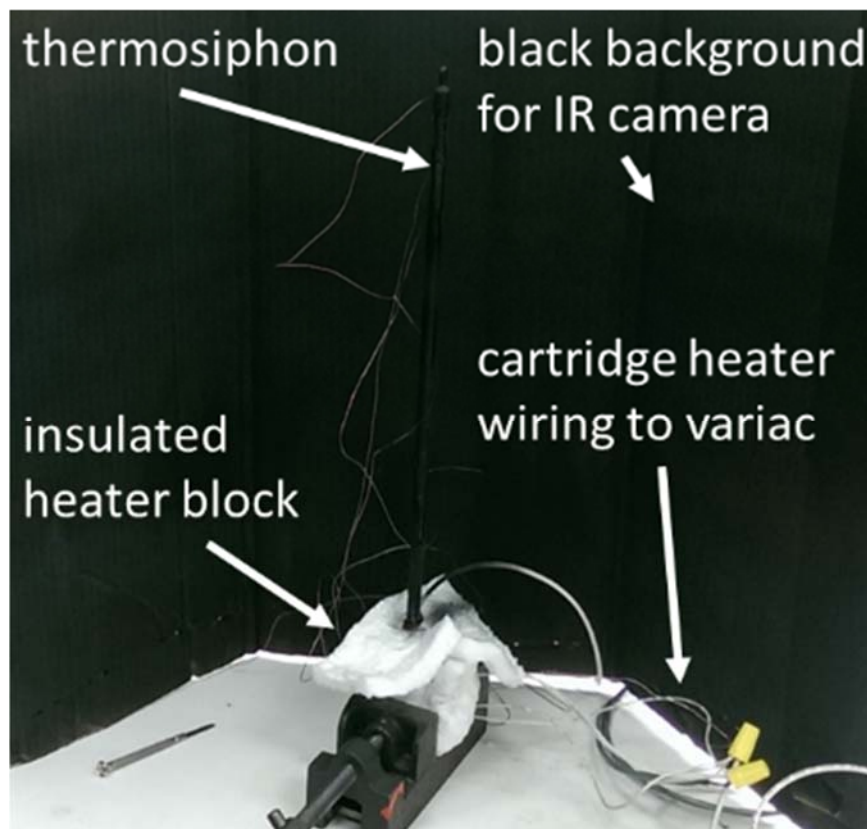
Figure 25: Aluminum/DI water vertical thermo-syphon in operation

In addition to DI water, four different inhibitor solutions were prepared as working fluids for testing. The first oxidizer solution contained chromates only. Three additional fluids were

Approved for public release: distribution is unlimited.

prepared using the same concentration of potassium dichromate but had different concentrations of potassium permanganate ranging from 2.5 $mmol/L$ to 10.0 $mmol/L$. The rationale was that chromium had demonstrated its utility as a direct-contact passivating fluid in the previous corrosion experiments. Therefore these tests would help determine if the same was true for thermosyphons, and, if not, would permanganate assist in preventing NCG or again produce oxygen gas NCG if in excess. If permanagates are useful, the theory behind their utility is that once the device is initially passivated by quickly reacting out all the permanganates the chromates in solution will be responsible for maintaining pH balance, coating stability, and oxide layer repair. The initial pH was selected for each fluid such that the final pH after all permanganate had reacted out of solution would not exceed 6.5. These calculations were performed using OLI Studio 9.2 to simulate the reaction of all permanganate to form the product $MnO_{2\ (s)}$. The design pH was obtained by adding $NaOH$ as needed. A $pH = 6.5$ was selected as the appropriate final pH based on Pourbaix diagram thermodynamics covered in Chapter 4 and fluid design considerations covered in Chapter 5.

The concentration of chromium ($\sim 80\ mmol/L$) in solution was selected to be consistent with previously tested fluids in Yao [35], as was the initial (2.5 $mmol/L$) concentration used of permanganate. The yellow color of the fluid collected after the completion of previous tests [27, 33, 35, 70], as well as the measured potential (E), indicates there was still a significant concentration of chromates remaining in solution. Observations of the fluid decoloring from the strong purple, indicative of the presence of permanganate, to bright yellow during flat heat pipe and other previous testing serves to further confirm the permanganate reacts out quickly and should be addressed first in experimental testing.

7.2 Results and Discussion

Each test was run with a constant heat input of $10\ W$. When the power was turned on this was considered time $t = 0\ secs$ and elapsed test time began from there. A summary of the experiments showing initial and final fluid pH and E conditions, fluid charge, and concentrations of oxidizers used for each thermo-syphon can be found below in Table 10.

Table 10: Natural convection, heater block experimental fluids used and E, pH measurements

Metal/Fluid	Tube	Charge (g)	Initial pH	Final pH	ΔpH	Initial E (mV SHE)	Final E (mV SHE)	ΔE (mV SHE)	$[Mn^{+7}]$ (mmol/L)	$[Cr^{+6}]$ (mmol/L)	Mn^{+7} (μmol)	Cr^{+6} (μmol)
Aluminum	1	1.4344	7.00	7.74	0.74	-281	-97	184	-	-	-	-
H_2O	2	1.3042	7.00	7.14	0.14	-281	-38	243	-	-	-	-
Copper	1	1.1964	-	-	-	-	-	-	-	-	-	-
H_2O	2	1.4009	-	-	-	-	-	-	-	-	-	-
	1	1.2235	6.24	6.73	0.49	571	225	-346	-	79.99	0.00	97.87
Aluminum	2	1.5451	6.24	6.74	0.50	571	243	-328	-	79.99	0.00	123.60
Mn-0,Cr-1	3	1.4128	6.24	6.71	0.47	571	220	-351	-	79.99	0.00	113.02
	4	1.3602	6.24	6.74	0.50	571	188	-383	-	79.99	0.00	108.81
Aluminum	1	1.4118	6.15	6.83	0.68	924	327	-597	2.49	80.02	3.51	112.97
Mn-1,Cr-1	2	1.3882	6.15	6.70	0.55	924	274	-650	2.49	80.02	3.45	111.08
	3	1.4143	6.15	6.81	0.66	924	248	-676	2.49	80.02	3.52	113.17
Aluminum	1	1.6439	6.07	6.68	0.61	939	444	-495	5.01	79.98	8.24	131.47
Mn-2,Cr-1	2	1.4662	6.07	6.55	0.48	939	245	-694	5.01	79.98	7.35	117.26
	3	1.4346	6.07	6.58	0.51	939	246	-693	5.01	79.98	7.19	114.73
	1	1.4646	5.87	6.73	0.86	972	312	-660	10.00	80.01	14.64	117.18
Aluminum	2	1.5026	5.87	6.66	0.79	972	379	-593	10.00	80.01	15.02	120.22
Mn-4,Cr-1	3	1.5458	5.92	6.55	0.63	974	381	-593	10.01	79.48	15.48	122.87
	4	1.5002	5.92	6.50	0.58	974	377	-597	10.01	79.48	15.02	119.24

All four inhibitor solutions contained $\sim 80\ mmol/L$ of $Cr(VI)$ (referred to as $Cr - 1$) added to solution in the form of potassium dichromate. Each of the four fluids ($Mn - 0$, $Mn - 1$, $Mn - 2$, $Mn - 4$) had increasing amounts of $Mn(VII)$ ($0.0\ mmol/L$, $2.5\ mmol/L$, $5.0\ mmol/L$, $10.0\ mmol/L$) added to solution using potassium permanganate. The pH was balanced using $NaOH$.

The tests were run at constant $10W$ input power for five hours unless they were failing catastrophically, in which case they were ended an hour or two early. IR images were taken throughout the experiment. Below, in Figure 26, IR images are shown for each test after 2 *hours* and 30 *mins* of elapsed test time.
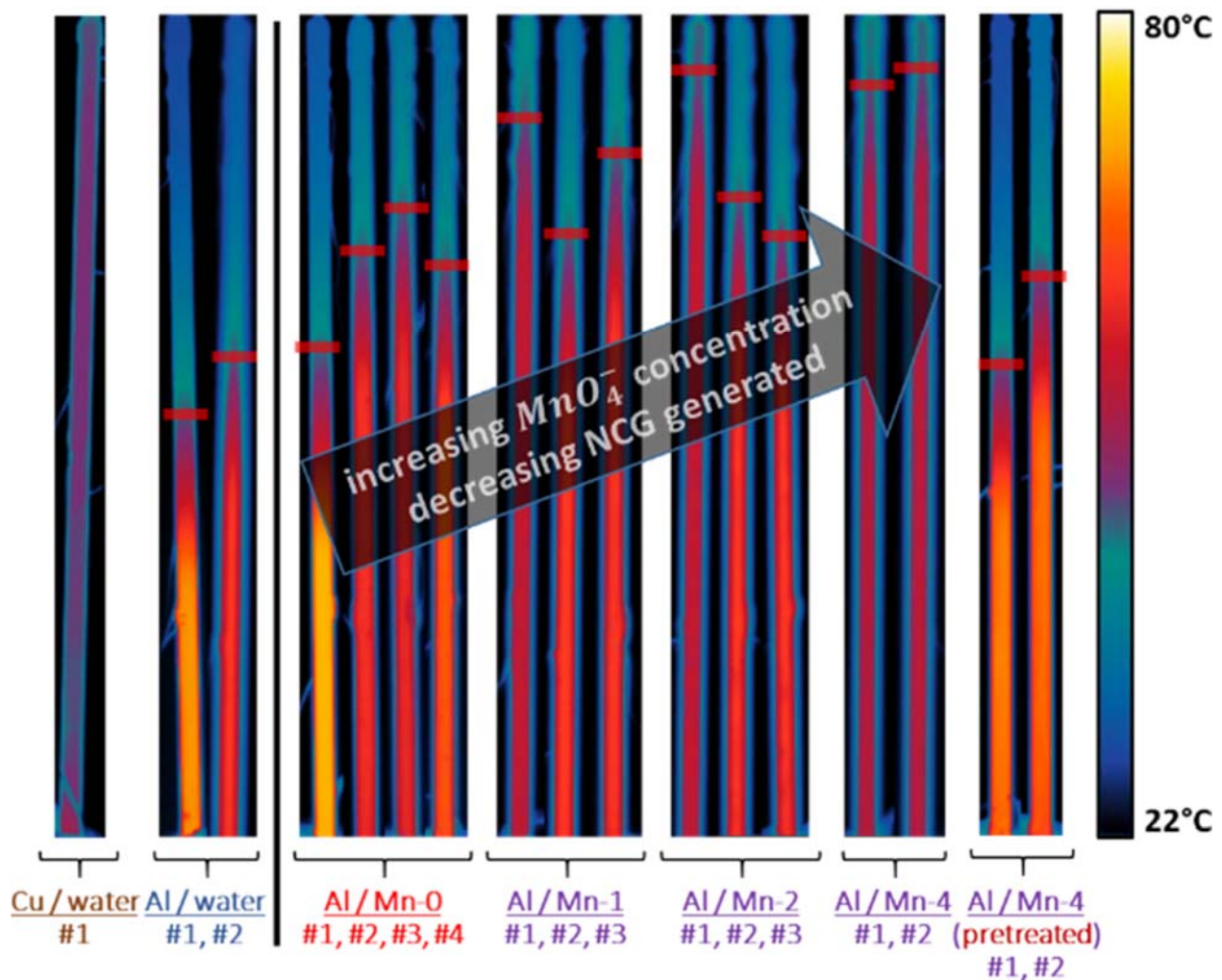
Figure 26: Natural convection, heater block infrared images, 2 hours 30 mins elapsed test time

All IR images are shown with the same scale which is displayed to the right of Figure 26. NCG shows up in the IR images as a cold region (blue to dark blue) which has coalesced at the top of the tube beneath which is a much hotter region (red to yellow) where hot steam is still at a constant

Approved for public release: distribution is unlimited.

temperature. The inactive, cold region is where the hydrogen gas has formed a slug of high resistance gas where little vapor is able to reach and condense. The bottom, hot region is still active to some degree and is where condensation is still taking place. Before delving into the specifics of the thermocouple measurements, the IR images in Figure 26 make it clear that chromium only will not fully passivate these aluminum thermo-syphons.

The following sections will discuss and compare the thermo-syphon experiments with each fluid using the temperature difference of the tube, defined by

$$\Delta T = H_{avg} - A4 \tag{68}$$

H_{avg} is the average of the nearly identical heater temperature readings and $A4$ is the top-most thermocouple as shown previously in Figure 24. The $A4$ thermocouple was chosen because as a potential NCG slug grows it will cause a larger and larger temperature difference between this top thermocouple and the heater temperature. This will allow for a rough comparison amongst different failing thermo-syphons to try to see which failed more or less before it was passivated.

Pourbaix diagrams with post-test fluid measurements are also included for each fluid. Diagrams are drawn for each fluid so that the actual concentrations of oxidizers used can be entered as the total amount of soluble species in solution. The upper bound temperature of 90°C was used because it was about 5°C to 10°C higher than the max temperature observed in the evaporator of any thermo-syphon test.

7.2.1 Copper/Water

Copper tubes were tested first, charged with DI water. This was important because it demonstrates what a properly functioning thermo-syphon of the same size and liquid charge should

Approved for public release: distribution is unlimited.

behave like. Below, Figure 27 shows the temperature difference for both copper/water tests #1 and #2. They both behaved very similarly with a generally constant ΔT of 15°C and 17°C, respectively.
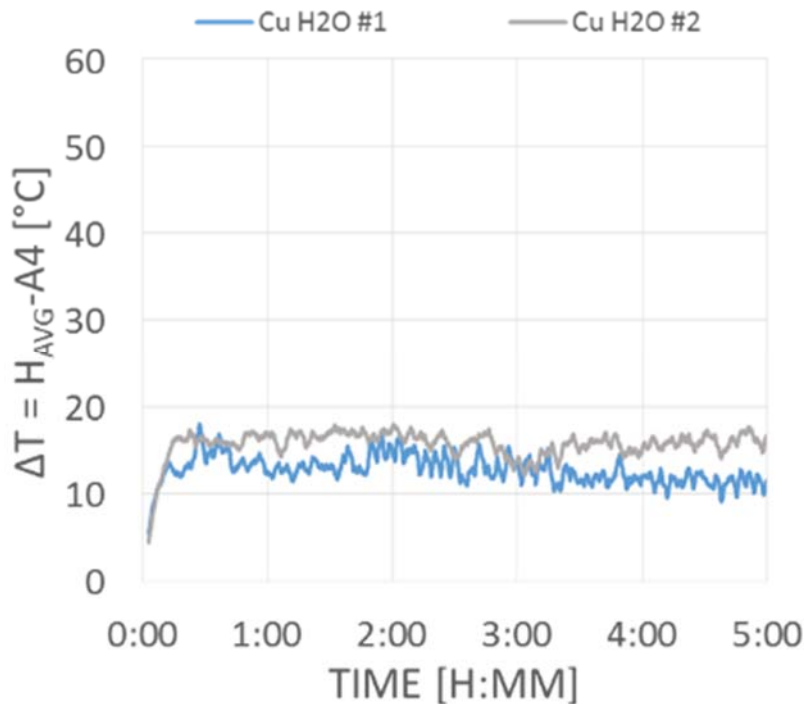
Figure 27: Copper/water #1, #2; $\Delta T = H_{avg} - A4$

Small differences such as these can be easily explained by slight differences in tube manufacturing or small fluid charge discrepancies. The most important observation is that not only did the temperature difference not increase over time, but the IR image in Figure 26 also show isothermal thermo-syphon behavior.

7.2.2 Aluminum/Water

Aluminum and water were tested next. Figure 28 shows the performance data vs time for both aluminum/water #1 and #2 tests.

Approved for public release: distribution is unlimited.
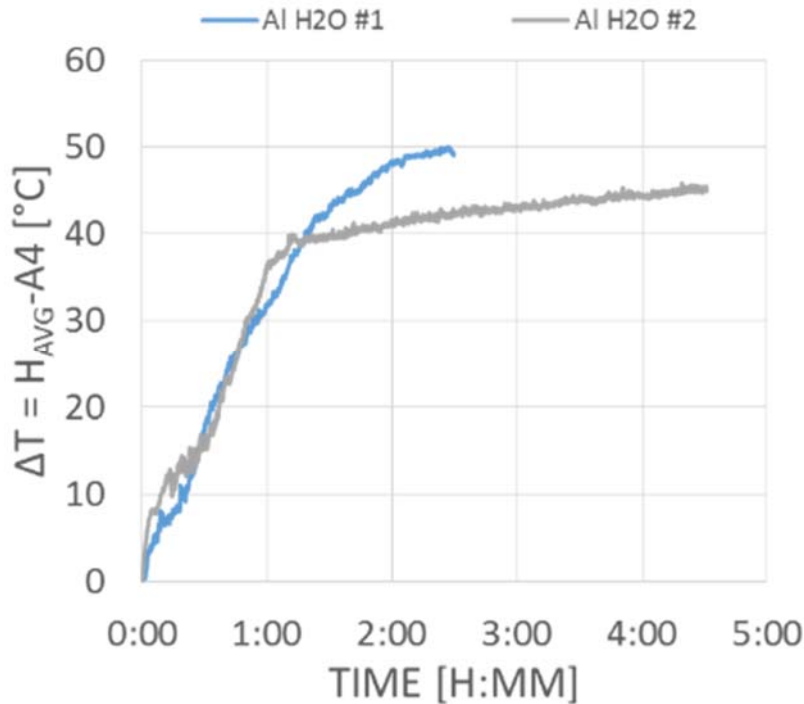
Figure 28: Aluminum/water #1, #2; $\Delta T = H_{avg} - A4$

When compared to the copper tests, there is clearly a significantly larger ΔT for the water/aluminum tests. Comparing the IR images as well shows that these tests generated the largest amount of NCG over the $2\ hours\ 30\ min$ time window. They also had the highest $\Delta T's$ of all the tests.

7.2.3 Aluminum/$Mn - 0$

The $Mn - 0$ (chromium only) fluid did not by itself resist NCG as it did in the direct submersion corrosion tests of Chapter 6. Instead, the chromium only fluid produced significant NCG and tested inconsistently compared to other fluids. Looking at Figure 29 below, it can be seen that two of the four tests performed about as poorly as the water tests, while the other two had much higher $\Delta T's$ than copper/water but plateaued at temperature differences lower than water/aluminum.
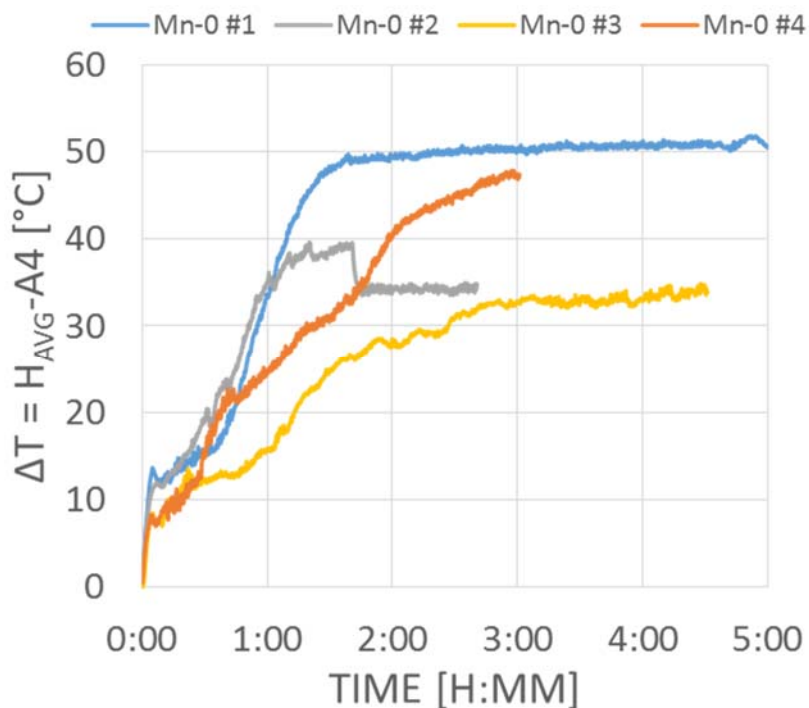
Figure 29: Aluminum/chromium only $(Mn - 0)$ fluid #1, #2, #3, #4; $\Delta T = H_{avg} - A4$

The IR images confirm the inconsistencies in the ΔT data and also corroborate this fluid as the second worst performing fluid in aluminum after water. The corrosion test performed in Chapter 6 with the same chromium only fluid in direct, fully-submersed contact with the aluminum sample resulted in no observable NCG over a much longer test time ($24\ hours$) at higher temperatures.

7.2.4 Aluminum/$Mn - 1$

The $Mn - 1$ fluid has a small amount of permanganate in it ($2.5\ mmol/L$) such that the concentration of both permangates and chromates in solution are the same as those used in Yao's fluids [35]. The ΔT plot vs. time is in Figure 30, below.
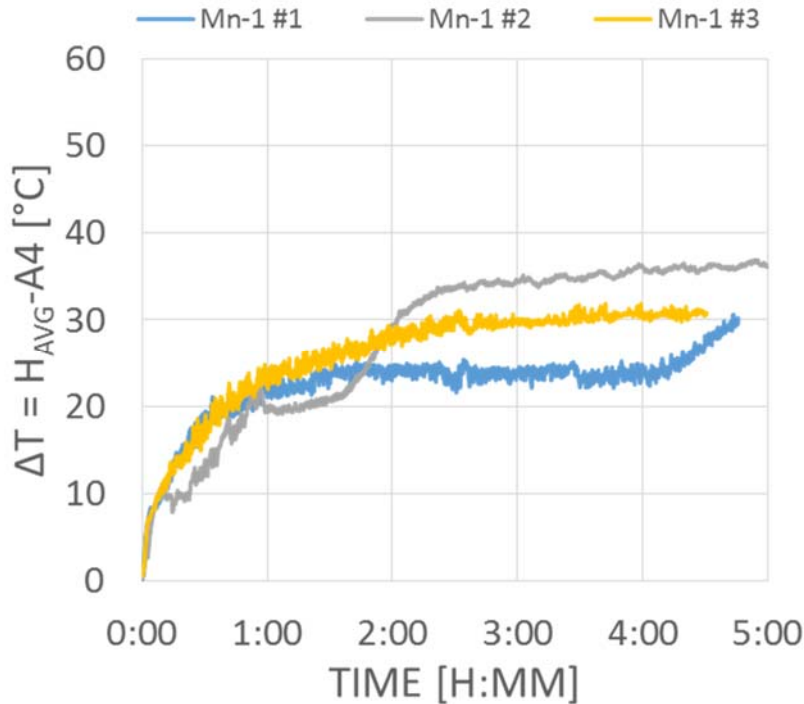
Figure 30: Aluminum/$Mn-1$ #1, #2, #3; $\Delta T = H_{avg} - A4$

The ΔT for all three of the thermo-syphons with the $Mn-1$ fluid demonstrated better consistency compared to the chromium only fluid. However, there was still obvious NCG generated as evidenced by the higher $\Delta T's$ compared to copper/water as well as the IR images showing there was NCG generated but less than the chromium only fluid and pure DI water. One explanation is that the permanganate's stronger oxidation ability is required to overcome the resistance of electron travel through the aluminum oxide and aluminum thermo-syphon tube to remote locations, thus providing slightly better NCG suppression for thermo-syphons than the chromium only fluid.

7.2.5 **Aluminum/$Mn-2$**

The $Mn-2$ fluid has $2x$ the permanganate in it ($5.0\ mmol/L$) compared to $Mn-1$ fluid and the same concentration of chromates. The $\varDelta T$ data for this fluid is given in Figure 31 and is similar to the $\varDelta T$ data for $Mn-1$.
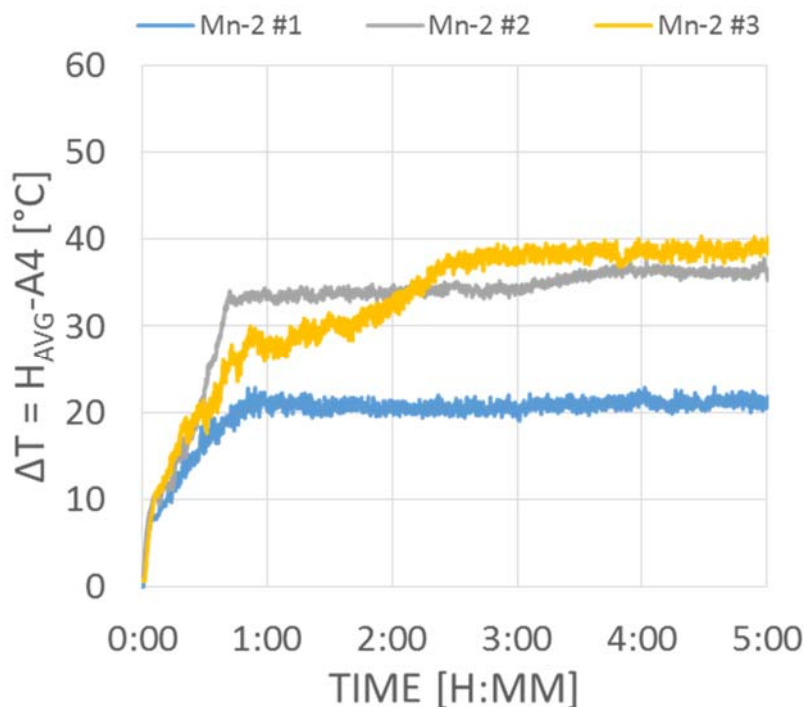
Figure 31: Aluminum/$Mn-2$ #1, #2, #3; $\Delta T = H_{avg} - A4$

$Mn-2$ tests #2 and #3 and $Mn-1$ fluids have temperature difference profiles in the same range around $35°C$. The $Mn-2$ fluid IR data also looks similar to $Mn-1$ for these two tests. The exception is $Mn-2$ test #1. This test has a much lower $\Delta T \sim 20°C$ that remains remarkably constant throughout the test duration. The IR image at $2\ hours\ 30\ mins$ also indicates this test performed better than the other two $Mn-2$ tests as well as the lower concentration Mn fluids and water.

7.2.6 Aluminum/$Mn-4$

The final fluid tested was $Mn-4$ which contained $10\ mmol/L$ of permanganate. A total of four tests were performed for this fluid. Two of these thermo-syphons were prepared in the same manner as all previous tubes (#1 and #2), while the other two thermo-syphons (#3 and #4) were prepared differently. The experiments using $Mn-0$, $Mn-1$, and $Mn-2$ fluids suggested that it might be beneficial to start with a more complete oxide layer at the start of the test. In $Mn-4$ tests #3 and #4 this was accomplished by adding more permanganate to solution and the effect was that two tests exhibited marginally better stability and the $Mn-2$ #1 exhibited much better overall performance. Therefore, $Mn-4$ tests #3 and #4 were pretreated in a solution of chromium only solution at ~80°C for $60\ mins$ before being rinsed in DI water and dried. Tubes were then assembled, charged, and tested in the normal manner. Below, Figure 32 contains the ΔT data for all four $Mn-4$ fluid tests.

Approved for public release: distribution is unlimited.
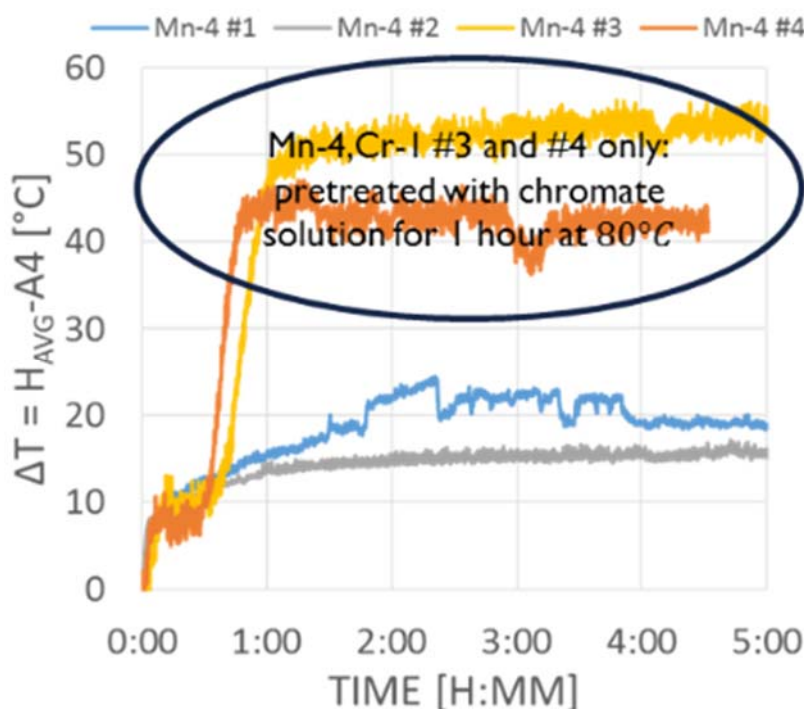
Figure 32: Aluminum/$Mn - 4$ #1, #2, #3, #4; $\Delta T = H_{avg} - A4$

The non-pretreated tests, #1 and #2, performed better than all of the tests performed with solutions containing lower amounts of permanganate. The ΔT's were lower, more stable, and the IR images show almost no NCG in the tubes after 2 $hours$ 30 $mins$ except for a very small area at the tip which is too small to be sure but is likely a very small amount of NCG. Regardless, the NCG growth rate was very small compared to all other tests.

The pretreated tests, #3 and #4 performed well initially with ΔT's of about $\sim 10°C$ for approximately 30 $mins$ before rapidly generating NCG and transitioning from what may have been the best performing thermo-syphons to tying the worst performance of pure DI water. It is unclear why the pretreatment worked for only 30 $mins$ and followed by identical rapid failure of both tubes. The IR images also indicate that by 2 $hours\ and$ 30 $mins$ of elapsed test time tests #3 and #4 looked similar to the pure water tests and had a large NCG slug present. It was expected that pretreatment would help passivation not cause more NCG generation. More treatment solution concentrations, temperatures, and treatment times should be investigated to learn more about pretreatment of the thermo-syphons before it is completely ruled out as a beneficial.

In terms of oxidizer concentrations, there was a small but noticed trend of decreased NCG generated as the concentration of permanganate was increased. Chromates were certainly not enough to suppress NCG as they did in the corrosion tests in Chapter 6. However, even the highest permanganate fluid showed what looked like small amounts of NCG generated. There is also the possibility that all tests generated some small amount of NCG due to a temperature constraint being reached such as the one described previously in Chapter 4.8. Pourbaix diagrams and test data will be used in the following subsection to determine if a temperature limit was reached.

7.3 Temperature Limit Investigation

In Chapter 4.8 it was shown that with increasing temperature the safe zone where aluminum oxide is stable will shift down and to the left on the Pourbaix diagrams with increasing temperature. This corresponds to a less strongly oxidizing solution and more acidic conditions. However, it was not yet known at the time how the solution E and pH will change with temperature. If they move in the same direction and with the same rate as the safe window then there will not be an additional temperature limit associated with maintaining the aluminum oxide stablility window. There will be a limit if the window moves faster than the solution E and pH or if the solution moves in the opposite direction. Post-test fluids for all tests were collected and their E and pH was measured. These fluids were measured at room temperature which is not the temperature at which the thermosyphon was tested, but it is desired to know how this changes as temperature incerases. OLI chemical modeling software was used to simulate what the measurements of each fluid would be as temperature increased from 25℃ (room temperature) to 150℃.

In order to simplify the calculations, a number of assumptions will first be addressed. First, it was assumed that permanganate was reacted out of solution completely. This assumption is supported by several pieces of evidence. The lack of any trace of permanganate's bright purple coloring indicates none is present. Even trace amounts will produce a strong color change of the fluid. Post-test fluids can be seen below in Figure 33.

Approved for public release: distribution is unlimited.
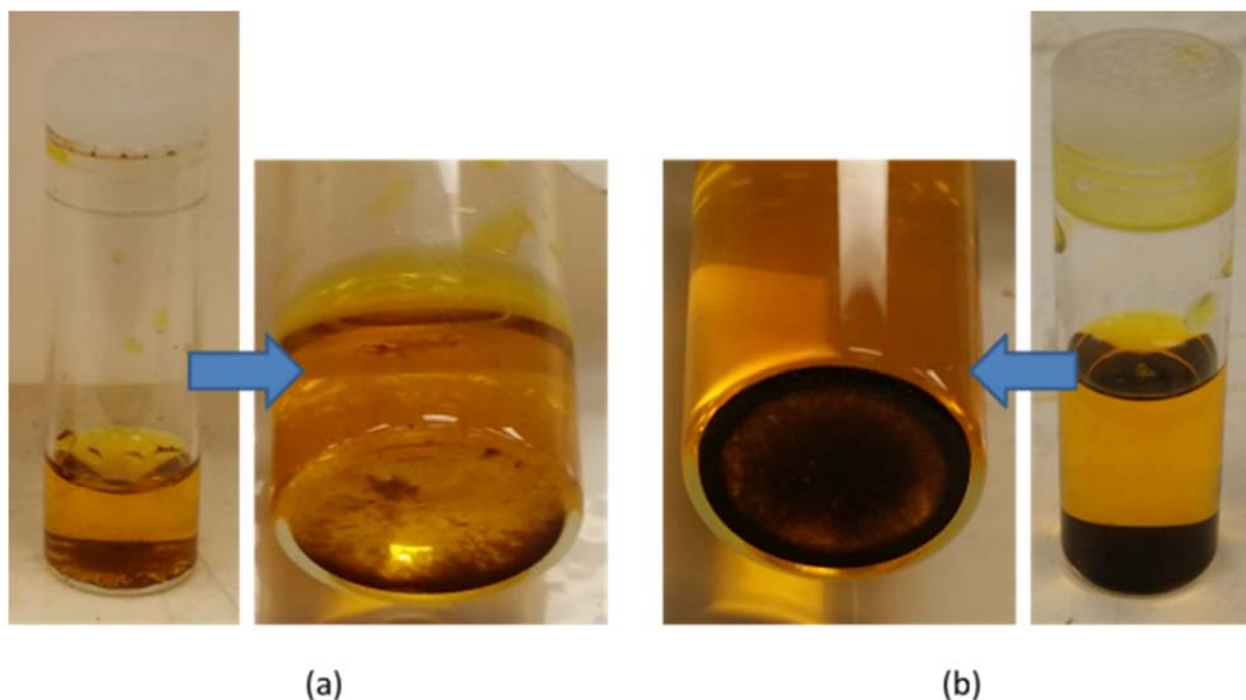
Figure 33: Post test fluids for (a) Mn-1 fluid, (b) Mn-4 fluid

The dark, black dust at the bottom of the vials is $MnO_{2\ (s)}$ and more is present for more permanganate in solution. Additional evidence is provided by the E and pH measurements of the fluids themselves after testing. The potential of the solution (E) would have to be greater than $\sim 900\ mV$ to indicate a presence of permanganate oxidizers of even $10^{-6}\ mol/L$. The measured values obtained were $\sim 550\ mV$ for each fluid, indicating the presence of chromates only.

Using the assumption that no permanganate was left in solution, OLI chemical modeling was used to simulate exactly how much chromate (Cr^{6+}) reacting out of each fluid would result in changes of E and pH. These graphs can be seen below in Figure 34 and Figure 35.
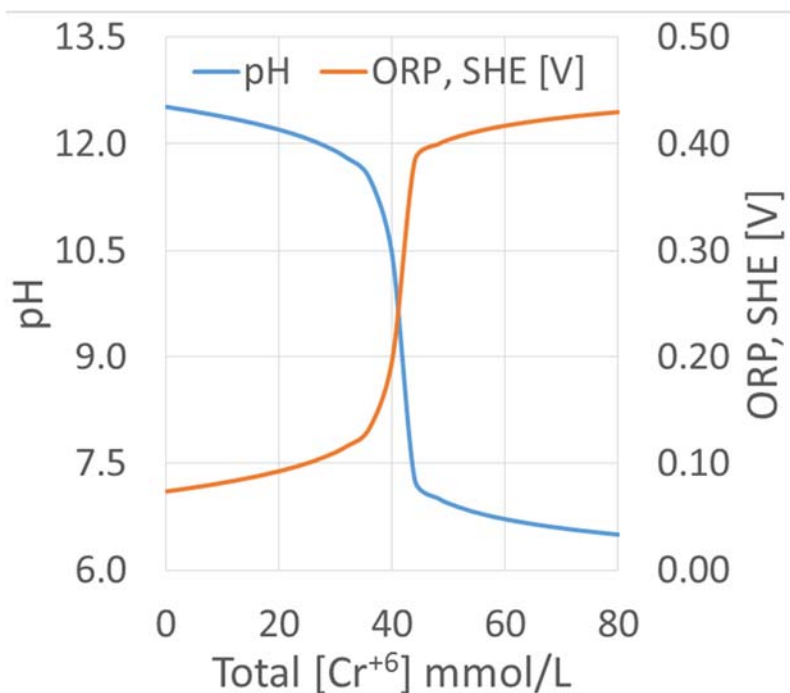
Figure 34: Fluid measurments as $Cr(VI)$ reacts out for final $pH = 6.50$ (lowest measured)
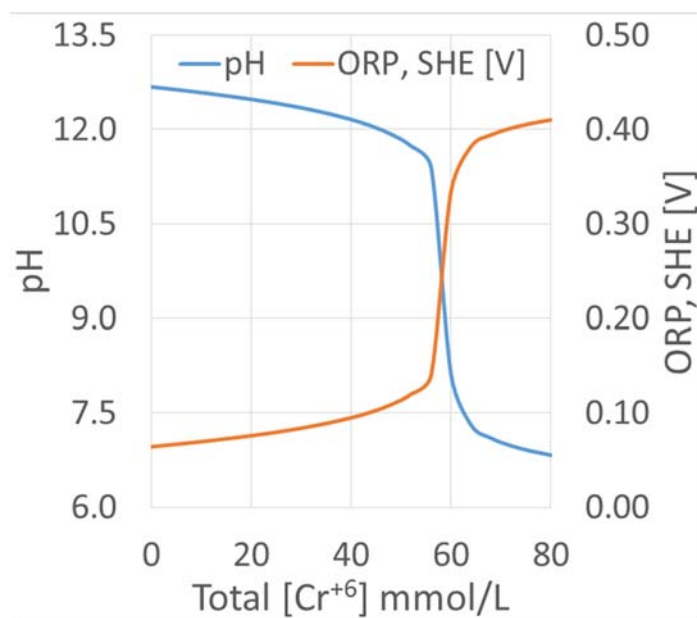
Figure 35: Fluid measurments as $Cr(VI)$ reacts out for final $pH = 6.83$ (lowest measured)

The results of these calculations indicate that for the changes seen in E and pH from before to after each test, it is unlikely that very much chromate reacted out of solution. For the lower final pH

Approved for public release: distribution is unlimited.

fluid, up to 50% may have reacted out, for the higher final pH up to only 25%. Even at 50% chromate reacted out of solution, the change is E and pH is largely negligible due to the buffering ability of chromates. Therefore, for the purposes of the temperature adjustment calculations to follow, it is assumed as a simplification that the final measurements of each fluid post-test are of a fluid with no permanganate and the starting concentration of chromate. These will be the inputs for oxidizer concentrations and fluid measurements for calculating the change in E and pH as a function of temperature using OLI, which was the original goal of these calculations. Both the lowest and highest post-test pH measurements from these experiments were used to calculate the changes of fluid E and pH as a function of temperature and the results can be found below in Figure 36 and Figure 37.
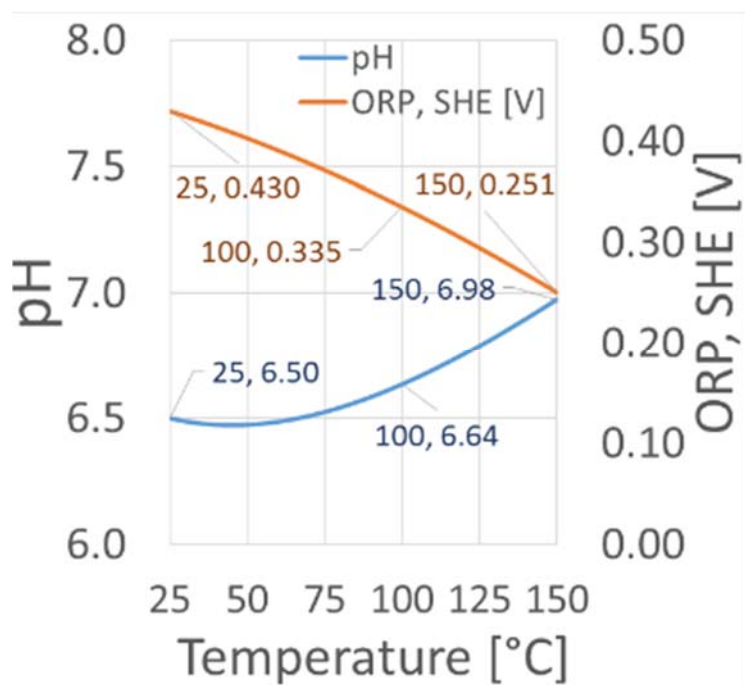
Figure 36: Fluid measurements vs. T for final $pH = 6.50$ (lowest measured)

Approved for public release: distribution is unlimited.
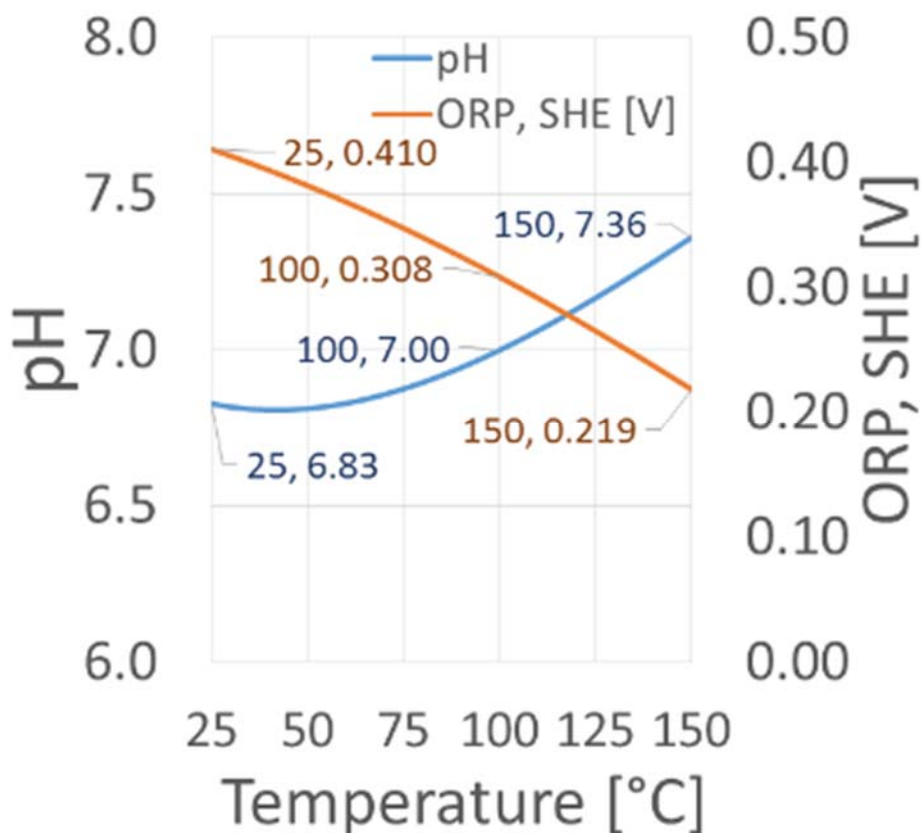
Figure 37: Fluid measurements vs. T for final $pH = 6.83$ (highest measured)

The results of these OLI calculations show that E (ORP – Oxidation Reduction Potential, SHE – Standard Hydrogen Electrode reference) decreases monotonically for both pH values by about $\sim 200\ mV$ as temperature increases from $25°C\ to\ 150°C$. The pH value increases monotonically for both final values by $\sim 0.5\ pH$. Both of these changes are in the opposite direction compared to the change in the safe zone for aluminum oxide stability on the Pourbaix diagram. This means there is the potential for a temperature limit to exist. To test whether or not this limit was reached for these particular tests a Pourbaix diagram was drawn with aluminum-water stability lines drawn for both 25°C and 90°C. The high temperature was chosen because no

test reached over 80°C, so 90°C was chosen to provide a small amount of margin for error in the drawing of the diagrams and/or fluid measurements. This diagram is shown below, in Figure 38.
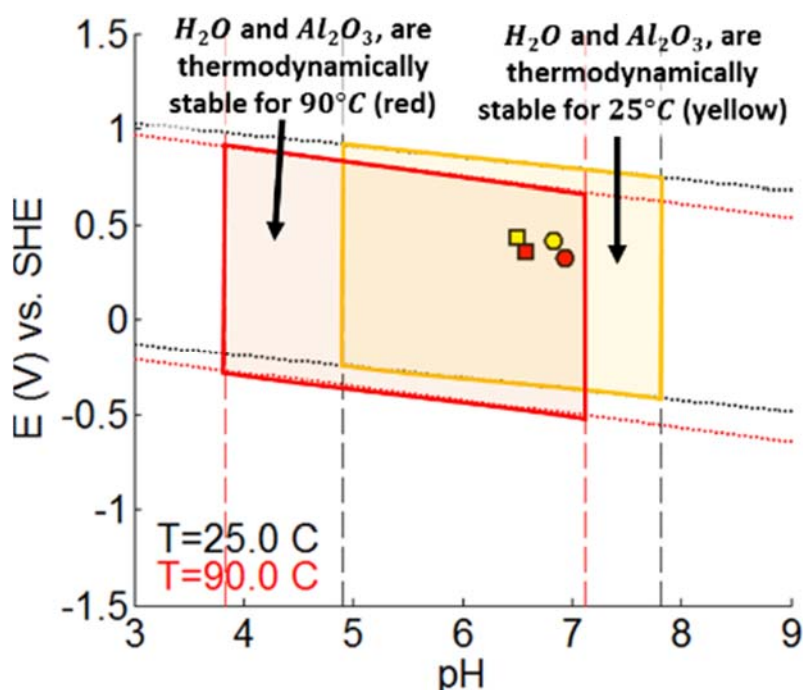
Figure 38: Pourbaix diagram for $Al - H_2O$ system at 25°C and 90°C, $C_{tot}[Al] = 10^{-6}\ mol/L$ to check for high temperature limit reached for heater block, natural convection thermo-syphons

The yellow box is the thermodynamically stable region for aluminum oxide at 25°C and the red box is for 90°C. The yellow and red points correspond to the same temperatures for fluid measurements both the actual measurements at room temperature and simulated high temperature points using OLI. The square points are for the lowest final pH measured and circle points are for the highest final pH measured (both low and high temperatures). The red points need to stay within the red box and yellow points within the yellow box for one to assume that the system remained within the aluminum oxide stability region over the entire range of fluids measured and through all of the temperatures potentially seen by each. The points did stay within their prescribed

Approved for public release: distribution is unlimited.

boundaries and so it was concluded the high temperature limit was not reached. However, there is the potential for an additional limit to be imposed if water itself can be oxidized by the Cr (VI) oxidizers.

7.4 High Temperature $Cr(VI)$ Limit

By looking at the Pourbaix diagram, Figure 15, found in Chapter 4 one notices that the water stability line for oxygen release is relatively close to the boundary between chromate and hydrogen chromate oxidizers and chromium oxide at the $pH\sim6$ used for the present inhibitor solutions. It is conceivable that at high temperature these lines may cross such that the water line is below the chromate/oxide stability line, indicating that water can now be oxidized by chromates, resulting in the release of oxygen gas, an NCG. To check for this possibility Pourbaix diagrams were generated for different temperatures until the lines crossed near where $pH\sim6$. The Pourbaix diagram showing where this eventually occurs is below in Figure 39.
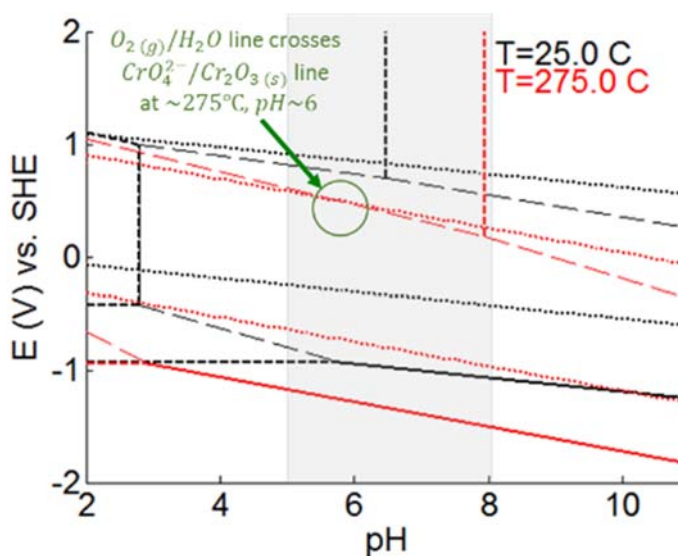
Figure 39: Pourbaix diagram for $Cr - H_2O$ system at 25°C and 275°C, $C_{tot}[Cr] = 80\ mmol/L$

The two lines do not cross until the temperature reaches 275°C, which is well above any planned tests for aluminum and water-based inhibitor fluids at this time. This limit was determined to not be a problem for the scope of this work.

7.5 Uncertainty Analysis

The 95% uncertainty of the type-T thermocouples used was ±1.21°C for a single temperature measurement and ±1.71°C for each ΔT measurement. The calculation for this is shown in Table 11.

Table 11: PDAQ 56, type-T thermocouple error

PDAQ 56: Type-T Thermocouple Error				
Source	Value (+/-)	Shape	Divisor	Std Unc (°C)
Resolution	0.005	Uniform	1.73	0.0029
DAQ+CJ	1.1	Normal	2	0.55
TC Wire (SLE)	0.5	Normal	2	0.25
T Combined Standard Uncertainty =				0.60
T Expanded Uncertainty (95%, std. dist.) =				1.21
ΔT Standard Uncertainty =				0.85
ΔT Expanded Uncertainty (95%, std. dist.) =				1.71

For an input power of 10 W, which was used for all thermo-syphon tests, the calculation of input power error through the Joule heating equation is broken down into resistance and voltage uncertainties, shown in Table 12 and Table 13.

Table 12: Omega HHM31 Multimeter, resistance uncertainty calculation

Omega HHM31 Multimeter: Resistance Error (e.g. R=55.8 Ω)				
Source	Value (+/-)	Shape	Divisor	Std Unc (Ω)
Resolution	0.05	Uniform	1.73	0.029
Accuracy	0.4% rdg + 4 dgts	Normal	2	0.31
Combined Standard Uncertainty =				0.31
Expanded Uncertainty (95%, std. dist.) =				0.63

Table 13: Omega HHM31 Multimeter, voltage uncertainty calculation

Omega HHM31 Multimeter: Voltage Error (e.g. V=23.63 v)				
Source	Value (+/-)	Shape	Divisor	Std Unc (Ω)
Resolution	0.05	Uniform	1.73	0.029
Accuracy	1% rdg + 4 dgts	Normal	2	0.32
Combined Standard Uncertainty =				0.32
Expanded Uncertainty (95%, std. dist.) =				0.64

Using these values, the total 95% confidence uncertainty for input power was calculated to be $\pm 0.40\ W$. This equates to about ~4% of the $10\ W$ input power.

The pH and E measurements were both done using Omega probes. The pH measurements have an accuracy of $\pm 0.02\ pH + 2d$ ($\pm 0.04\ pH$ units) while the E measurements are $\pm 0.5\% + 2d$, giving accurate measures for each fluid. Typical electrode potential error was between $\pm 2\ mV$ for values measuring near zero and up to $\pm 7\ mV$ for the highest E values measuring near $900\ mV$.

7.6 Conclusions

Two to four identical aluminum thermo-syphons were tested using a heater block evaporator section and natural convection cooling over the exposed length of the tube. Fluids containing 0.0, 2.5, 5.0, and 10.0 $mmol/L$ of permanganate all with the same $80\ mmol/L$ of chromate were tested as well as pure DI water. Copper thermo-syphons of the same size and liquid charge were also tested with DI water for comparison. An infrared camera was used to visualize the NCG slug after $2\ hours\ and\ 30\ mins$ of test time. Temperature difference data and final E and pH measurements of the working fluid post-test were also compared.

The IR images and ΔT data both indicate that the higher the concentration of permanganate in the solution, the less NCG was formed over the course of the test. This also led to more stable operation and significantly lower $\Delta T's$ compared to working fluids with less permanganate. It is

believed that the more powerful oxidizer permanganate helped more thoroughly passivate the tube during initial operation so the aluminum oxide started with fewer random defects and the chromium species were conserved for buffering E and pH during operation and repairing defects or washed off oxide over the course of the test. This trend was even noticed in $Mn - 2$ test #1 which was accidentally overcharged by $\sim 12\%$ compared to the other tests, resulting in the same concentration but a larger quantity of both oxidizers.

Despite the suppression of NCG with increasing permanganate concentration, even the highest concentration of permanganate tested likely exhibited small amounts of NCG generation. Temperature limts for the stable aluminum oxide window and oxidation of water by chromates at high temperatures were checked and found to not be the cause of NCG generation for these tests. No temperature limit was reached for either scenario.

While chromate oxidizers were enough for the corrosion tests where aluminum samples were directly submerged in inhibiting solution, this was found to not be enough to suppress NCG reliably in the vertical thermo-syphons tested. For the short duration of these tests, higher concentrations of permanganate oxidizers in addition to the chromates resulted in significantly suppressed NCG generation. Longer tests are needed to determine if this trend continues to be repeatable for extended thermo-syphon lifetimes.

Approved for public release: distribution is unlimited.

8 Natural Convection, High Temperature Constant Bath Thermo-syphon Experiments

While there were clear trends in the performance of the natural convection cooled thermo-syphons heated with heater blocks, it was desired to run additional thermo-syphons in a constant temperature heated bath experiment to more precisely fix the evaporator temperature and allow for much longer test durations for the aluminum thermo-syphon experiments. Similar to the constant temperature corrosion tests in Chapter 6, the heated bath will provide a stable evaporating temperature, and thus internal pressure, to allow for better comparison of the NCG slug formed in the thermo-syphons using the infrared camera. The biggest advantage of this test setup over the previous one is that the constant temperature bath makes it easier to run longer duration tests because it is safer to leave overnight and eliminates the need for an insulated heater section which can cause inadvertent variability between tests.

8.1 Max Operating Temperature

Before starting the next test program, the same analysis performed in Chapter 7.3 was repeated to determine what the max temperature limit actually was since it was only known at that point that it was not reached at 90℃. The most conservative (highest) final pH value was used from the previous Chapter 7 experiments. Pourbaix diagrams were produced at even higher temperatures until the high temperature (red points) finally did cross the right edge of the aluminum oxide boundary in the alkaline direction. This is shown below in Figure 40.

Approved for public release: distribution is unlimited.
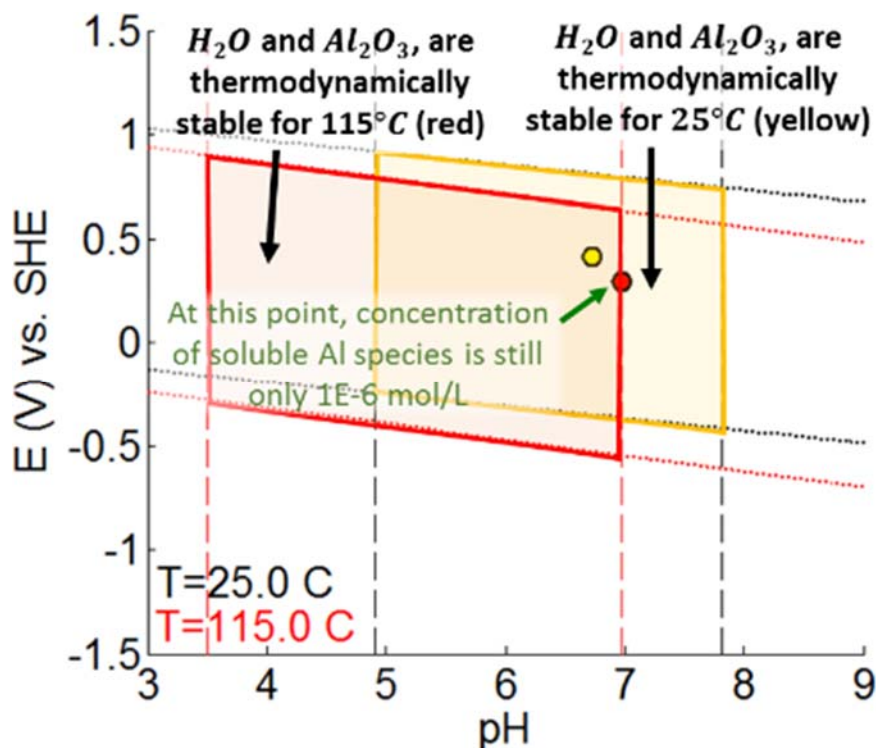
Figure 40: Pourbaix diagram for $Al - H_2O$ system at 25°C and 115°C, $C_{tot}[Al] = 10^{-6}\ mol/L$ to estimate high temperature limit before bath tests

The high temperature adjustment for the final $pH = 6.83$ point from the previous tests shows that it will not cross the boundary until $T = 115°C$. Even at this point the concentration of soluble aluminum species $(Al(OH)_4^-)$ is still only $10^{-6}\ mol/L$ which is the limit above which corrosion is considered to have occurred by most corrosion science conventions. In order to provide even more small margin for error the temperature of the constant temperature bath evaporator in this experimental chapter will be set to $T = 110°C$. Once the experiments have been run the fluids will again be measured post-test and actual final pH values will be used to replace the values from the previous chapter to check that the limit holds.

8.2 Test Setup

Using the silicone oil heated bath from the corrosion tests as the heat input, a new thermo-syphon experimental setup was built to study additional inhibitor fluids in aluminum thermo-syphons. A side view of the setup can be seen below in Figure 41.
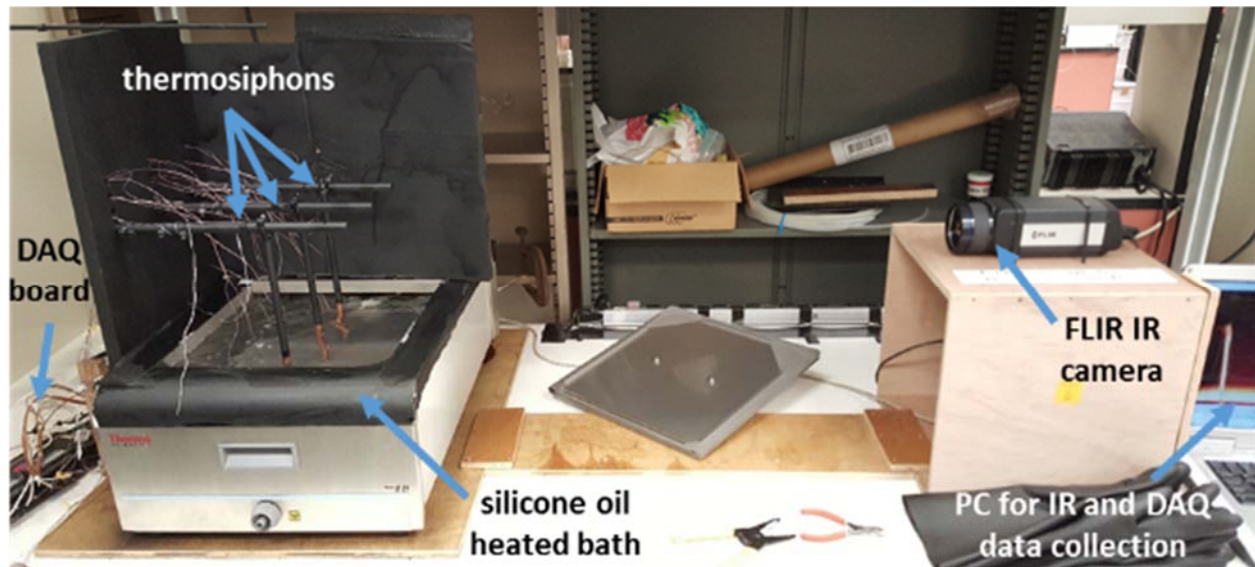
Figure 41: Side view of heater bath thermo-syphon test setup

Natural convection was again used for heat rejection in the condenser of the thermo-syphons. Figure 42 shows back and front views of the test setup where the thermocouples, DAQ board and bath are more visible.
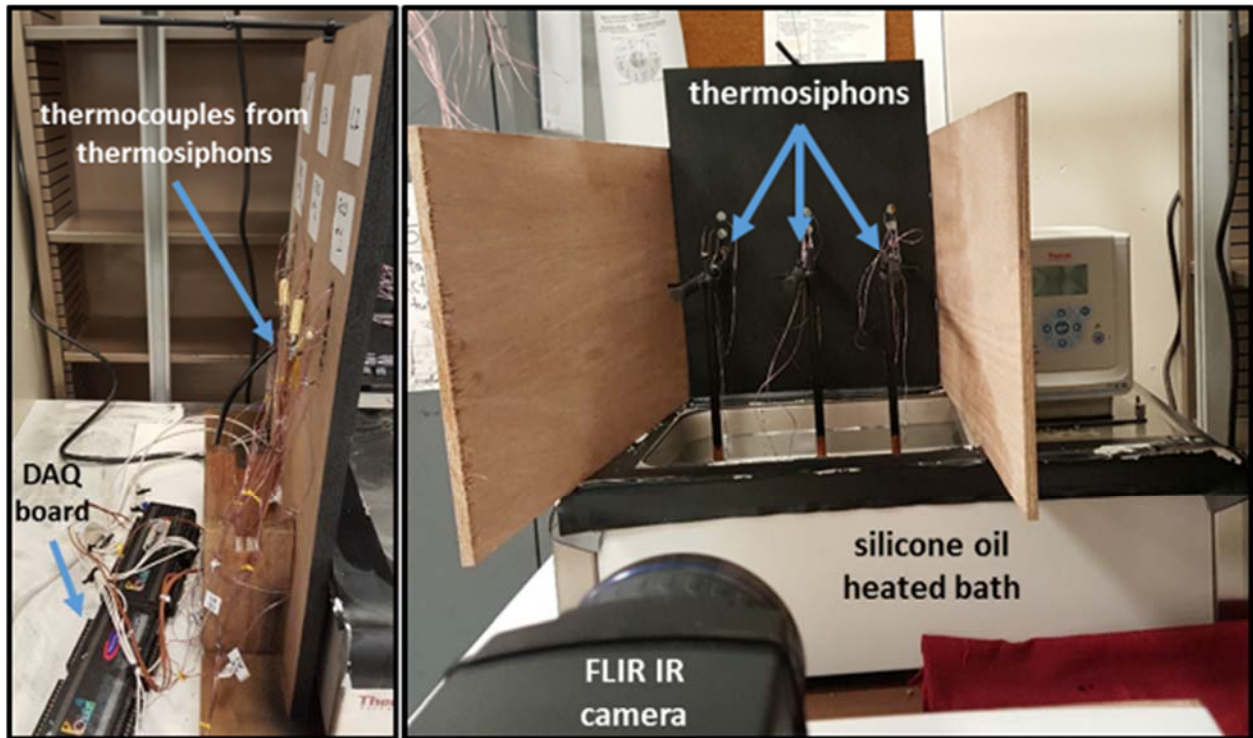
Figure 42: Back (left) and front (right) views of heated bath thermo-syphon test setup

Figure 43 provides a birds' eye view of the setup to show locations of the different thermo-syphons and a map of the names of each of the six possible thermo-syphons; front or back attached to one of three dowel rods supporting the top of the tube.
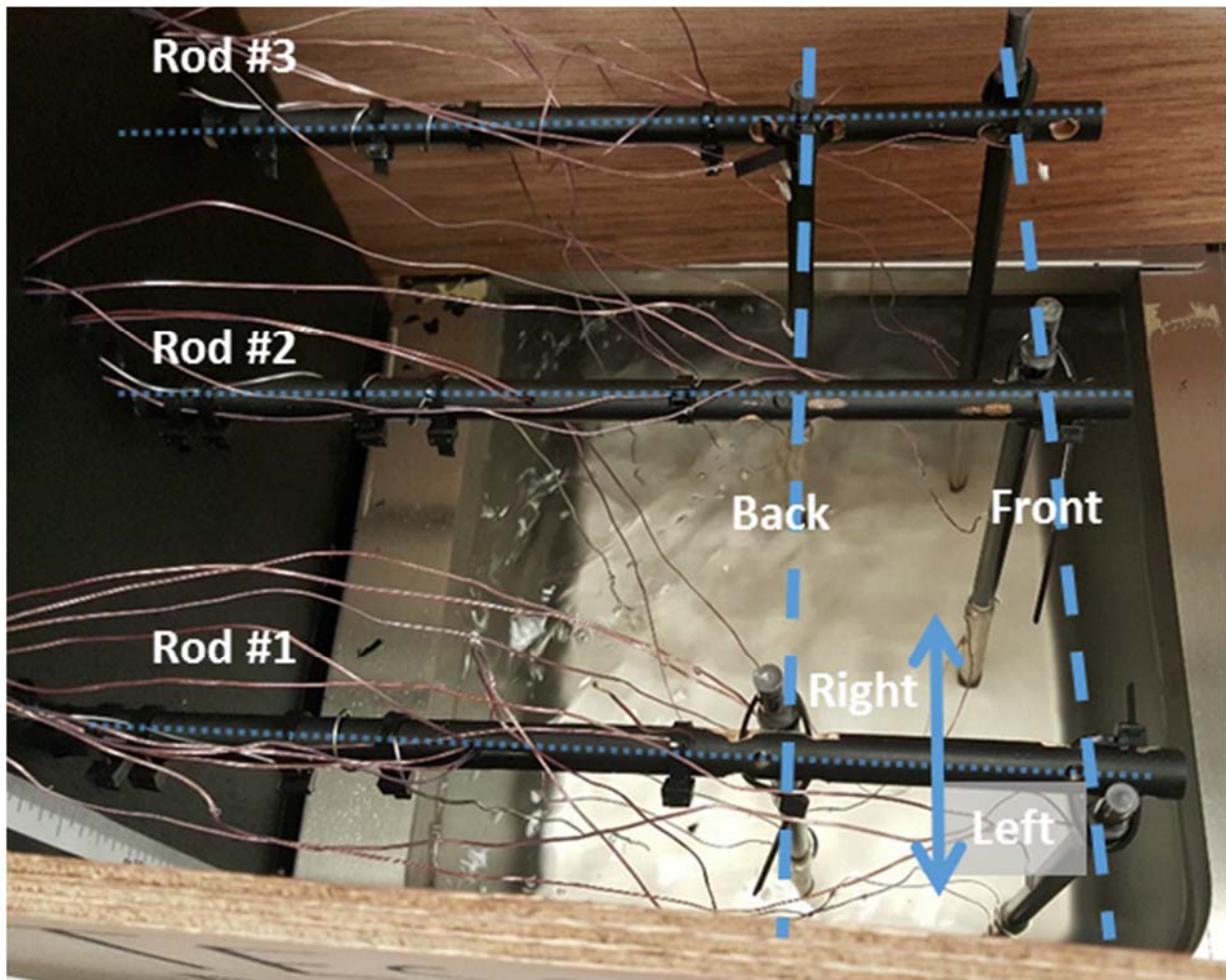
Figure 43: Top view of heated bath showing thermo-syphon location naming convention

Thermo-syphons for this test were made of the same aluminum 6061-T6 alloy with the same OD and ID dimensions as previous tests. Tube assembly including cap sizes, fill tube, and JB weld sealing were the same as previous tests as well. One difference in tube geometry from the tests of Chapter 7 was that the overall tube length and heater length were changed. These thermo-syphons were 30 cm in length and the heated bath liquid height, the evaporator length, was 12.5 cm. The change was necessary because of the minimum liquid height required for the heated bath circulator to function. Following the same charge volume convention used previously, a larger liquid charge of 3.0 mL was used for all tests in this experiment due to larger evaporator length.

This had the added benefit of decreasing the percent variability between charge volumes as well.

A schematic of all dimensions and thermocouple placement can be found below in Figure 44.
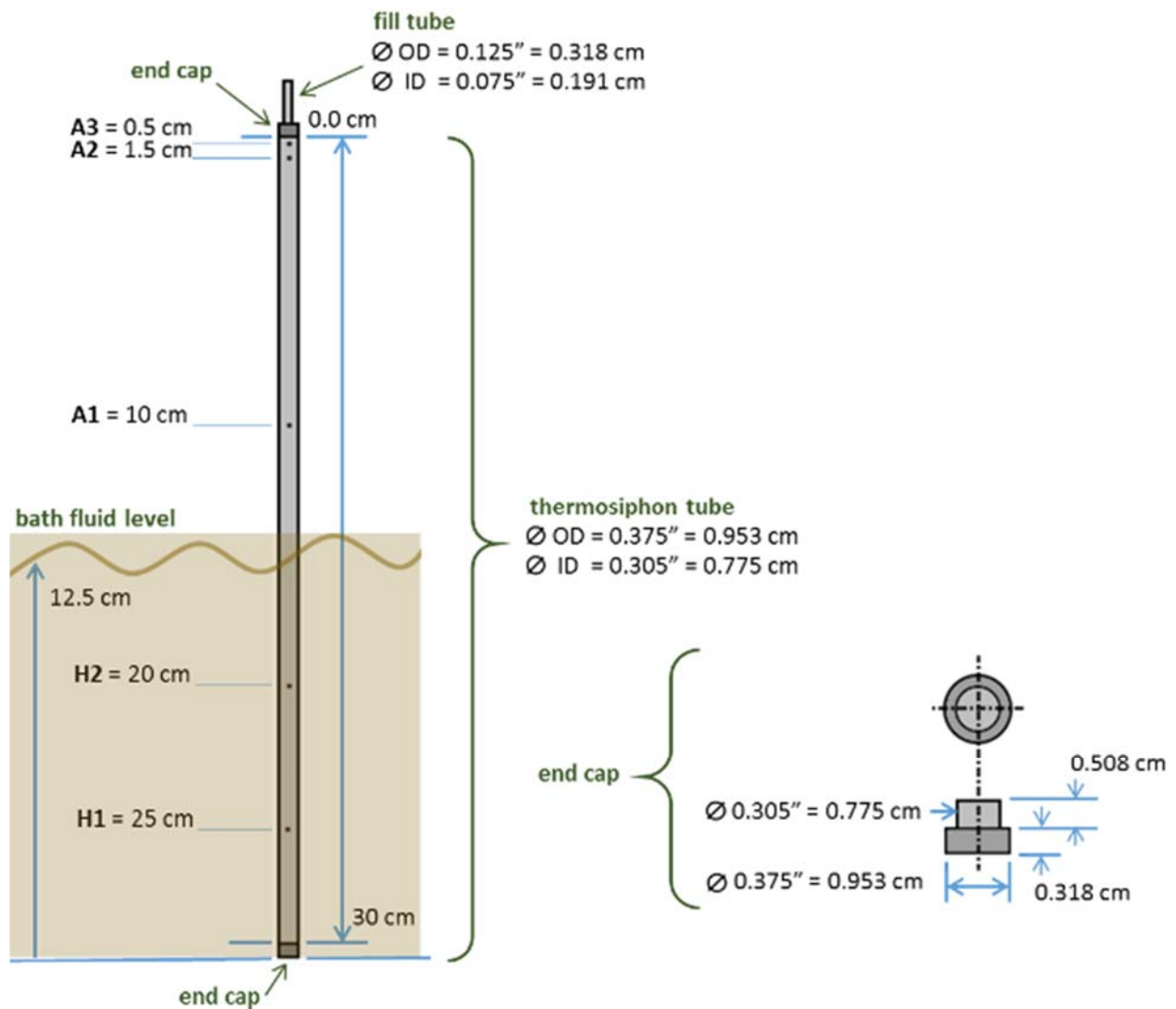
Figure 44: Thermo-syphon and heated bath dimensions with thermocouple map

The bath temperature was kept at a constant 110°C for all tests which resulted in a consistent temperature measurement on the thermo-syphon itself of 106°C. Once tube assembly, sealing, and charging were performed identically to the methods used in Chapter 7, the instrumented thermo-syphons were first attached to the rods without dunking them in the heated bath while thermocouples were threaded through the back of the wooden board behind the bath

Approved for public release: distribution is unlimited.

and connected to the DAQ56 board. Type-T thermocouples with SLE were once again used. The thermo-syphons were then carefully lowered into the heated bath at temperature using a temperature resistant glove to prevent burns hands during the process. High temperature zip ties were used to secure the excess fill tube portion of the thermo-syphon to each rod with the bottom end firmly fixed to the floor of the bath, keeping them in vertical orientation. Thermocouple temperature data and IR images were recorded throughout the experiment test time.

8.3 Results and Discussion

For this experiment, only two inhibitor fluids from the previous tests were used. $Mn - 0$ (chromium only) fluid was selected to see if the shorter tubes, different evaporator configuration or other modifications had any impact on the passivation potential of the chromium only fluid. The $Mn - 4$ fluid was selected because it was the best performing fluid from the last set of thermo-syphons. A new fluid named $Mn - 3, Cr - 3$ was also made containing $8.35\ mmol/L$ of permanganate ($\sim 3x$ the amount in $Mn - 1$ fluid) and $231.47\ mmol/L$ of chromate ($\sim 3x$ the amount in all other fluids, $Cr - 1$ designation). This fluid was made to provide more chromium backup oxidizers for repair passivation along with a slightly smaller permanganate concentration to scale the concentration with the 25% shorter length of the thermo-syphons, corresponding roughly to a reduction in available aluminum surface area to be reacted. Aluminum/water and copper/water combinations were also tested for reference. Table 14 shows the exact fluid concentrations used, before and after E and pH measurements, fluid charge volumes and test names for each thermo-syphon.

Table 14: Bath test thermo-syphon test matrix and fluid information

Metal/Fluid	Tube	Charge (g)	Initial pH	Final pH	ΔpH	Initial E (mV SHE)	Final E (mV SHE)	ΔE (mV SHE)	$[Mn^{+7}]$ (mmol/L)	$[Cr^{+6}]$ (mmol/L)	Mn^{+7} (μmol)	Cr^{+6} (μmol)
Al/H$_2$O	D1	3.0006	7.00	8.74	1.74	-281	454	735	0.00	0.00	0.00	0.00
	D2	3.0423	7.00	9.73	2.73	-281	462	743	0.00	0.00	0.00	0.00
	D3	2.9882	7.00	9.23	2.23	-281	424	705	0.00	0.00	0.00	0.00
Cu/H$_2$O	C1	3.0682	-	-	-	-	-	-	0.00	0.00	0.00	0.00
	C2	2.9487	-	-	-	-	-	-	0.00	0.00	0.00	0.00
	C3	2.8588	-	-	-	-	-	-	0.00	0.00	0.00	0.00
Al/Mn-0,Cr-1	E3	3.0017	6.33	6.46	0.13	524	497	-27	0.00	79.56	0.00	238.82
	E4	4.0762	6.33	6.44	0.11	524	520	-4	0.00	79.56	0.00	324.31
	E5	2.9995	6.33	6.52	0.19	524	480	-44	0.00	79.56	0.00	238.65
Al/Mn-4,Cr-1	E1	3.0966	5.92	6.36	0.44	974	499	-475	10.01	79.48	31.01	246.13
	E2	3.0911	5.92	6.39	0.47	974	520	-454	10.01	79.48	30.95	245.70
	E6	3.0965	5.92	6.80	0.88	974	493	-481	10.01	79.48	31.00	246.12
	F2	3.1701	5.92	6.61	0.69	974	506	-468	10.01	79.48	31.74	251.97
Al/Mn-3,Cr-3	G1	3.0382	6.23	6.54	0.31	981	453	-528	8.35	231.47	25.37	703.26
	G2	3.2081	6.23	6.50	0.27	981	496	-485	8.35	231.47	26.79	742.59
	G3	6.7926	6.23	6.55	0.32	981	501	-480	8.35	231.47	56.73	1572.30

The same performance metric was used for measuring degradation due to NCG growth with a temperature difference metric,

$$\Delta T = H_{avg} - A3 \tag{69}$$

which is the same as the previous 7 tests. The $A3$ thermocouple is 0.5 *cm* from the top of the tube exactly like it was for the 45 *cm* long thermo-syphons. Figure 45, Figure 47, and Figure 49 are below containing *ΔT* data for all tests on each graph for the first 5, 24, and 72 hours of test time, respectively. The same data was split into three figures so that more detail was visible for shorter test times due to the large amount of data presented. Each fluid used corresponds to its own line color, as indicated in the legends, with each test identified with the tube name on the data line to which it belongs.
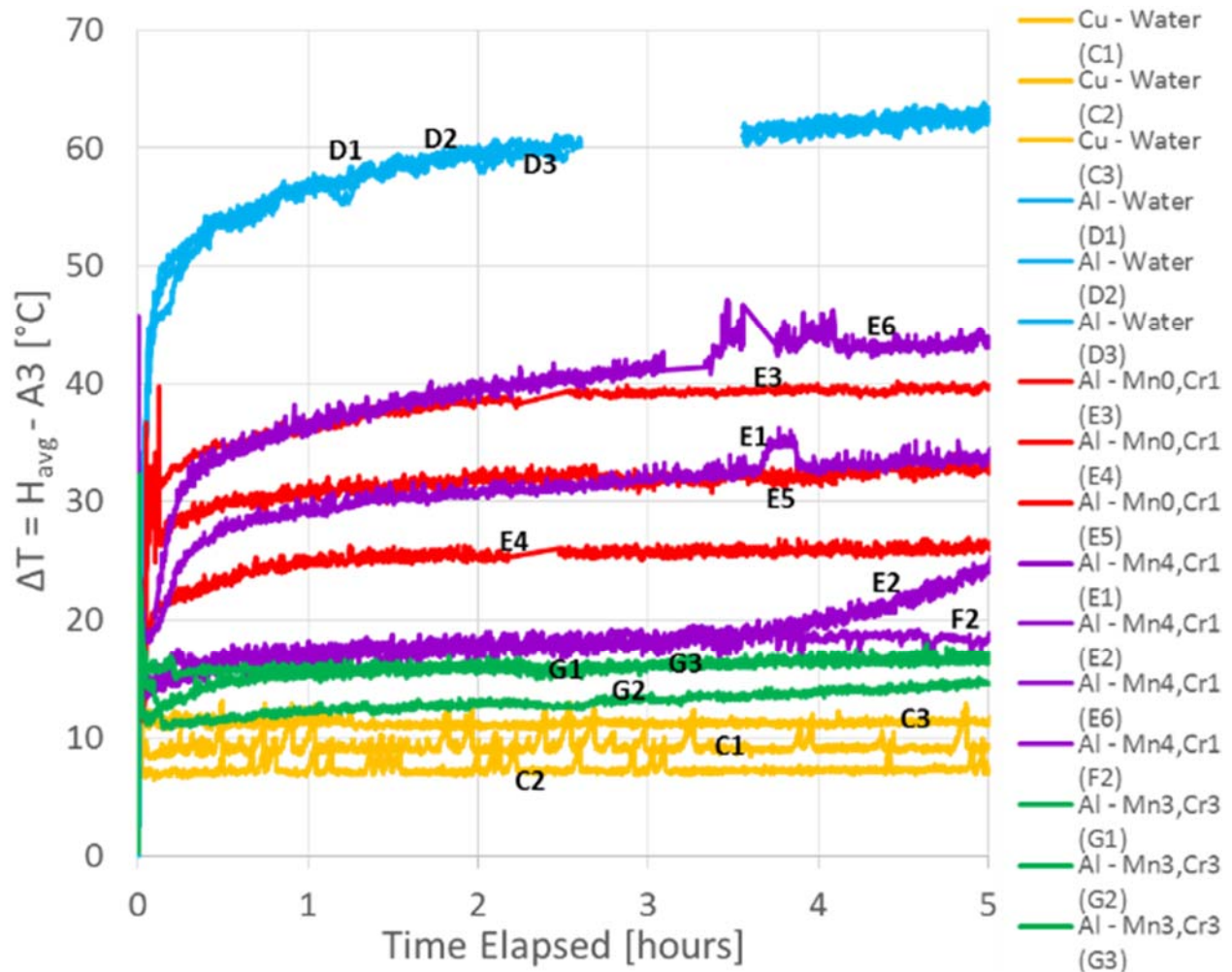
Figure 45: Bath test, $\Delta T = H_{avg} - A3$ vs. time, 1st 5 $hours$, all tests

From Figure 45, showing the first 5 $hours$ of test time, it is already apparent that water immediately generated a very large amount of NCG. The three copper/water thermo-syphons performed with low ΔT and showed no change over the course of the entire 72 hour test. Fluids with the $Mn - 3, Cr - 3$ fluid performed second best within the first 5 $hours$, followed by two of the four $Mn - 4$ tests. The other two $Mn - 4$ tests performed inconsistently much like the $Mn - 0$ tests. IR images at exactly 5 $hours$ of elapsed test time are shown in Figure 46.

Approved for public release: distribution is unlimited.
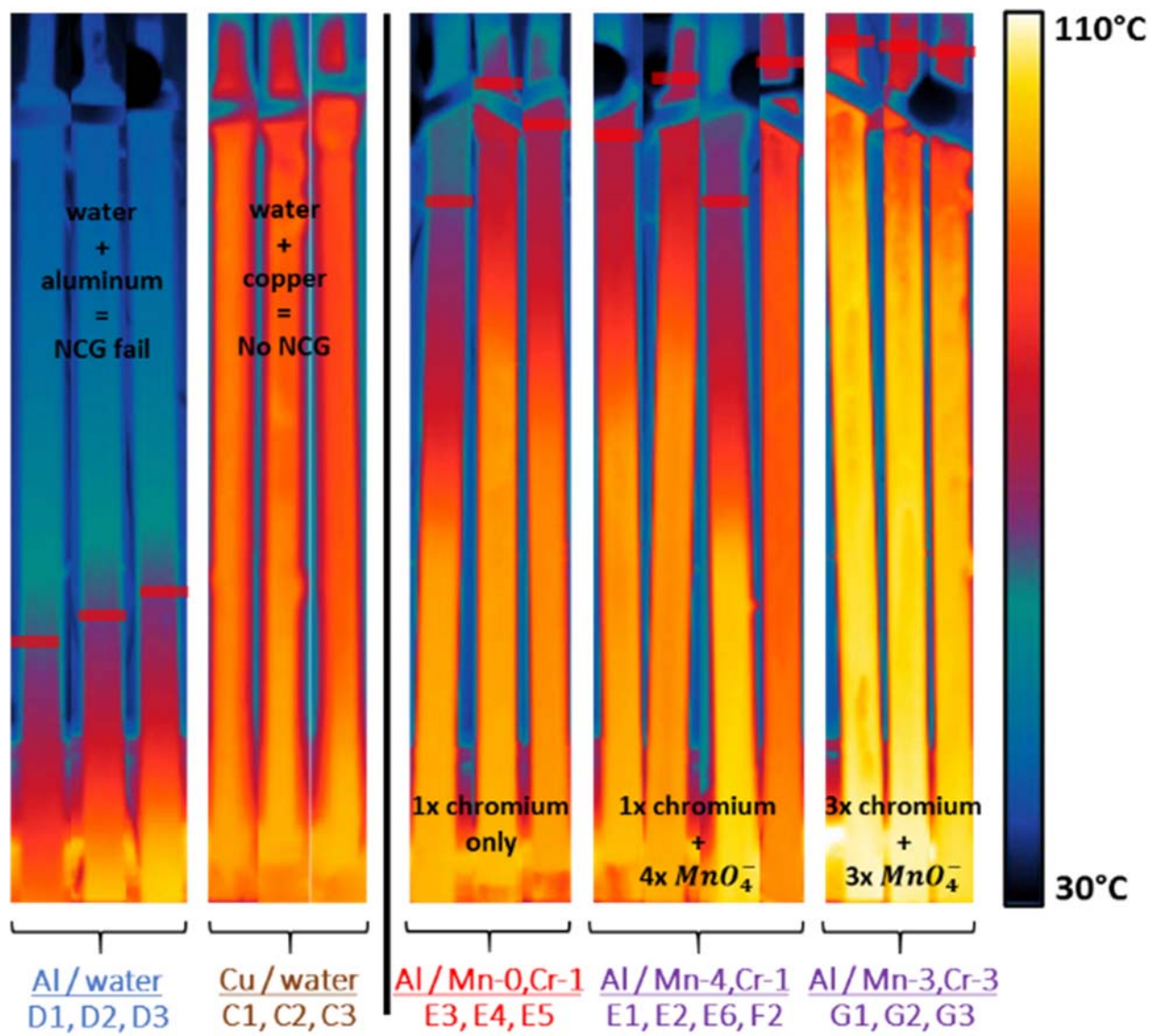
Figure 46: Natural convection, constant temperature bath infrared images, 5 $hours$ elapsed test time

The IR images agree with the ΔT data showing that all the water/aluminum tests are already almost entirely filled with NCG while the copper/water tubes show no NCG and are nearly isothermal. The thermo-syphons charged with $Mn - 3, Cr - 3$ also perform well and do not appear to show any NCG in the IR images after 5 $hours$. The $Mn - 0$ and $Mn - 4$ fluids fall randomly roughly halfway in between the isothermal thermo-syphons and completely gas-filled aluminum water tests.

It is worth noting that $Mn-0$ test $E4$ was accidentally overcharged to $4.0762\ mL$ and $Mn-3, Cr-3$ test $G3$ was significantly overcharged to $6.7926\ mL$. The other tests were all within $\sim7\%$ of the intended $3.0\ mL$ charge, and most were within $\sim4\%$. The ΔT data in Figure 47 shows the first 24 hours of test time. It shows that some of the tests which initially performed well begin to generate large amounts of NCG after the first 5 $hours$ have passed. Specifically, all three $Mn-3, Cr-3$ tests and the two best performing $Mn-4$ tests $(E1, E2)$ increased ΔT such that after 24 hours of test time they had performance almost identical to water.
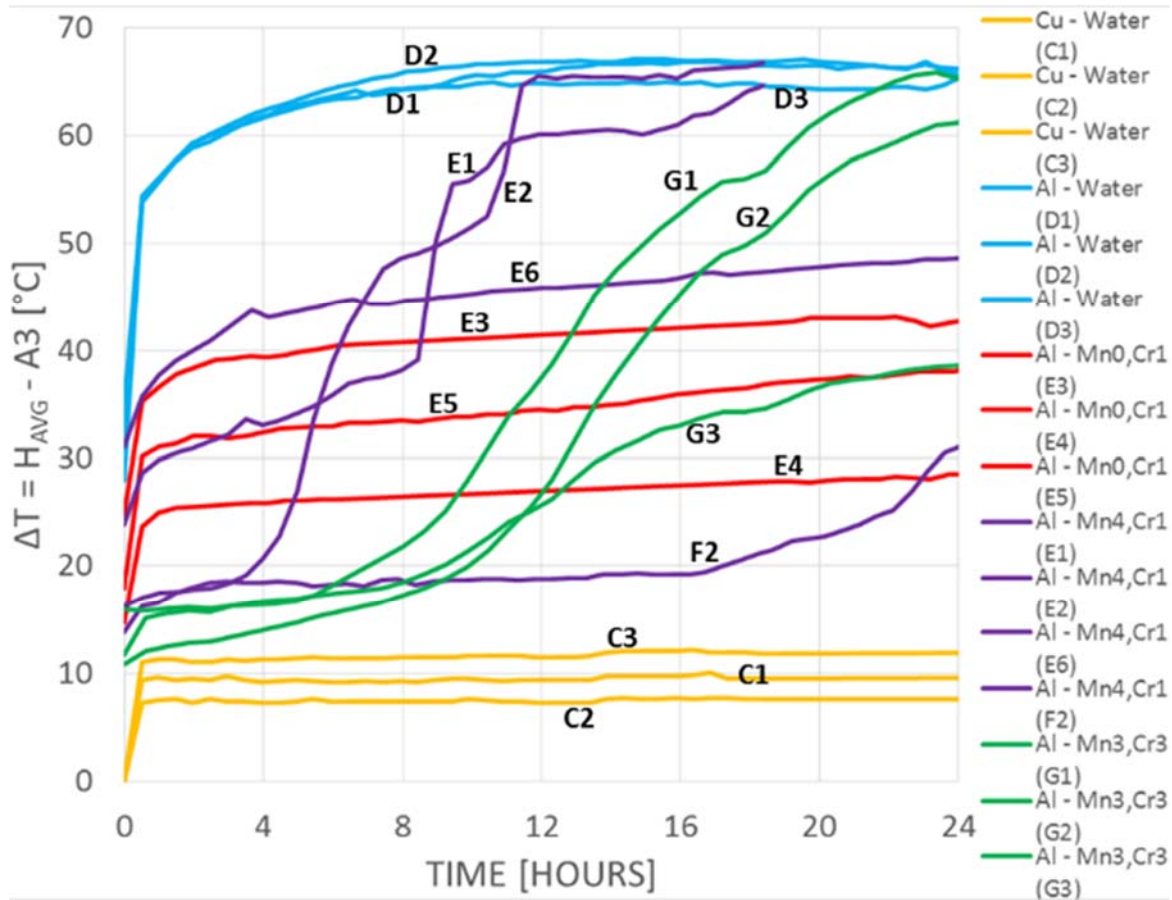
Figure 47: Bath test, $\Delta T = H_{avg} - A3$ vs. time, 24 $hours$, all tests

Figure 48 contains the IR images at exactly 24 hours of elapsed test time and visually shows the large increase in NCG generation between hour 5 and hour 24.
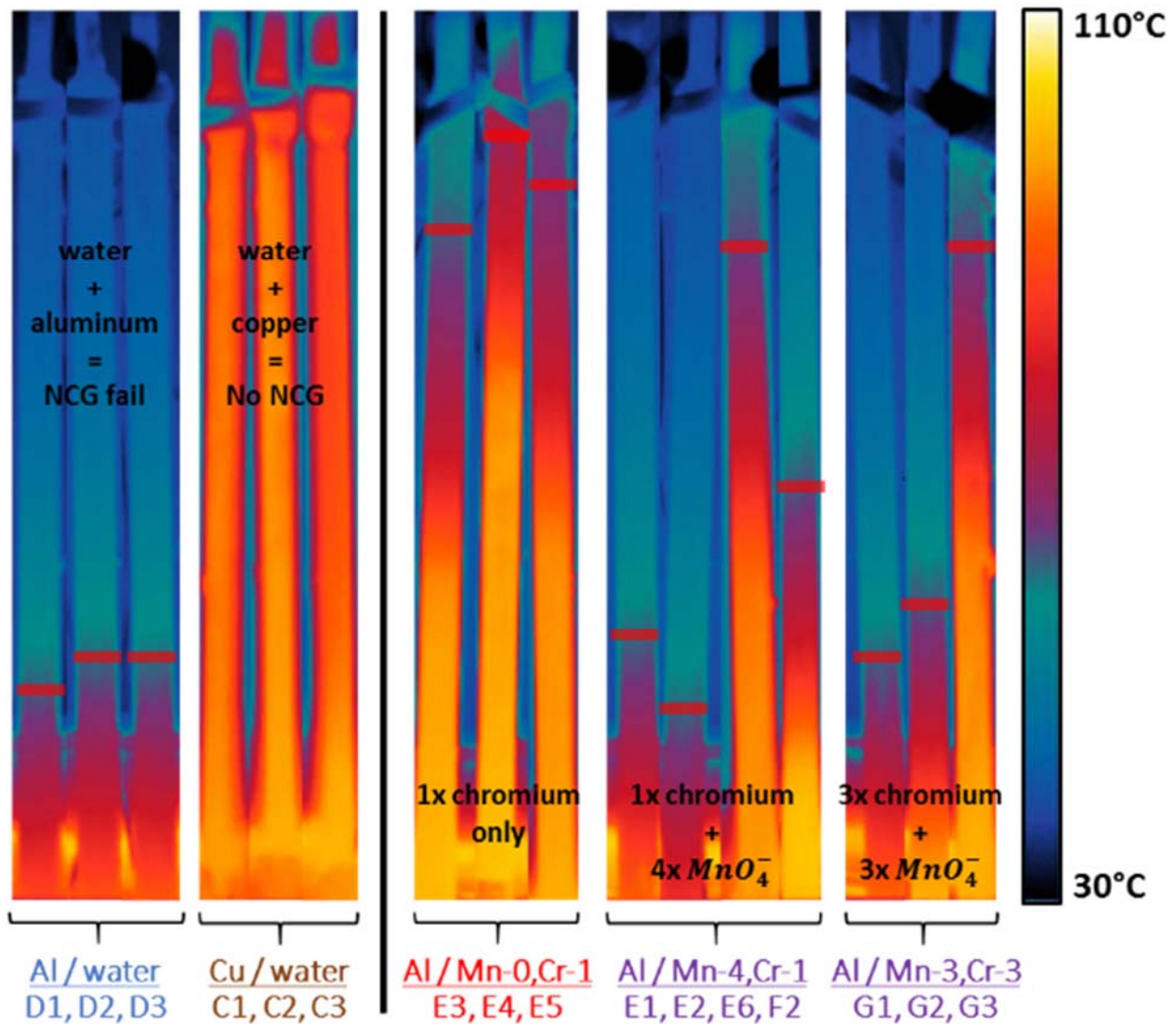
Figure 48: Natural convection, constant temperature bath infrared images, 24 $hours$ **elapsed test time**

The best performing fluids with aluminum thermo-syphons are now the $Mn - 0$ tests by virtue of not generating significantly more NCG between hour 5 and hour 24. They have increased $\varDelta T$ about 5℃ each at a mostly constant rate. Their IR images also exhibit only a slightly larger NCG slug at hour 24 versus hour 5.

Figure 49 contains the entire 72 $hours$ of test time. Some tests were discontinued before this limit if they reached significant amounts of NCG generation so that other tests could be started

in their place since there was only room for up to 6 tests at once and usually not more than three because it obstructed the IR camera's view.
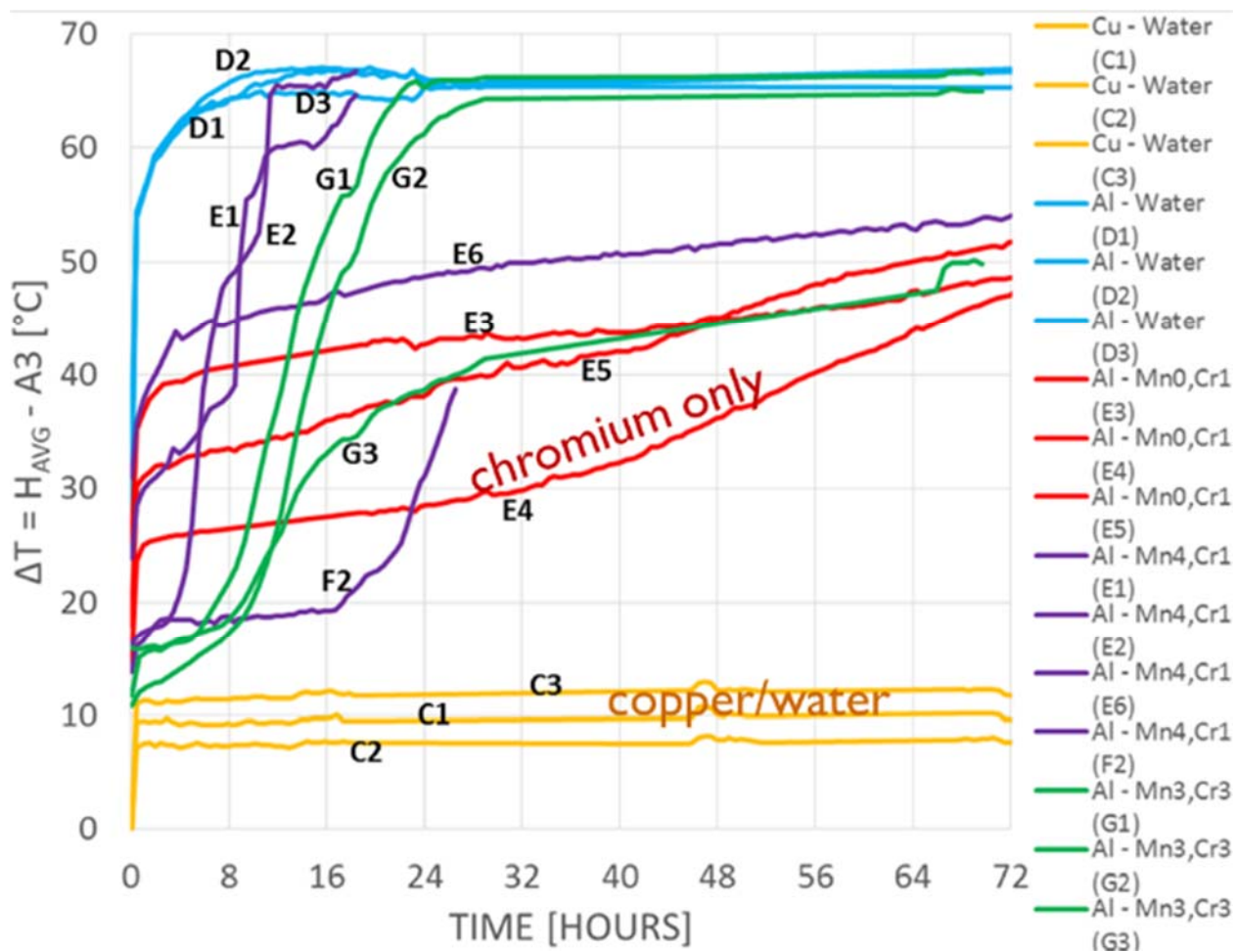
Figure 49: Bath test, $\Delta T = H_{avg} - A3$ vs. time, 72 $hours$, all tests

After 72 $hours$ the copper thermo-syphons continued to perform the same while most of the aluminum thermo-syphons have increased ΔT to that of water at this point. The exceptions are the three $Mn - 0$ tests, one of the $Mn - 3, Cr - 3$ tests ($G3$), and one of the $Mn - 4$ tests ($E6$) which all continued to generate NCG at a unacceptable but still constant rate.

The high temperature limit calculated earlier in this chapter, using the previous thermo-syphon experimental fluid measurements of Chapter 7, can now be updated with the actual E and

pH measurements from the current experiments. This was performed and checked against a Pourbaix diagram shown below in Figure 50.
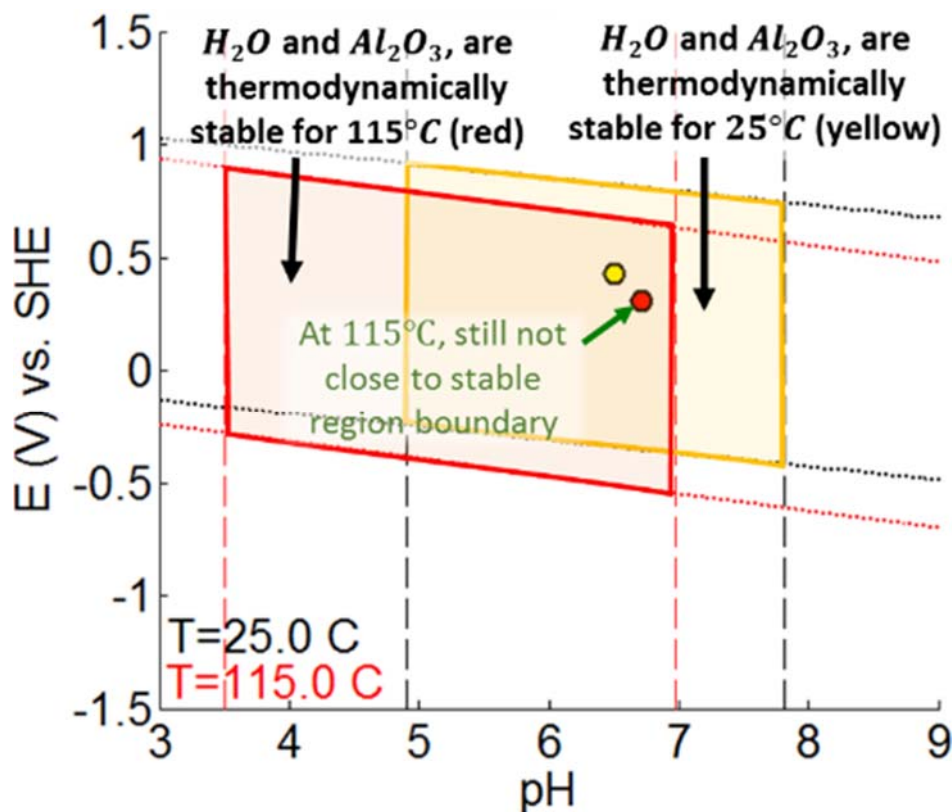
Figure 50: Pourbaix diagram for $Al - H_2O$ system at 25℃ and 115℃, $C_{tot}[Al] = 10^{-6} \, mol/L$ to check high temperature limit estimate made before bath tests

The results show that the previous estimate using prior fluid measurements was conservative and that no high temperature limit was reached for the current bath heated thermo-syphons. This is likely because the max final pH for this set of experiments was only $pH = 6.50$.

It can be concluded that for short periods of time both natural convection thermo-syphon experiment sets indicate that higher concentrations of permanganate oxidizer are beneficial for short time periods, about 5 $hours$. For tests running longer than that, thermo-syphons with chromates only significantly outperform any tube with permanganate. The fact that the 5 $hour$ data trends are the same for both experiment types and that the current test continued to fail more

Approved for public release: distribution is unlimited.

after that period suggest that another mechanism is at play causing NCG generation. One likely cause of this is discontinuous return flow which would not affect the readings in the evaporator fluid measurements because with the circuit disconnected the chromates would not be consumed, thus explaining the higher potentials measured, despite the NCG generation.

8.4 Uncertainty Analysis

The 95% uncertainty of the type-T thermocouples used was $\pm 1.21°C$ for a single temperature measurement and $\pm 1.71°C$ for each ΔT measurement. The calculation for this is shown in Table 15.

Table 15: PDAQ 56, type-T thermocouple error

PDAQ 56: Type-T Thermocouple Error				
Source	Value (+/-)	Shape	Divisor	Std Unc (°C)
Resolution	0.005	Uniform	1.73	0.0029
DAQ+CJ	1.1	Normal	2	0.55
TC Wire (SLE)	0.5	Normal	2	0.25
T Combined Standard Uncertainty =				0.60
T Expanded Uncertainty (95%, std. dist.) =				1.21
ΔT Standard Uncertainty =				0.85
ΔT Expanded Uncertainty (95%, std. dist.) =				1.71

The pH and E measurements were both done using Omega probes. The pH measurements have an accuracy of $\pm 0.02\ pH + 2d$ ($\pm 0.04\ pH$ units) while the E measurements are $\pm 0.5\% + 2d$, giving accurate measures for each fluid. Typical electrode potential error was between $\pm 2\ mV$ for values measuring near zero and up to $\pm 7\ mV$ for the highest E values measuring near $900\ mV$.

8.5 Conclusions

Aluminum thermo-syphons with different oxidizer inhibitor solutions as the working fluid were tested in a vertical, natural convection cooled test setup heated by a constant temperature silicon oil bath fixed at a constant 110°C. Temperature difference data, IR images, electrode potential, and pH measurements were given for each test over the course of 72 hour experiments. The results indicate that none of the designed fluids were capable of fully resisting NCG generation but were successful, to varying degrees, at suppressing the formation of hydrogen gas. Over the first 5 *hours* of test time, for both the current experiments in the heated bath and previous thermo-syphons from Chapter 7, higher permanganate concentrations helped resist NCG generation. For longer tests chromium only fluids significantly outperformed any test thermo-syphon containing permanganate.

The utility of the permanganates for short term tests is likely because they help provide stronger oxidizing ability near the start of the test to reduce initial NCG generation. However, it is very difficult to add permanganate without having extra chemicals left in solution after the brief initial passivation period. The leftover permanganate likely disassociates into oxygen gas and manganaese oxide, thereby forming more NCG than chromates alone for longer duration experiments.

The fact remains that no tests thus far have entirely resisted NCG generation despite the efforts using different inhibitor concentrations, test configurations, temperatures, and even tube preparation method. The working theory on why the thermodynamics predict passivation while the experimental results indicate NCG gas was formed is due to the flow regime of the liquid backflow which is required to complete the electrochemical circuit and return excess H^+ ions from

Approved for public release: distribution is unlimited.

the remote parts of the thermo-syphon to the liquid in the evaporator. The shorter tube length and higher liquid charge amount apear to have helped somewhat in forcing a more continuous flow but not enough to prevent an unacceptable amount of NCG from forming. The next chapter will introduce this failure mode and how it might be overcome through careful design of the next thermo-syphon experiments.

9 Indirect Passivation and Continuous Backflow

9.1 Electrochemical Cycle

The previous Chapters 4 and 5 discussions of chromate and permanganate oxidizer effects on an aluminum surface reflect what will occur when they are in direct contact. However, in a PCHT device the inhibitors may or may not always be in direct contact with the exact location which requires oxide coating or repair. Electrochemistry describes chemical reactions between an electrolytic solution [71] and an electron conductor (aluminum surface) that result in electron transfer between the metal electrode and the electrolyte solution. The application in the case of using IAS in an aluminum PCHT device is to use electrochemistry to prevent hydrogen generating reactions by providing alternative reactions which are preferred by the aluminum surface resulting in a protective oxide coating throughout the tube.

Without this circuit, shown below in Figure 51, it is believed that the aluminum oxidation and passivating oxide coating would only exist in the evaporator section and the pipe would fail.
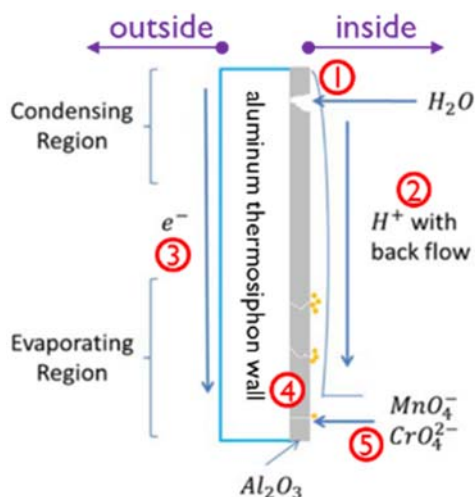

Figure 51: Electrochemical circuit enabling remote aluminum surface passivation [35]

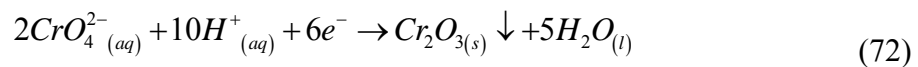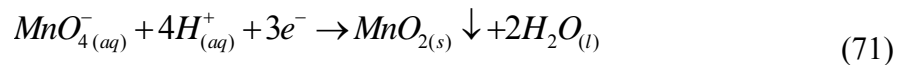Approved for public release: distribution is unlimited.

This would result because evaporated IAS fluid contains only water vapor and this would then react with the bare aluminum which would remain unprotected in this scenario.

The circuit shown in Figure 51 is described with the following steps, also shown on the diagram above. If the aluminum surface contacts pure water in a region not in direct contact with oxidizers (i.e. condenser and/or adiabatic sections), it will undergo the following reaction steps:

1) Each aluminum atom is oxidized and loses 3 electrons and forms aluminum oxide at that location while releasing excess H^+ ions into the water via the following half-reaction,

$$2Al_{(s)} + 3H_2O_{(l)} - 6e^- \rightarrow Al_2O_{3(s)} \downarrow + 6H^+_{(aq)} \tag{70}$$
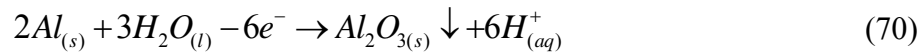
2) Excess H^+ ions are carried back to the evaporator section with the condensed liquid.

3) Electrons conduct through the aluminum tube.

4) Electrons conduct across the oxide layer in the evaporator.

5) Permanganate or chromate are reduced in the evaporator, consuming the excess H^+ ions and generating either manganese or chromium oxide via the following half reactions,

$$MnO_{4\,(aq)}^- + 4H^+_{(aq)} + 3e^- \rightarrow MnO_{2(s)} \downarrow + 2H_2O_{(l)} \tag{71}$$

$$2CrO_{4\,(aq)}^{2-} + 10H^+_{(aq)} + 6e^- \rightarrow Cr_2O_{3(s)} \downarrow + 5H_2O_{(l)} \tag{72}$$

The electrochemical circuit described presents a method by which the aluminum surface can be passivated and protected everywhere, continuously, despite the fact that oxidizers exist only in the evaporator section of the heat pipe. Aluminum oxide is compact and generally known as an electrical insulator but it is not generated as a single continuous sheet. Some electrons are able to be transported through gaps between different pieces of oxide coating but the insulating nature of the oxides may diminish the maximum electron flux which can be transported through the

aluminum device and ultimately be a limiting factor in device passivation. Using a fluid flow analogy, this conduit must be large enough to support the electron flux through the aluminum tube.

9.2 Discontinuous Flow

If the returning liquid condensate flow from the condensing region is interrupted then the H^+ ions will remain in the condensing region and not complete their required journey back to the evaporator to combine with the oxidizers. This problem is illustrated below in Figure 52.
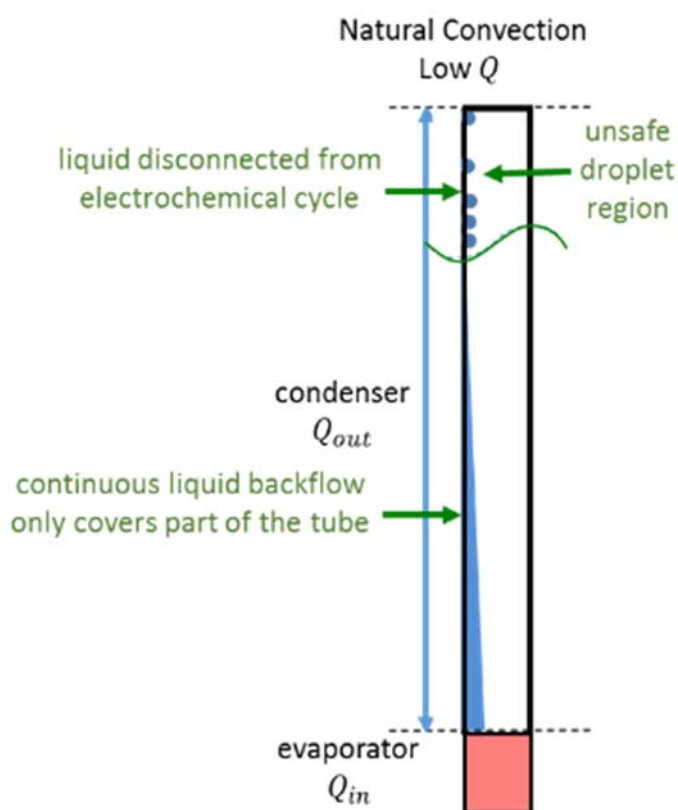
Figure 52: Demonstration of how natural convection cooling for thermo-syphons will create an unsafe droplet condensation region

The low condensation flux for natural convection cooled thermo-syphons poses a problem for establishing a continuous return liquid flow. This is because the overall heat transfer for natural convection thermo-syphons is low and using such a large area of the tube body for condensation

Approved for public release: distribution is unlimited.

area results in an even lower condensation flux. This makes it more difficult for a liquid film to form at the top of the tube and droplet condensation is likely to occur. The unsafe droplet region will have pure liquid water disconnected from the electrochemical cycle and hydrogen gas will be formed there as it would in a thermo-syphon without inhibitors. It is critical to understand how to shrink this region. Below, in Figure 53, methods for reducing the droplet region are shown.
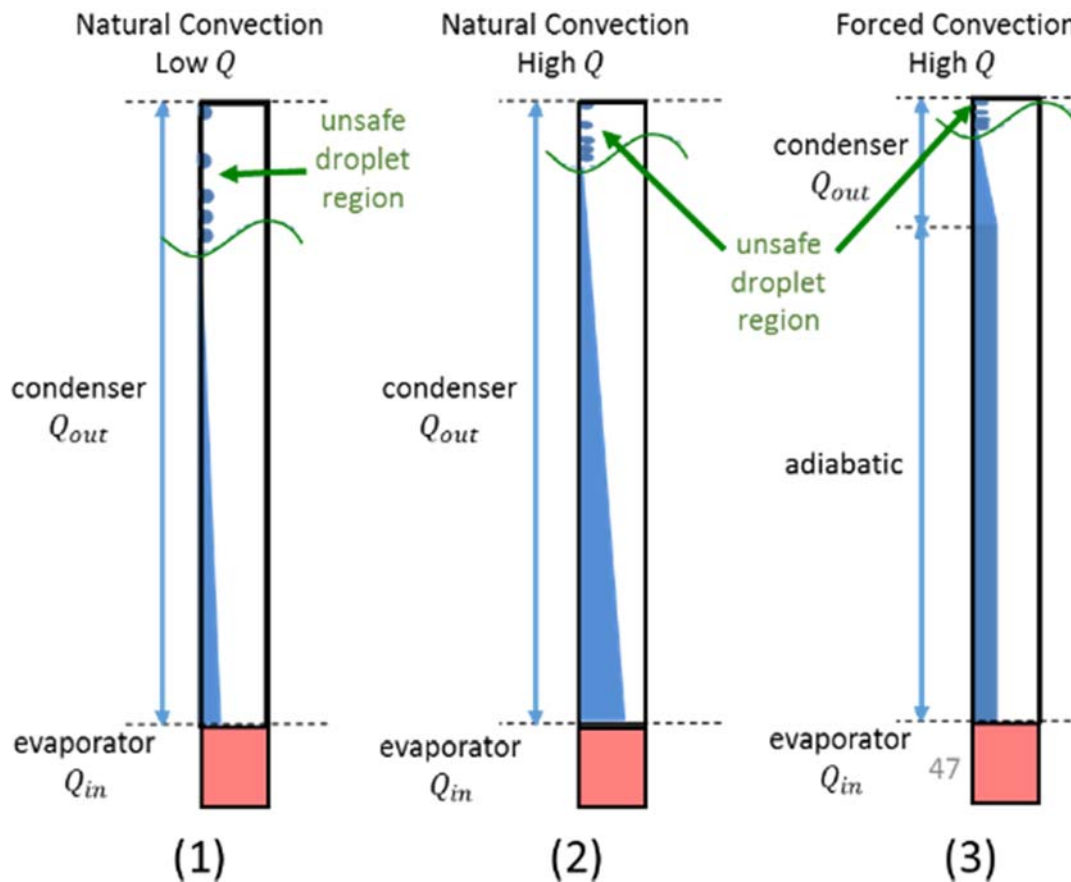
Figure 53: How to reduce the size of the unsafe droplet region in thermo-syphons

Thermo-syphon (1) represents the thermo-syphons tested in Chapter 7 where the condensing area was very large and overall Q through the thermo-syphon was low, $10\,W$. Thermo-syphon (2) represents the thermo-syphons teste in Chapter 8 where input power was higher and the area for condensation was much smaller, but natural convection cooling was still

Approved for public release: distribution is unlimited.

used. Thermo-syphon (3) represents the case where a small area, forced convection condenser is used such that overall Q through the thermo-syphon is high and condensing area is low, resulting in a much higher condensing flux than either thermo-syphon (1) or (2). The thermo-syphon (3) case will result in a much smaller unsafe droplet region and less NCG generated. This theory will be tested in the following experimental chapter using forced convection cooling blocks.

Approved for public release: distribution is unlimited.

10 Forced Convection, Heater Block Thermo-syphon Experiments

A thermo-syphon experimental setup identical to that used in Chapter 7 was created with the exception that it is now cooled via forced water convection through a cooling block and it is insulated throughout the adiabatic region. This change was made so that the more capable and smaller condenser section would lead to a more continuous liquid backflow to maintain a complete electrochemical circuit with greater reliability and produce less NCG when lone water droplets stagnate on the surface of the aluminum tube interior away from the evaporator section where the inhibitors reside. The unsafe droplet region will be smaller and less NCG should be generated for these tests.

10.1 Test Setup

This new experiment uses tubes with the exact geometry, assembly method, and charging methods as those used in Chapter 7. A schematic overview of this setup is shown below in Figure 54.
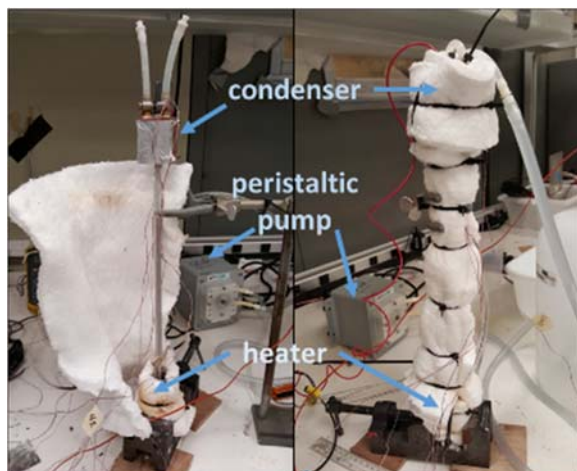
Figure 54: Forced convection, vertical thermo-syphon test setup

The thermo-syphons are 45 cm in length again and heated by a copper heating block fitted with ceramic cartridge heaters. Figure 55 below shows dimensions of all test components and a map of the thermocouple locations used.
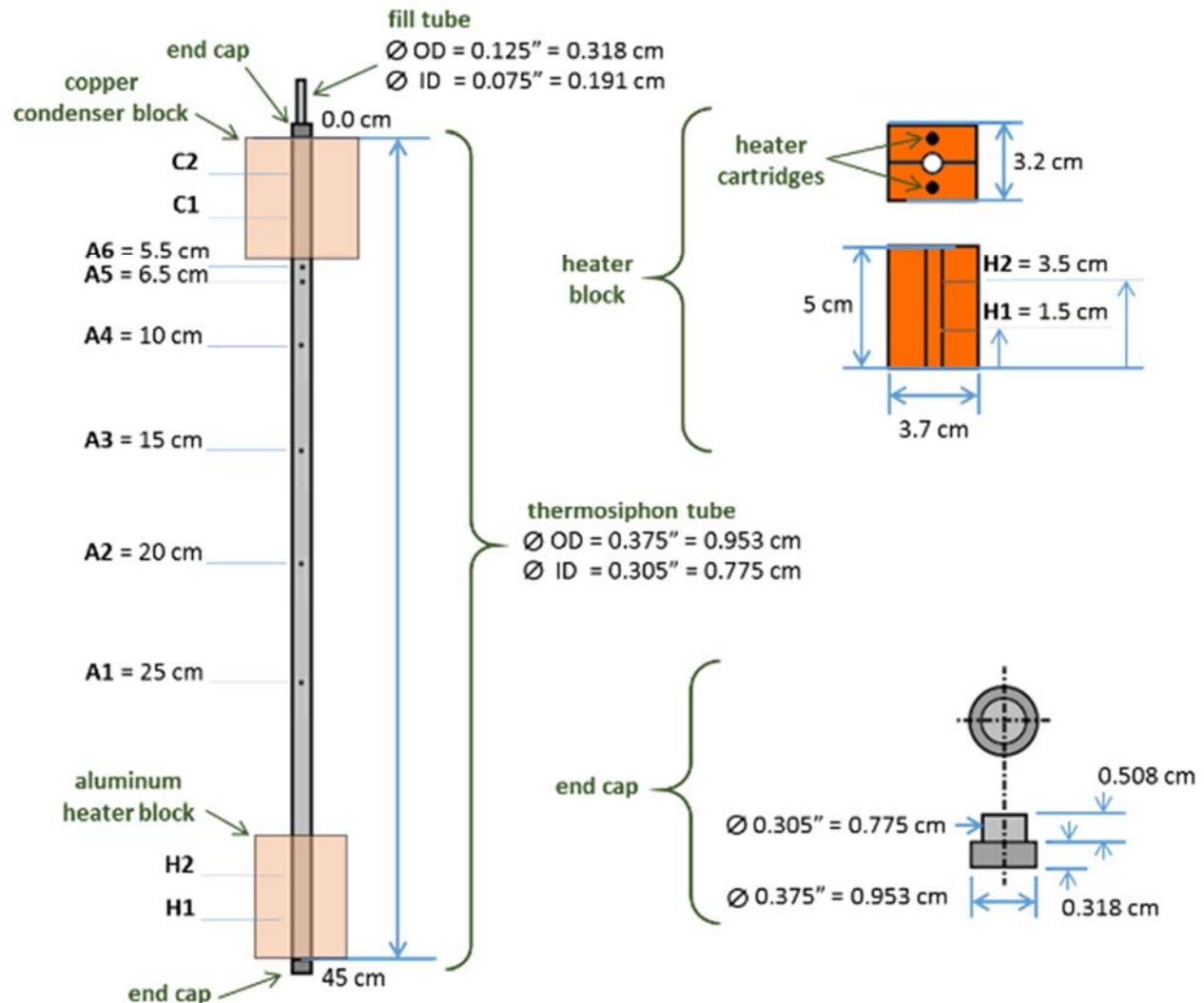
Figure 55: Forced convection, vertical thermo-syphon dimensions and thermocouple map

A peristaltic pump was used to circulate room temperature cooling water through a copper cooling block acting as the condenser. A schematic of this condenser block and its dimensions are shown in Figure 56.
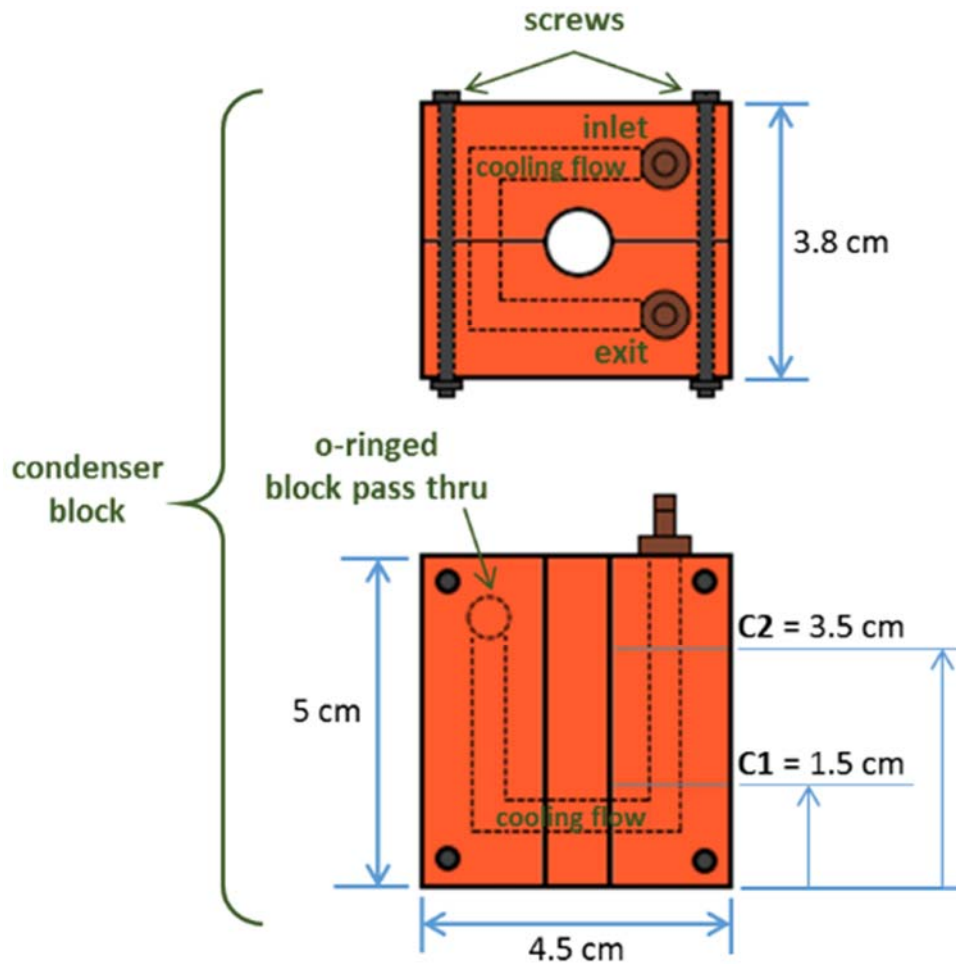
Figure 56: Forced convection, vertical thermo-syphon cooling block schematic and dimensions

Thermo-syphons were prepared and charged in the same manner as they were in Chapter 7 using the same liquid charge of 1.45 mL. Once each tube was fully prepared, instrumented, and charged with working fluid it was wrapped in fiberglass insulation held firmly in place with cloth ties as seen in Figure 54. The twist connect water cooling lines were attached to the cooling block and the thermo-syphon was fixed vertically using lab stands and clamps.

Two different test types were conducted. First constant input power tests were conducted to see if NCG generation is suppressed by changing the condensation method. Second, input power was increased starting with 20 W, increasing by 20 W until 100 W and then by 40 W until dryout

or catastrophic NCG failure occured to study overall performance and see the effect of purposely going above the safe temperature limit previously established in Chapter 8 of ~115°C. Steady state at each input power typically took about 15 to 20 *mins* to reach at which point temperature values were recorded for later analysis. Input power for all tests was calculated using Joule heating from the ceramic cartridge heaters embedded within a copper heater block.

With no IR camera viewing capabilities due to the condenser block and insulation obsuring the view, NCG was detected by test hysteresis. Each test was conducted as described three times. Two definitions for temperature difference are calculated and presented as well as both condenser and evaporator thermal resistances were plotted as a function of input power. All tests with a single thermo-syphon are plotted on a single figure for each metric. The first temperature difference is now defined as,

$$\Delta T = T_h - T_c \tag{73}$$

or average evaporator temperature minus average condenser temperature. The second temperature difference is defined as,

$$\Delta T = A5 - A6 \tag{74}$$

Which is the difference in temperature between the thermocouple 1.5 *cm* away from the condenser and the thermocouple 0.5 *cm* away from the condenser. Condenser and evaporator thermal resistances are defined as,

$$R_{th,cond} = \frac{T_a - T_c}{Q_{in}} \tag{75}$$

$$R_{th,evap} = \frac{T_h - T_a}{Q_{in}} \tag{76}$$

Evaporator and condenser thermal resistances are important to monitor because without the infrared images, these will help determine if NCG is generated. For the constant power tests condenser resistance should remain constant over time, indicating that no NCG has formed to block the condenser section. Similarly for the stair-step power tests, consecutive tests with the same thermo-syphon, at the same power levels, will show NCG generation if the condenser resistances increase for the same power level for each consecutive test. Matching results would indicate the thermo-syphon performance is repeatable and no NCG formation during or between repeated tests is taking place.

10.2 Constant Power Tests: Experimental Results and Discussion

The constant power tests were conducted first. Input powers of $100\,W$ and $180\,W$ were chosen to correspond to vapor temperatures of $\sim85°C$ and $\sim100°C$. These temperatures were chosen to be under the $115°C$ limit and also close to the test temperatures of the previous two natural convection experimental sections. Unfortuneately, equipment allowing for long test times was not available and, thus, were limited to $\sim4-7\,hours$. Three consecutive tests with two identical thermo-syphons were conducted. The first test was at $180\,W$ for $3.5\,hours$, the second was at $180\,W$ again for $3.5\,hours$, and the third was at $100\,W$ for $6.5\,hours$. The fluid $Mn-1$ was chosen as the test fluid for both thermo-syphons tested. Thermo-syphons were allowed to cool fully in between each consecutive test before starting the next experiment. Condenser resistance data for both thermo-syphon $T3$ and $T4$ are shown below in Figure 57 and Figure 58, respectively.

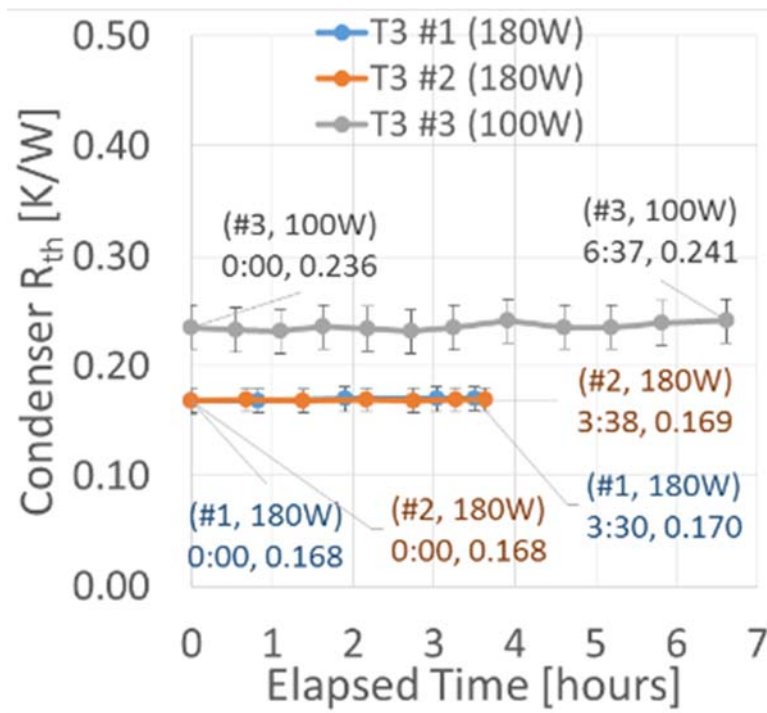Approved for public release: distribution is unlimited.

Figure 57: Aluminum/$Mn-1$, constant power, forced convection, time vs. condenser R_{th}, thermo-syphon $T3$
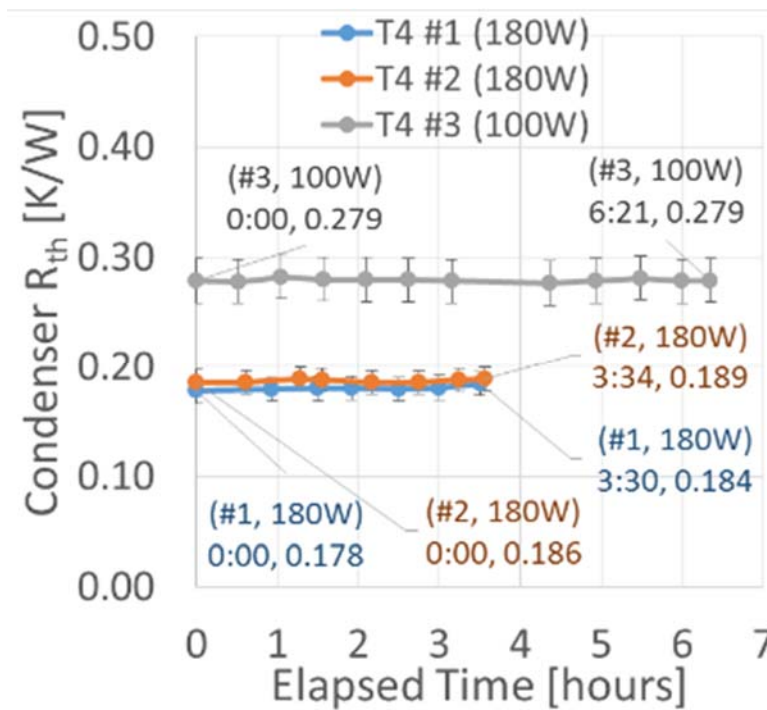

Figure 58: Aluminum/$Mn-1$, constant power, forced convection, time vs. condenser R_{th}, thermo-syphon $T4$

NCG was unable to be detected in either thermo-syphon tested for any of the constant power levels tested. This indicates that the change in condenser geometry and type resulted in a significant decrease in NCG generated compared to either of the natural convection experimental sets. This supports the discontinuous flow hyporeport and unsafe droplet region inroduced previously in Chapter 9. The next section will test more thermo-syphons, this time increasing the input power by $20\,W$ until steady-state is reached.

10.3 Stair-Stepped Power Tests: Experimental Results and Discussion

Once the constant power tests indicated that discontinuous flow was indeed a real problem for aluminum thermo-syphon passivation, more standard performance tests were ran using the same forced condenser setup. A larger portfolio of test fluids was used to both subjectively compare performance to copper/water baseline thermo-syphons and also investigate the effect of intentionally surpassing the 115℃ limit. Input power was increased starting with $20\,W$ and increasing by $20\,W$ until $100\,W$ and then by $40\,W$ until dryout or catastrophic NCG failure occured. The thermo-syphon was then allowed to fully cool and then this test procedure was repeated three times for each themosiphon. Multiple thermo-syphons for each fluid were tested.

Aluminum thermo-syphons were charged with four different inhibitor fluids: $Mn-0$, $Cr-0$, $Mn-1$, and $Mn-4$. The fluid $Cr-0$ (which has same permanganate concentration as $Mn-1$) is a new fluid which contains only permanganate and no chromium compounds. It is considered for thoroughness only and is not expected to operate at all due to its naturally high $pH = 8.12$ which is already outside the known pH boundary for aluminum oxide stability. Once again, copper/water and aluminum/water tests were also conducted for comparison. Table 16

shows a summary of the starting concentrations in each fluid used, the before and after E and pH measurements, fluid volume charged, and test name for each thermo-syphon tested.

Table 16: Forced convection thermo-syphon test matrix and fluid information

Metal/Fluid	Tube	Charge (g)	Initial pH	Final pH	ΔpH	Initial E (mV SHE)	Final E (mV SHE)	ΔE (mV SHE)	[Mn^{+7}] (mmol/L)	[Cr^{+6}] (mmol/L)	Mn^{+7} (mmol)	Cr^{+6} (mmol)
Al/H$_2$O	Q1	1.4624	7.00	7.71	0.71	-281	500	781	0.00	0.00	0.00	0.00
	Q2	1.4416	7.00	8.36	1.36	-281	478	759	0.00	0.00	0.00	0.00
Cu/H$_2$O	R1	1.4499	-	-	-	-	-	-	0.00	0.00	0.00	0.00
	P1	1.3960	-	-	-	-	-	-	0.00	0.00	0.00	0.00
	P2	1.5800	-	-	-	-	-	-	0.00	0.00	0.00	0.00
Al/Mn-1,Cr-0	U1	1.4275	8.12	10.68	2.56	940	346	-594	2.78	0.00	3.97	0.00
	U2	1.4133	8.12	9.16	1.04	940	275	-665	2.78	0.00	3.93	0.00
Al/Mn-0,Cr-1	T5	1.2846	6.33	6.88	0.55	524	495	-29	0.00	79.56	0.00	102.21
	T6	1.4746	6.33	6.78	0.45	524	509	-15	0.00	79.56	0.00	117.32
Al/Mn-1,Cr-1	T1	1.4002	6.15	6.81	0.66	924	590	-334	2.49	80.02	3.48	112.04
	T2	1.5078	6.15	6.79	0.64	924	682	-242	2.49	80.02	3.75	120.65
Al/Mn-4,Cr-1	Q4	1.6491	5.92	6.81	0.89	984	585	-399	9.96	79.55	16.43	131.18
	Q5	1.4906	5.92	6.68	0.76	984	598	-386	9.96	79.55	14.85	118.57
	S1	1.4495	5.92	6.87	0.95	984	608	-376	9.96	79.55	14.44	115.30

10.3.1 Copper/Water

Three copper thermo-syphons ($P1$, $P2$, and $R1$) with identical dimensions and charge volume to that used with the aluminum tubes were each run two times. The performance data for both ΔT definitions as a function of input power can be found below in Figure 59. Evaporator and condenser thermal resistances as a function of input power are shown in Figure 60.

Approved for public release: distribution is unlimited.

Figure 59: Copper/water, forced convection, Q vs. $\Delta T = T_h - T_c$, & Q vs. $\Delta T = A5 - A6$, thermo-syphons: $R1/P1/P2$

Figure 60: Copper/water, forced convection, Q vs. evaporator & condenser R_{th}, thermo-syphons: $R1/P1/P2$

The copper test data shows consistent results across different thermo-syphons and amongst each repetition. Dryout was found to be approximately $120\ W$. Note the low thermal resistances, particularly for condenser thermal resistance as well as its repeatability upon subsequent testing with the same thermo-syphon. With reuse, the results remain the same.

10.3.2 **Aluminum/Water**

Thermo-syphons $Q1$ and $Q2$ were made of aluminum and charged with pure DI water. The performance data for both ΔT definitions as a function of input power can be found below in Figure 61. Evaporator and condenser thermal resistances as a function of input power are shown in Figure 62.
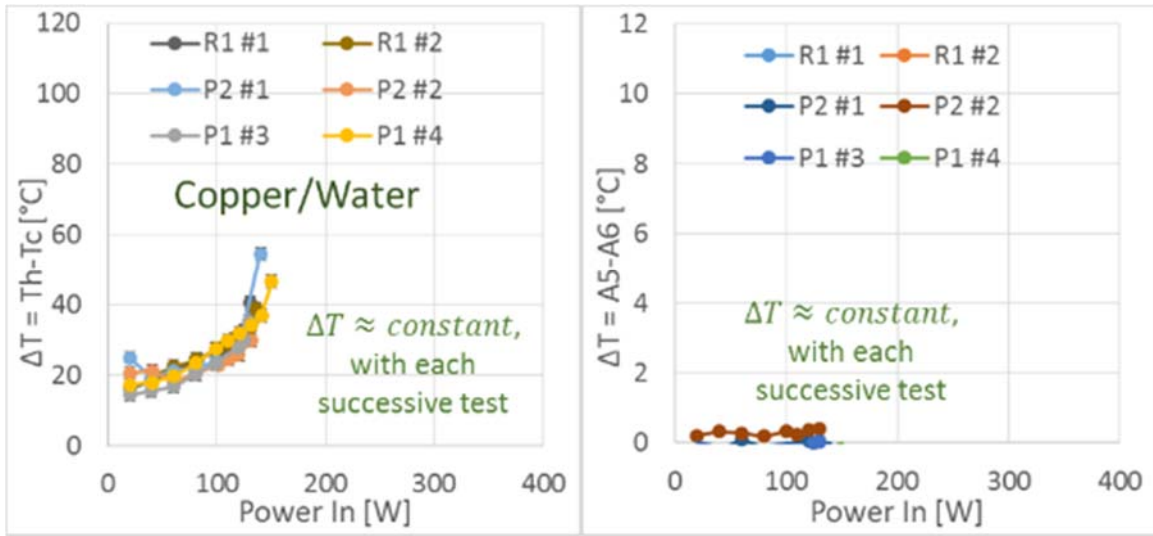

Figure 61: Aluminum/water, forced convection, Q vs. $\Delta T = T_h - T_c$, & Q vs. $\Delta T = A5 - A6$, thermo-syphons: $Q1/Q2$
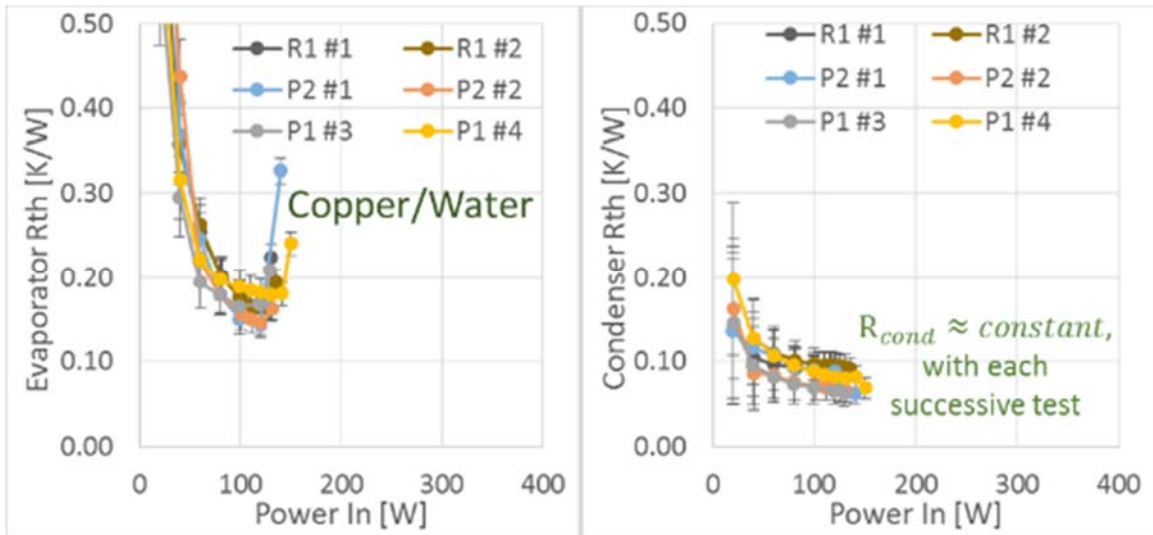

Figure 62: Aluminum/water, forced convection, Q vs. evaporator & condenser R_{th}, thermo-syphons: $Q1/Q2$

As expected, the aluminum/water tests both failed by forming hydrogen NCG. Hydrogen gas generation was severe enough that few input powers were able to be tested and subsequent

tests were deemed unsafe and unnecessary. NCG was detected by observing extremely large increases in ΔT at low input powers that continued to increase and did not reach steady state. Condenser thermal resistances were also extremely high, note that the axes for both resistances had to be changed in order to fit the data on the graph.

10.3.3 Aluminum/$Cr - 0$

Aluminum thermo-syphons $U1$ and $U2$ were charged with the new fluid containing permanganate only. The performance data for both ΔT definitions as a function of input power can be found below in Figure 63. Evaporator and condenser thermal resistances as a function of input power are shown in Figure 64.
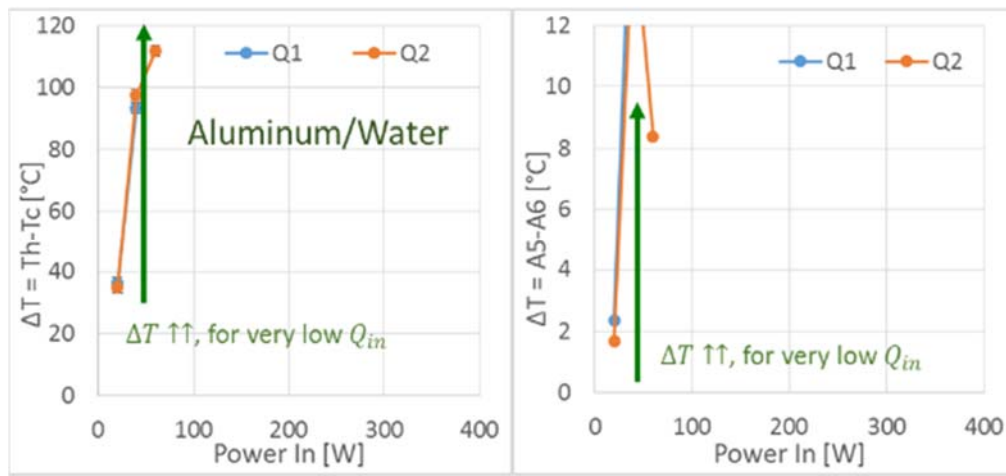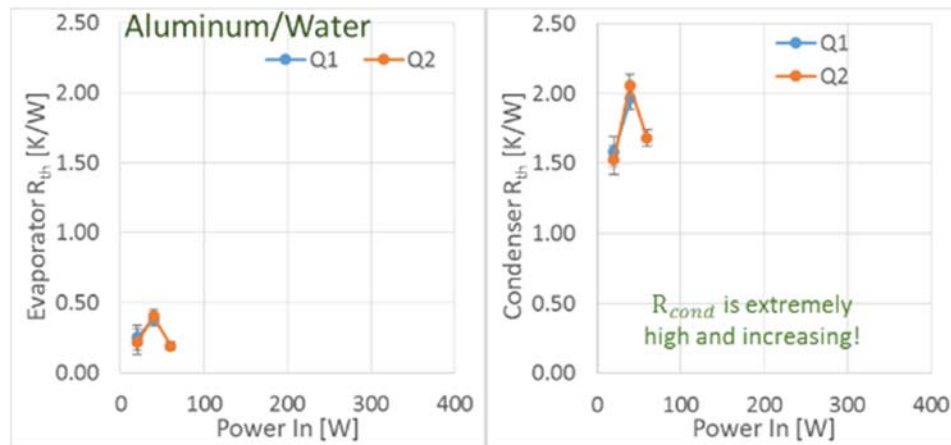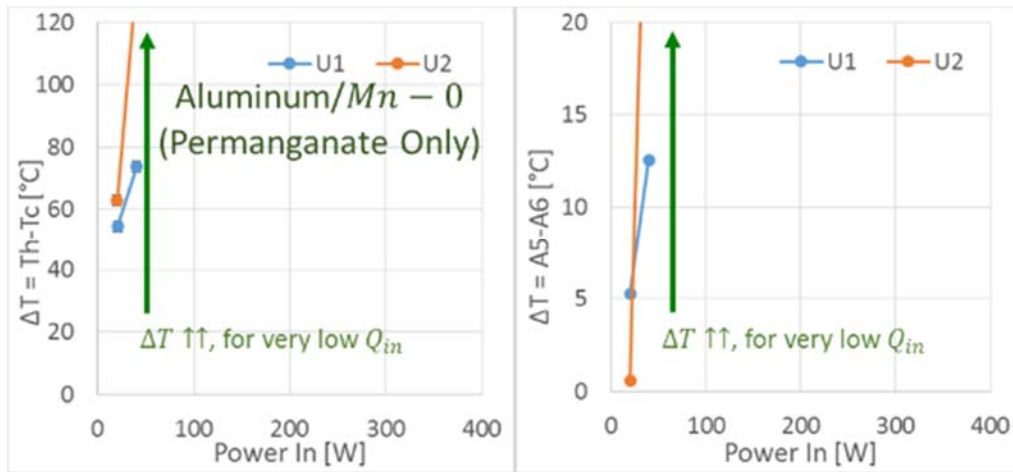

Figure 63: Aluminum/$Cr - 0$, forced convection, Q vs. $\Delta T = T_h - T_c$, & Q vs. $\Delta T = A5 - A6$, thermo-syphons: $U1/U2$

Figure 64: Aluminum/$Cr - 0$, forced convection, Q vs. evaporator & condenser R_{th}, thermo-syphons: $U1/U2$

This test fluid had no chance of success because the initial pH of the fluid was already well outside the stability region for aluminum oxide. The ΔT and thermal resistance data also shows that significant NCG was generated and the overall results are very similar to those of pure water and aluminum, or worse. It is now clear that for even modest NCG suppression chromates are required in solution.

10.3.4 Aluminum/$Mn - 0$

Aluminum thermo-syphons $T5$ and $T6$ were charged with $Mn - 0$ fluid containing chromate only. The $T5$ performance data for both ΔT definitions as a function of input power can be found below in Figure 65. Test $T5$ evaporator and condenser thermal resistances as a function of input power are shown in Figure 66.

Approved for public release: distribution is unlimited.

Figure 65: Aluminum/$Mn - 0$, forced convection, Q vs. $\Delta T = T_h - T_c$, & Q vs. $\Delta T = A5 - A6$, thermo-syphon: $T5$
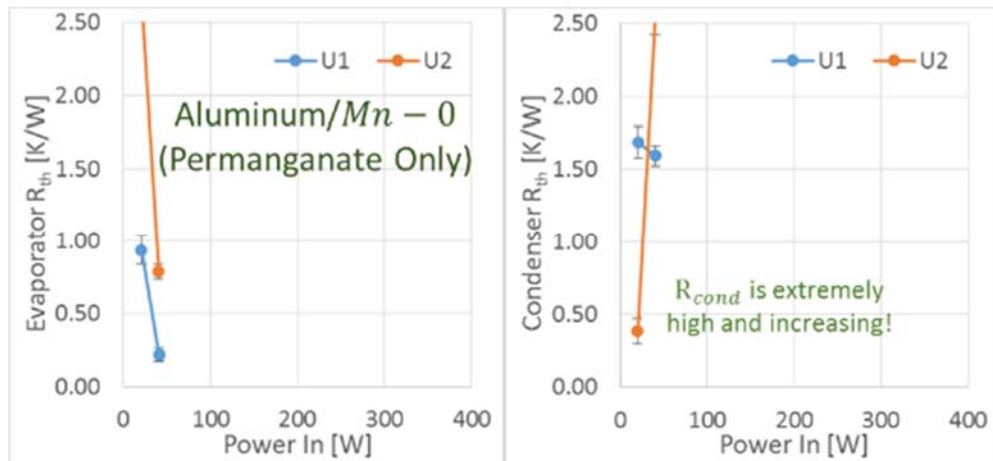

Figure 66: Aluminum/$Mn - 0$, forced convection, Q vs. evaporator & condenser R_{th}, thermo-syphon: $T5$

The $T5$ condenser resistances start out relatively high (especially at low input powers where low temperatures allow NCG expansion) and increase only slightly with subsequent testing, suggesting the bulk of the NCG present was generated prior the first test. Additional NCG was

mainly generated between $T5$ #1 and $T5$ #2, indicating that after this point condenser resistances were constant from test to test.

The $T6$ performance data for both ΔT definitions as a function of input power can be found below in Figure 67. The $T6$ thermo-syphon evaporator and condenser thermal resistances as a function of input power are shown in Figure 68.

Figure 67: Aluminum/$Mn - 0$, forced convection, Q vs. $\Delta T = T_h - T_c$, & Q vs. $\Delta T = A5 - A6$, thermo-syphon: $T6$

Figure 68: Aluminum/$Mn - 0$, forced convection, Q vs. evaporator & condenser R_{th}, thermo-syphon: $T6$

Thermo-syphon $T6$ performed almost identically to $T5$. Again, condenser resistances started out high and increased only between $T6$ #1 and $T6$ #2.

Compared to the pure DI water or permanganate only $(Cr - 0)$ fluids, the chromium only $(Mn - 0)$ fluid performed significantly better. NCG generation was suppressed enough such that meaningful thermo-syphon performance results were obtained. However, NCG was determined to have been generated which was observed in the increasing condenser resistances measured in each subsequent test with the same thermo-syphon. Additionally, the temperature difference along the tube increased with each subsequent test. This is another sign of the formation and slow growth of a hydrogen NCG slug.

10.3.5 Aluminum/$Mn - 1$

The $T1$ performance data for both ΔT definitions as a function of input power can be found below in Figure 69. Test $T1$ evaporator and condenser thermal resistances as a function of input power are shown in Figure 70.
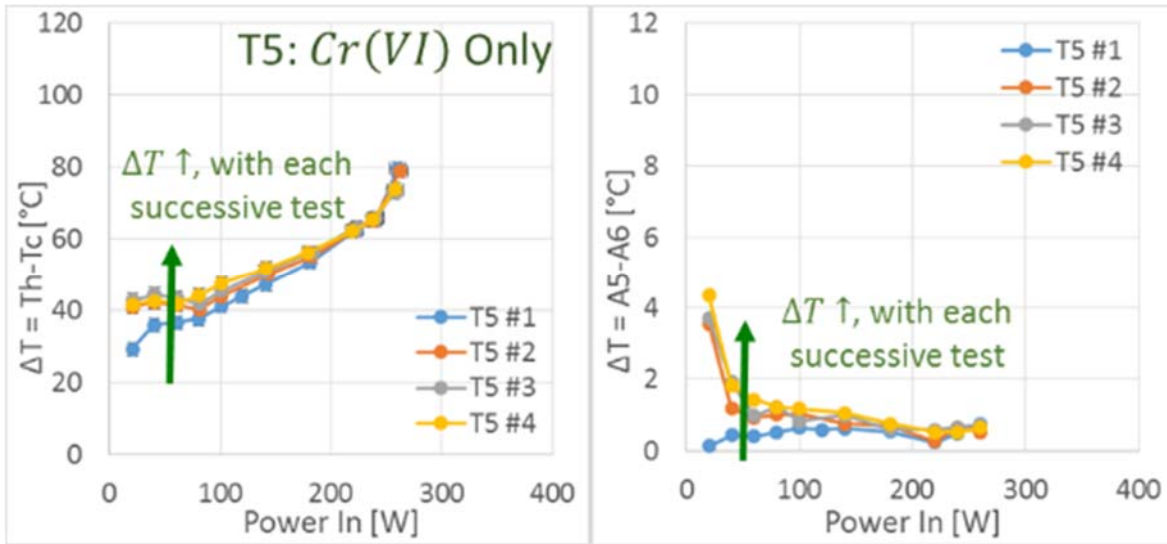

Figure 69: Aluminum/$Mn - 1$, forced convection, Q vs. $\Delta T = T_h - T_c$, & Q vs. $\Delta T = A5 - A6$, thermo-syphon: $T1$
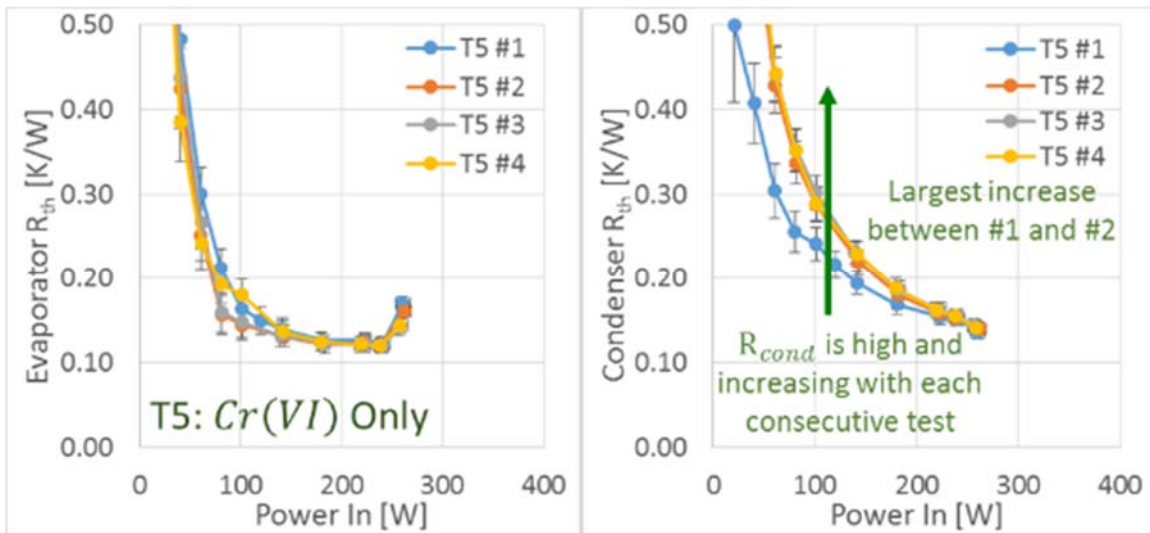
Figure 70: Aluminum/$Mn - 1$, forced convection, Q vs. evaporator & condenser R_{th}, thermo-syphon: $T1$

The $T2$ performance data for both ΔT definitions as a function of input power can be found below in Figure 71. Test $T6$ evaporator and condenser thermal resistances as a function of input power are shown in Figure 72.
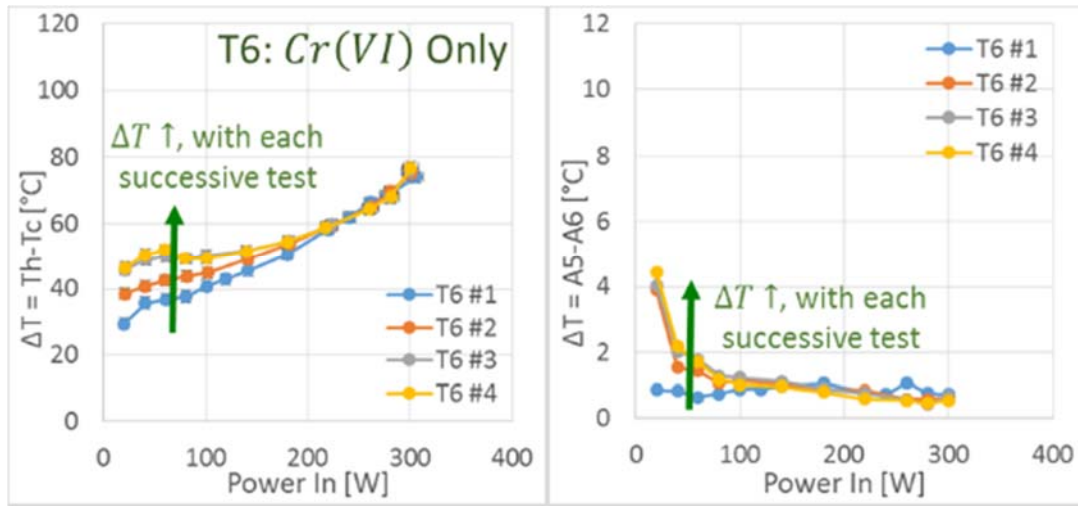

Figure 71: Aluminum/$Mn - 1$, forced convection, Q vs. $\Delta T = T_h - T_c$, & Q vs. $\Delta T = A5 - A6$, thermo-syphon: $T2$
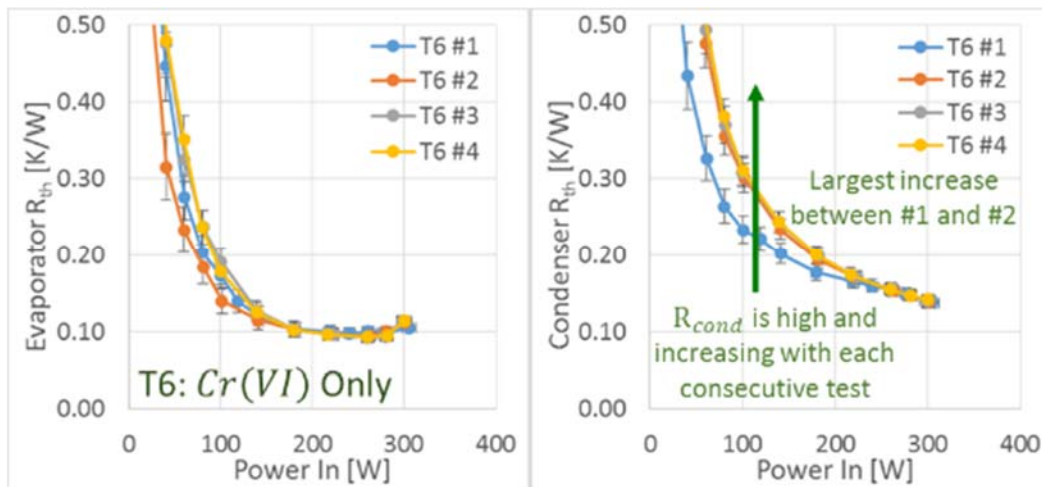
Figure 72: Aluminum/$Mn - 1$, forced convection, Q vs. evaporator & condenser R_{th}, thermo-syphon: $T2$

10.3.6 Aluminum/$Mn - 4$

The $Q4$ performance data for both ΔT definitions as a function of input power can be found below in Figure 73. Test $Q4$ evaporator and condenser thermal resistances as a function of input power are shown in Figure 74.

Figure 73: Aluminum/$Mn - 4$, forced convection, Q vs. $\Delta T = T_h - T_c$, & Q vs. $\Delta T = A5 - A6$, thermo-syphon: $Q4$

Figure 74: Aluminum/$Mn - 4$, forced convection, Q vs. evaporator & condenser R_{th}, thermo-syphon: $Q4$

Relative to the $Cr - 0$ (permanganate only) fluid or DI water, thermo-syphon $Q4$, using the $Mn - 4$ ($4x$ permanganate) solution, performed better and was able to produce meaningful performance results without runaway NCG growth. However, slow NCG growth was detected, as it was for all inhibitor solutions. Compared to the lower concentration permanganate fluid ($Mn - 1$) thermo-syphon $Q4$ started out with higher condenser resistances and increased substantially with each subsequent test. The temperature difference between the top two thermocouples, shown in the right hand side of Figure 73, indicate increases of $2 - 3°C$ for this small $0.5\ cm$ distance alone due to NCG slug growth. It is worth noting that this thermo-syphon performed the poorest of all those tested in this chapter. This is most likely because it reached the highest heat fluxes before dryout and thus the highest temperatures which accelerates NCG generation.

The $Q5$ performance data for both ΔT definitions as a function of input power can be found below in Figure 75. Test $Q5$ evaporator and condenser thermal resistances as a function of input power are shown in Figure 76.
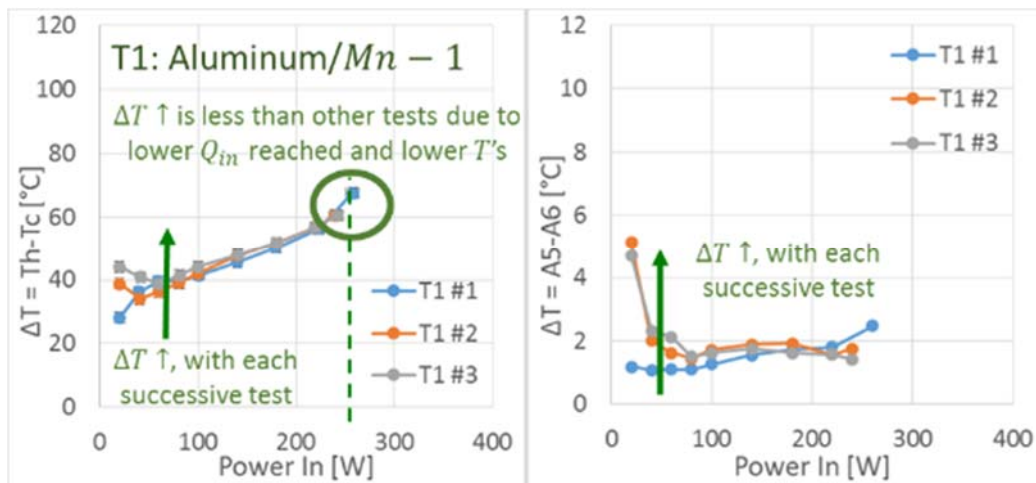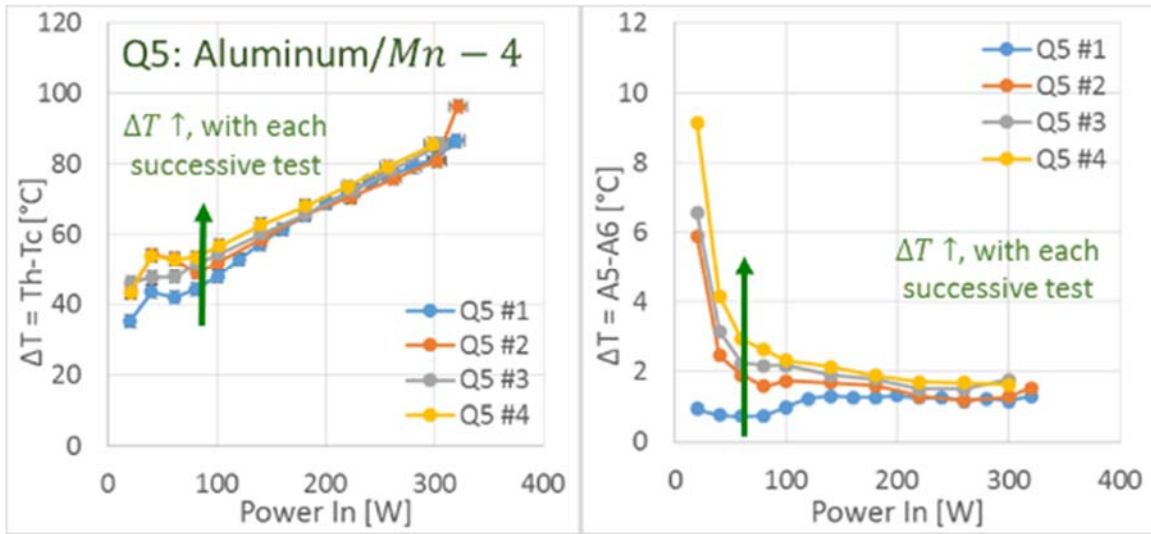
Figure 75: Aluminum/$Mn - 4$, forced convection, Q vs. $\Delta T = T_h - T_c$, & Q vs. $\Delta T = A5 - A6$, thermo-syphon: $Q5$
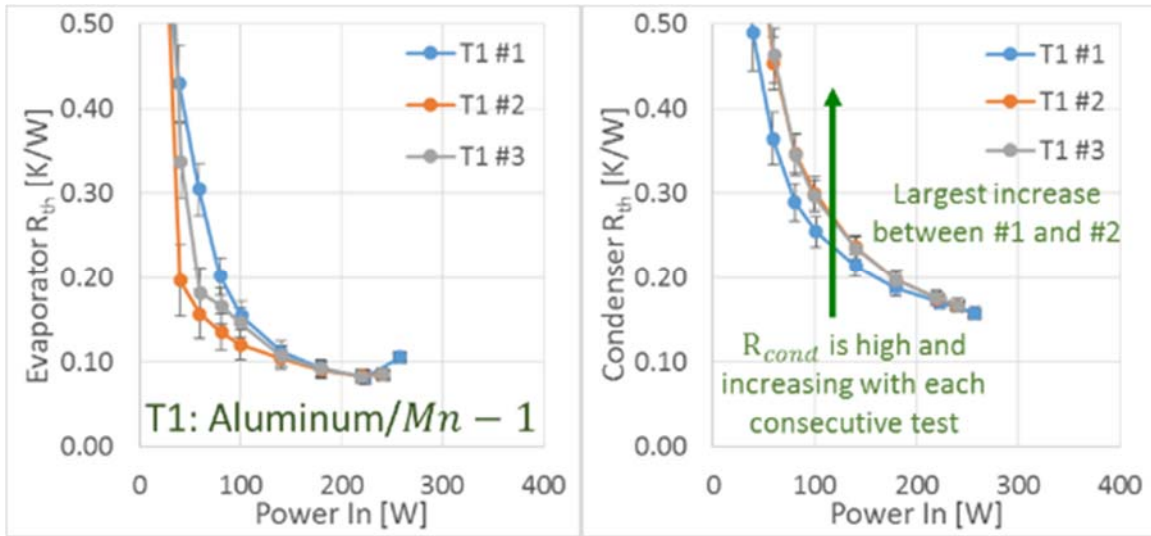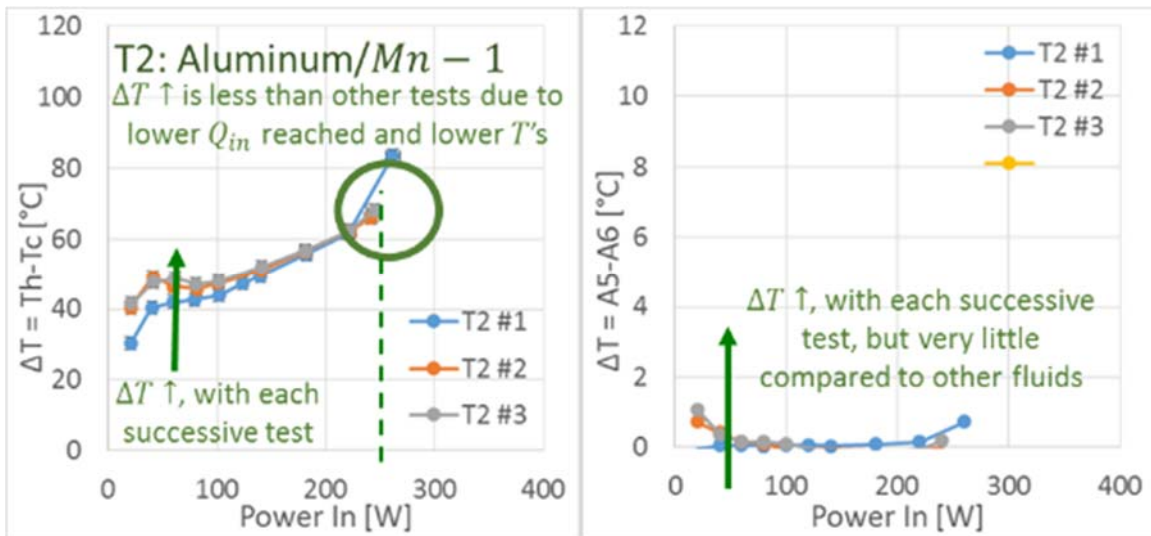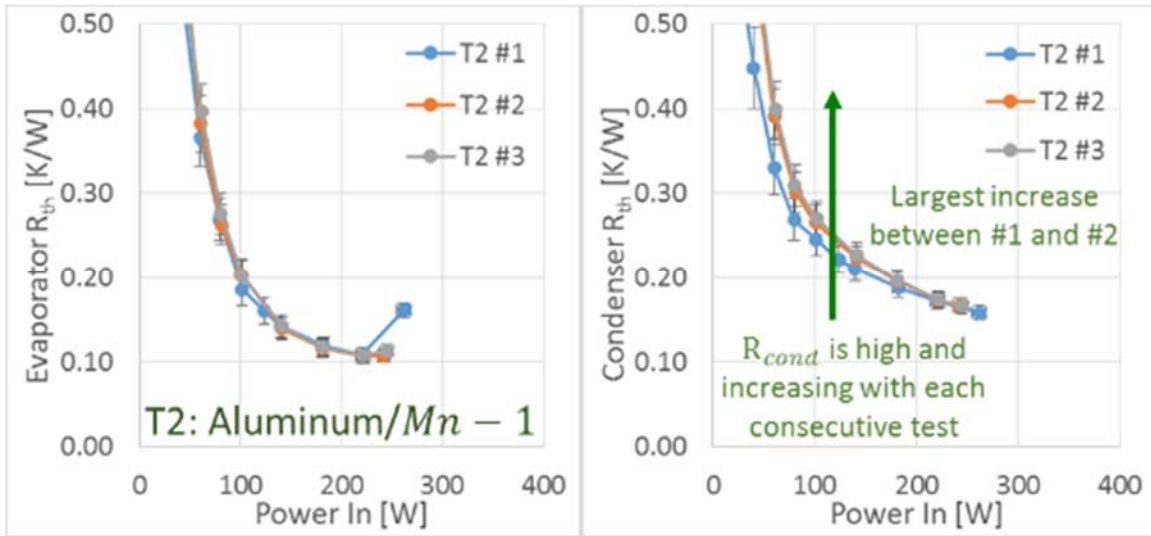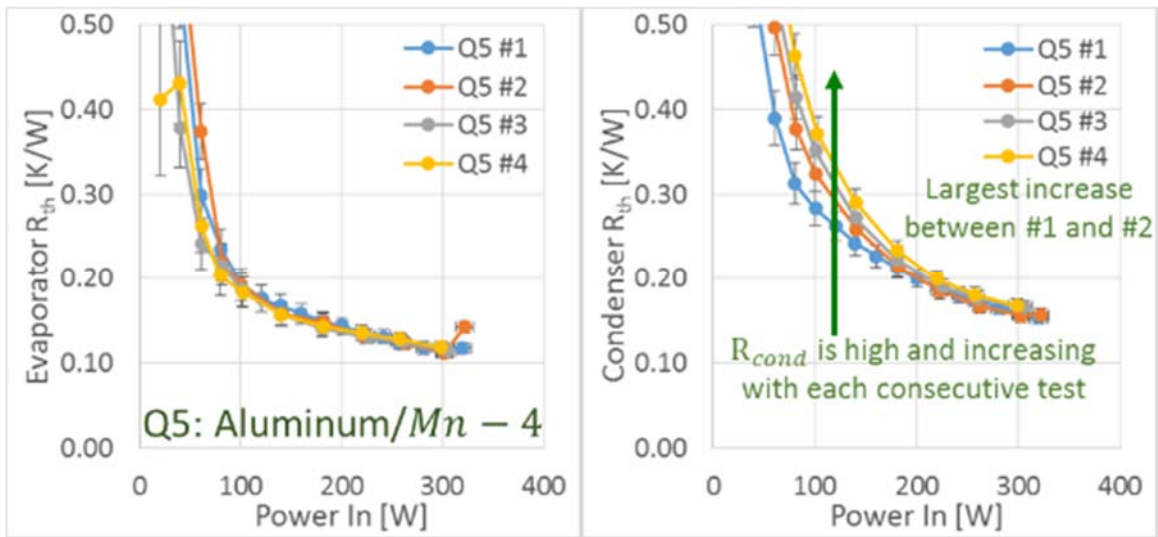

Figure 76: Aluminum/$Mn - 4$, forced convection, Q vs. evaporator & condenser R_{th}, thermo-syphon: $Q5$

Thermo-syphon $Q5$ exhibited the same trends as $Q4$ which was charged with the same fluid. One notable difference is that the magnitude of NCG generated between successive tests was slightly less, likely due to lower overall temperatures reached in the evaporator.

The $S1$ performance data for both ΔT definitions as a function of input power can be found below in Figure 77. Test $S1$ evaporator and condenser thermal resistances as a function of input power are shown in Figure 78.
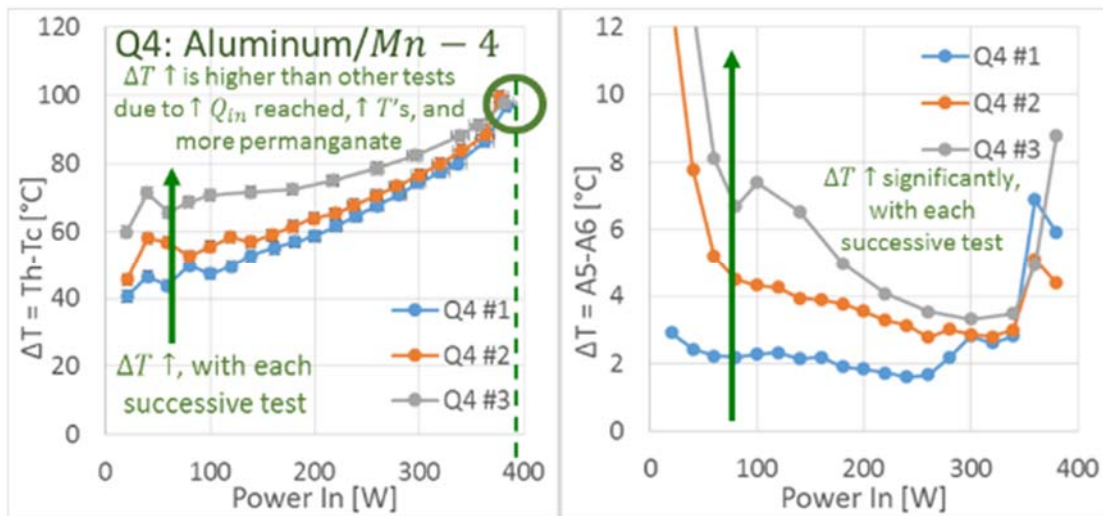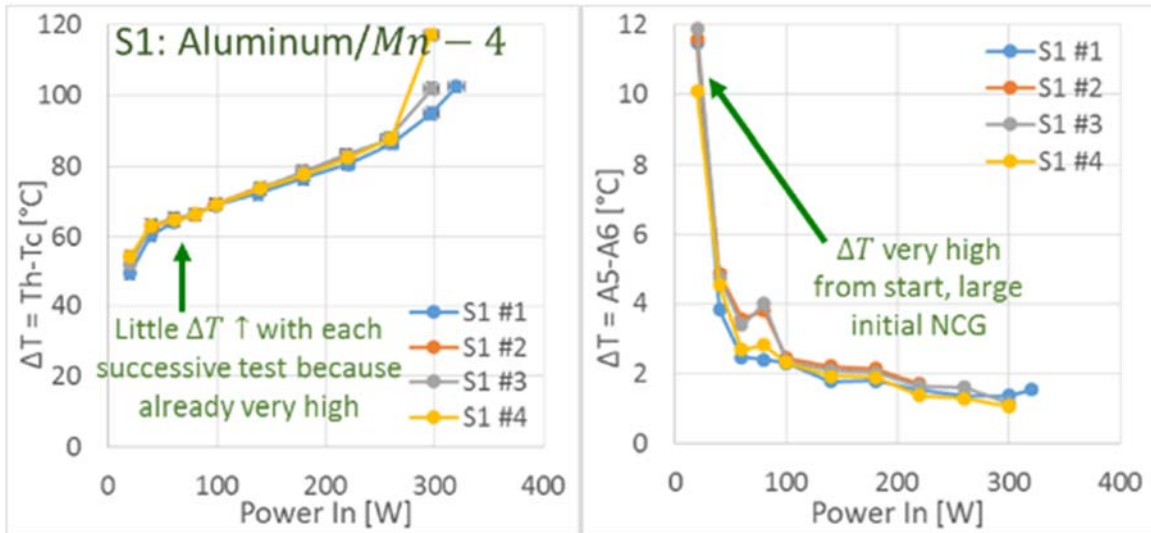

Figure 77: Aluminum/$Mn - 4$, forced convection, Q vs. $\Delta T = T_h - T_c$, & Q vs. $\Delta T = A5 - A6$, thermo-syphon: $S1$
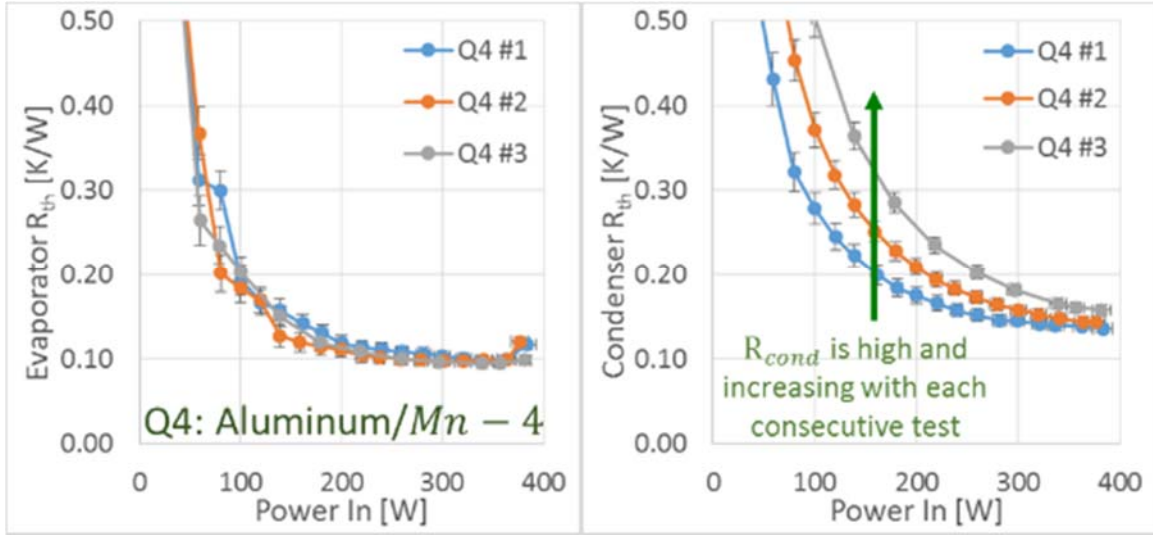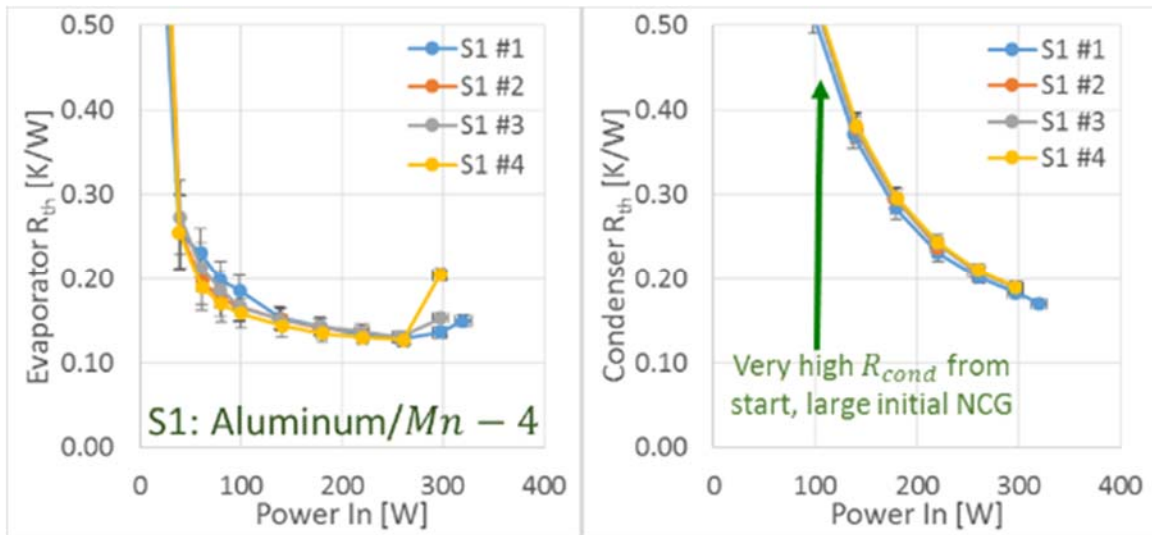

Figure 78: Aluminum/$Mn - 4$, forced convection, Q vs. evaporator & condenser R_{th}, thermo-syphon: $S1$

The $S1$ thermo-syphon exhibited the highest overall starting condenser resistances and tube $\Delta T's$ of all experiments. However, it also increased the least with each subsequent experiment

Approved for public release: distribution is unlimited.

conducted. It is believed that some mechanism initiated NCG growth up to a large amount before the first test was begun and at then quickly passivated upon operation. This could also have been caused by the large amount of permanganate used in the $Mn - 4$ fluid.

The aluminum thermo-syphons with $Mn - 4$ produced the largest amount of NCG judging by their condenser resistance values and increases in ΔT with each subsequent test. Also, increases in power and temperature will compress an NCG slug and reduce the disparity between condenser resistances at high input powers. This was observed for all fluids tested but was most obvious for $Mn - 4$ (largest amount of permanganate present) fluid. The $Mn - 1$ and $Mn - 0$ (chromium only) fluids both performed similarly but the $Mn - 0$ was shown to produce slightly less NCG, likely because it had no permanganate present instead of $Mn - 1$ which had a small amount.

Dryout behavior for aluminum with inhibitor solutions was very different than copper/water. All aluminum tubes with designed fluids exhibited dryout points up to $3x$ higher than copper/water. This is an interesting phenomenon because the copper/water tubes, while stable and consistent, had low dryout heat fluxes near $120 \, W$. Some aluminum tests resisted dryout until $300 \, W +$. This was also observed by Yao [35] when dealing with copper thermo-syphons and working fluids with compositions similar to those used in this work. Yao proposed the cause was due to the hydrophilic chromate salts in solution which act to extend the evaporating meniscus and increase the overall area of high evaporation rates, thereby delaying maximum heat flux dryout.

The stair-step power thermo-syphons all reached temperatures as high as 150°C or even 180°C when they were near dryout. This is likely a contributing factor to the NCG which was generated in every test that was not seen when the power levels were kept constant with tube

temperatures well below the 115°C limit. This adds more support to the temperature limit established in the previous natural convection thermo-syphon experiments of Chapters 7 and 8.

10.4 Uncertainty Analysis

The 95% uncertainty of the type-T thermocouples used was ±1.30°C for a single temperature measurement and ±1.84°C for each ΔT measurement. The calculation for this is shown in Table 17.

Table 17: PDAQ 3000, type-T thermocouple error

Source	Value (+/-)	Shape	Divisor	Std Unc (°C)
PDAQ 3000: Type-T Thermocouple Error				
Resolution	0.005	Uniform	1.73	0.0029
DAQ+CJ	1.8	Normal	3	0.60
TC Wire (SLE)	0.5	Normal	2	0.25
T Combined Standard Uncertainty =				0.65
T Expanded Uncertainty (95%, std. dist.) =				1.30
ΔT Standard Uncertainty =				0.92
ΔT Expanded Uncertainty (95%, std. dist.) =				1.84

Example problems for uncertainties of resistance and voltage can be found below in Table 18 and Table 19. These uncertainties were used to calculate the 95% confidence uncertainty for each data point plotted in this chapter's figures made from experimental temperature and Q data. The error bars associated with this have been added to the appropriate figures.

Table 18: TENMA 72-7765 multimeter, resistance error

Source	Value (+/-)	Shape	Divisor	Std Unc (Ω)
TENMA 72-7765 Multimeter: Resistance Error (e.g. R=38.2 Ω)				
Resolution	0.05	Uniform	1.73	0.029
Accuracy	1% rdg + 2 dgts	Normal	2	0.29
Combined Standard Uncertainty =				0.29
Expanded Uncertainty (95%, std. dist.) =				0.58

Table 19: TENMA 72-7765 multimeter, voltage error

TENMA 72-7765 Multimeter: Voltage Error (e.g. V=61.9 v)				
Source	Value (+/-)	Shape	Divisor	Std Unc (Ω)
Resolution	0.05	Uniform	1.73	0.029
Accuracy	1.2% rdg + 3 dgts	Normal	2	0.52
Combined Standard Uncertainty =				0.52
Expanded Uncertainty (95%, std. dist.) =				1.04

The pH and E measurements were both done using Omega probes. The pH measurements have an accuracy of $\pm 0.02\,pH + 2d$ ($\pm 0.04\,pH$ units) while the E measurements are $\pm 0.5\% + 2d$, giving accurate measures for each fluid. Typical electrode potential error was between $\pm 2\,mV$ for values measuring near zero and up to $\pm 7\,mV$ for the highest E values measuring near $900\,mV$.

10.5 Conclusions

Aluminum thermo-syphons were tested in a vertical orientation and charged with different inhibitor solutions designed to help suppress NCG gas formation within these active metal PCHT devices. A heater block was attached to one end and chilled water condenser block to the other. The thermo-syphons were first run with constant power levels of $180\,W$, $180\,W$, and then $100\,W$ for up to 7 hours, consecutively. The results did not show any signs of NCG generation. These tests were kept below the established temperature limit of $115°C$. The conclusion from these experiments is that the discontinuous flow theory introduced in Chapter 9 has an effect on the performance of inhibitor solutions for aluminum thermo-syphons. When a much stronger condensing flux was used for the thermo-syphons, the amount of NCG generated significantly decreased.

The next experiments increased the input power step by step, recording temperature values at steady state. Using these temperatures, resistance of the evaporator and condenser were

calculated along with ΔT data. The data collected indicate that every test produced at least some amount of NCG gas. However, a comparison of their behavior when a test was repeated indicate that the $Mn - 4$ fluid ($4x$ permanganate, $1x$ chromate) tests performed the worst and exhibit the largest slug compression as the test reaches high temperatures. $Mn - 1$ ($1x$ permanganate, $1x$ chromate) and $Mn - 0$ ($0x$ permanganate, $1x$ chromate or a.k.a. chromium only) both generated less NCG. The fluid containing permanganate only did not work at all and was as poor as water when it came to resisting NCG growth. Water/aluminum tests all failed rapidly as well and copper/water tests performed with no NCG and were repeatable. The NCG generated in these tests occurred because they all reached over the 115°C temperature limit towards the dryout point and NCG was generated at that time, demonstrating that surpassing this limit causes more NCG generation.

In terms of inhibitor concentrations, future studies are recommended to use lower concentrations of permanganate and higher concentrations of chromium than currently used when tested in forced convection thermo-syphons. This is because the excess permanganate is likely not needed and is causing oxygen gas release as seen in high concentration permanganate tests performed in Chapter 6. Shorter tubes or a lower temperature condenser might also facilitate a more reliably continuous liquid backflow of excess hydrogen ions which are required to complete the electrochemical circuit and passivate remote locations of the device outside the evaporator.

The enhanced dryout performance of the stair-step tests due to hydrophilic salts of chromium caused an almost $3x$ increase in the max input power compared to copper/water before total dryout. The high temperatures this exposed the thermo-syphons to pushed them outside the aluminum oxide stability region for high temperatures, according to the Pourbaix diagrams made

Approved for public release: distribution is unlimited.

and test fluids plotted on them. Low temperature tests are recommended for future work, not to

exceed 115℃ in temperature.

11 Conclusions and Future Work

11.1 Summary Results and Discussion

11.1.1 Background

Typically, aluminum and water are a heat pipe combination that is not considered due to the rapid noncondensable gas (NCG) generation. This report investigated the effects and limits of using oxidizers and solution pH to suppress hydrogen gas NCG generation in aluminum thermo-syphons. The literature was reviewed showing that, while aluminum and iron are both commonly passivated as a means to resist material corrosion and degradation, little research was found regarding the suppression of NCG for closed-systems at low pressure like thermo-syphons and heat pipes. Strong oxidizers were chosen as a means of potentially stopping NCG based on similar schemes used for open air corrosion protection. The oxidizers chosen were permanganate and chromates.

11.1.2 Thermodynamics and Chemical Reactions

Thermodynamic data was compiled as a function of temperature for all relevant metal/water interactions regarding water, aluminum, manganese, chromium and their soluble and oxidized species. This data was used to make Pourbaix diagrams which can predict thermodynamic stability of different species in an aqueous system. These figures were used to bound the window of E and pH needed to promote a protective aluminum oxide film for the internal aluminum surface of a thermo-syphon at any given operating temperature. It was observed that the region of oxide stability, or "safe zone" moved to more reducing (down) and acidic (left) conditions as temperature increases. Depending upon the movement of the system E and pH, this created the

Approved for public release: distribution is unlimited.

potential for a temperature limit if the two should meet, thus moving the system outside of the safe zone.

11.1.3 Corrosion Tests

There was high confidence that the use of these inhibitors would fully prevent NCG generation if the aluminum surface were to remain fully submersed in the solution at near-neutral pH conditions. Before beginning tests with thermo-syphons, a corrosion reaction vessel was built so that fluids could be tested with simple aluminum samples when the system was vacuumed, degassed, and the sample submersed in fluid at an elevated constant temperature. There were two questions to be answered:

1) Are chromium oxidizers enough to passivate a fully submersed sample by themselves?

2) Would the use of excess quantities of permanganate oxidizers generate oxygen gas (another NCG) through disassociation at high temperature?

The test results of the corrosion experiments indicated that, yes, chromium oxidizers were enough when aluminum is fully submersed and that, yes, excess permanganate will generate significantly more NCG than pure DI water alone.

11.1.4 Natural Convection, Heater Block Thermo-syphon Tests

The first thermo-syphon experiments used a heater block and natural convection condenser so that an IR camera could visualize any NCG slug generated within the tube. Solutions containing chromates and varying concentrations of permanganate oxidizers were tested in vertical thermo-syphons $45\ cm$ in length. Input power was held constant at $10\ W$ for all tests. For these short term tests ($\sim 5\ hours$) it was found that increased levels of permanganate helped prevent NCG

generation in the thermo-syphons. The E and pH of each fluid was measured before and after it was tested. OLI was used to simulate what these room temperature measurements would be at the elevated temperatures seen within the thermo-syphons. High temperature Pourbaix diagrams were also contstructed to help recreate the necessary conditions at operating temperature for a stable aluminum oxide layer. It was found that the system and safe zone did indeed move in opposite directions as temperature increases but that the limit of 120°C was not reached for these particular set of experiments. The Pourbaix diagrams were also used to demonstrate that chromium oxidizers will not oxidize water (another possible route of forming NCG) until very high temperatures ~275°C. Longer tests were desired to further investigate the effects of oxidizers in aluminum thermo-syphons.

11.1.5 Natural Convection, Constant Temperature Bath Thermo-syphon Tests

The next set of thermo-syphon tests used a constant temperature silicon oil bath as the heat source to stabilize the vapor temperature among the tests but mainly to allow for experiments to be run indefinitely with consistent, reliable, and safe conditions. Natural convection was again chosen as the condensation method to continue to use the IR camera. Tests were not run indefinitely, rather, they were run for $\sim 72 \ hours$. This was because all thermo-syphons tested, regardless of the fluid used, produced some amount of NCG and longer tests were not necessary. For these longer tests, permanganate again helped with preventing NCG over short time periods. However, for anything longer than a few hours any amount of permanaganate in the solution was found to produce higher NCG generation than thermo-syphons tested with chromates only. This was similar to the findings of the corrosion tests.

11.1.6 Electrochemical Cycle and Discontinuous Flow

Since the best performing, chromium only fluid still produced NCG at reduced rates over time in the bath tests, the cause was hypothesized to result from the condenser section where condensed liquid was pure water. This region is protected by an electrochemical cycle requiring electron transfer through the aluminum tube and simultaneously a continuous liquid backflow to return H^+ ions, generated from the half-reaction with the bare aluminum surface, to the evaporator section where the oxidizer chemicals exist in solution. The low condensation rates of low-power, natural convection cooled thermo-syphons with large condensing surface areas leads to small condensing fluxes. This was shown to increase the likelihood of a large droplet condensation region where hot, pure water droplets were isolated from the rest of the system and can potentially generate hydrogen NCG. This dangerous region can be reduced in size by using a smaller, forced convection condenser which promotes high condensation rates of liquid film rather than isolated droplets.

11.1.7 Forced Convection Thermo-syphon Tests

The final thermo-syphon tests used a water cooled forced convection condenser only $5\ cm$ in length to address the discontinuous flow problem and reduce the risk of isolated droplets condensing in the thermo-syphon. Tests at $180\ W$ and $100\ W$ were conducted for up to $\sim 4\ hours$ and then repeated twice for a total test time of $\sim 15\ hours$. The nature of the experimental setup prevented extended tests with the available equipment. No signs of NCG generation were found for either of the thermo-syphons tested using $Mn-1$ solution.

The high temperature limit which had previously been avoided was next tested by running additional thermo-syphons with forced convection condensers at incrementally increasing input

Approved for public release: distribution is unlimited.

powers, reaching steady-state conditions in between. It was found that aluminum thermo-syphons with chromate solutions had dryout limits $\sim 3x$ higher than an identical copper/water thermo-syphon. However, when high temperatures well above the 115°C limit found previously were reached, NCG was generated in amounts depending on how high the temperatures went.

11.2 Conclusions

Permanganate and chromate oxidizers were investigated to determine the effects and limits of using inorganic oxidizers in aqueous solutions charged in aluminum thermo-syphons for the purposes of NCG suppression. It was found that if the aluminum surface is directly submersed in a solution with $\sim 80\ mmol/L$ of chromate oxidizers at a $pH \sim 6$ then NCG could be suppressed below detection levels of the equipment in this work over a $24\ hour$ time period, if the temperature is kept below 115°C.

When the same solution is used inside a thermo-syphon device NCG suppression was observed for all concentrations of both oxidizers when natural convection cooling was used. However, increasing concentrations of permanganate oxidizers will help reduce initial NCG generation but only for a few hours before actually causing a significantly higher amount of NCG to form in the thermo-syphon. Therefore, permanganates are not recommended.

If a forced convection condenser is used, NCG was suppressed below the detection capability of the equipment used when the temperature was, again, kept below 115°C. This was because the much higher condensing flux of this condenser boundary condition promoted a continuous liquid backflow to return H^+ ions to the evaporator. The film-wise return of condensed liquid, rather than isolated droplet condensation, completes the electrochemical cycle which protects the thermo-syphon interior if bare aluminum is present due to a washed off oxide film.

Approved for public release: distribution is unlimited.

11.3 Recommendations for Future Work

In general, thermo-syphons were found to be a difficult candidate for passivation due to their method of liquid return. If they are to be used, a high condensing flux condenser is required, likely in the form of a forced convection boundary condition. However, thermo-syphons are not recommended for future work due to the difficulty in remotely passivating the condenser and adiabatic region through the electrochemical cycle. The requirement of a continuous liquid backflow, even if a strong condenser is used, makes it difficult to reliably say that a thermo-syphon will never have any isolated droplets near the top that could produce NCG. The randomness in where the droplet/film line exists leads to difficulty in tightly controlling the expected lifetime of such a thermo-syphon used in industry.

One possible way around this limitation would be to use a wick to maintain all surfaces of the device wetted with chemical containing liquid so that the discontinuous flow problem is avoided. Applications which lend themselves strongly to this are micro heat pipes, TGPs, flat heat pipes, extruded grooved heat pipes (such as those used on satellites), oscillating heat pipes, etc. Oscillating heat pipes are particularly interesting due to their inherent ability to resist the effects of NCG more than standard heat pipes simply due to their method of operation and liquid transport.

Future work is also recommended that repeats many of the experiments performed in this report with additional concentrations of chromate oxidizers to establish a minimum required amount for different applications and potentially tie that requirement to internal surface area of the device being charged. In many markets chromates are highly regulated and the reduction of their required concentration would be beneficial. Future research is also recommended to continue to investigate methods of pretreatment to compliment the inhibitors used in solution. One method

Approved for public release: distribution is unlimited.

that may be useful is pretreating the interior surface of the aluminum tube with high temperautre ($\sim300°C$) air to establish a strong base of protective aluminum oxide layer before assembling and charging the heat pipe. Another area for investigation is to determine if the 115°C temperature limit found in this report can be increased by decreasing the initial pH of the inhibiting solution. By looking at the Pourbaix diagrams it can be seen that there is some margin to do this but it is left to future researchers to determine the extent and its effect on device temperature limit.

This report's investigation of chromate and permanganate oxidizer effects on suppressing NCG generation in aluminum heat pipes opens the door for additional studies to be done with other active metal heat pipes such as with iron or steels. The methods used for thermodynamic analysis using Pourbaix diagrams and experimental methods could easily be applied to any metal and even any soluble inorganic oxidizer such as those with cobalt, cerium, or others. Significant inroads were made through this work towards future aluminum heat pipe devices that can utilize a water-based solution. This eventual goal would provide an excellent option for heat pipe engineers desiring an intermediate temperature range fluid with a high max heat tranfer capability.

References

[1] Chi, S., <u>Heat pipe theory and practice,</u> Washington, DC, Hemisphere Publishing Corp.; New York, McGraw-Hill Book Co., 1976.

[2] Reay, D., and Kew, P. A., <u>Heat pipes: Theory, design and applications</u>, Butterworth Heinemann, 2006.

[3] Heuer, C. E., "The application of heat pipes on the Trans-Alaska pipeline," C. R. R. a. E. Laboratory, ed., Hanover, NH, USA, p. 33, 1979.

[4] Semenic, T., and Catton, I., "Experimental study of biporous wicks for high heat flux applications," *International Journal of Heat and Mass Transfer*, 52(21), pp. 5113-5121, 2009.

[5] Faghri, A., "Heat Pipes: Review, Opportunities, and Challenges," *Frontiers in Heat Pipes (FHP)*, 5(1), 2014.

[6] Wikipedia, "Heat Pipe," https://en.wikipedia.org/wiki/Heat_pipe., accessed prior to 12/9/16.

[7] Reay, D. A., "The Perkins Tube—a noteworthy contribution to heat exchanger technology," *Journal of Heat Recovery Systems,* 2(2), pp. 173-187, 1982.

[8] ACT, 2016, "Heat Pipe Working Fluid Selection," https://www.1-act.com/merit-number-and-fluid-selection/, accessed prior to 12/9/16.

[9] Terdtoon, P., Charoensawan, P., and Chaitep, S., "Corrosion of tubes used in thermosyphon heat exchanger for waste heat recovery system: A case of internal surface," *Heat Transfer Eng*, 22(4), pp. 18-27, 2001.

[10] Van Oost, S., and Aalders, B., "Cryogenic Heat Pipe Ageing," *Proc. 10th International Heat Pipe Conference*, Stuttgart, Germany, 2011.

[11] Basiulis, A., and Filler, M., "Operating characteristics and long-life capabilities of organic fluid heat pipes," *Proc. AIAA 6th Thermophysics Conference*, Tullahoma, Tennessee, 1971.

[12] Basiulis, A., and Prager, R., "Compatibility and reliability of heat pipe materials," Proc. AIAA 10th Thermophysics Conference, Denver, CO, 1975.

[13] Kreeb, H., Groll, M., and Zimmerman, P., "Lifetest investigations with low-temperature heat pipes," *Proceeding of 1stIHPC*, Sttutgart, Germany, October 1973, Paper(4), p. 1, 1973.

[14] Busse, C., Loens, J., and Campanile, A., "Hydrogen generation in water heat pipes at 250 C," Proc. Preprints of the First International Heat Pipe Conference, Stuttgart, Federal Republic of Germany, 1973.

[15] Gerrels, E. E., and Larson, J., "Brayton cycle vapor chamber (heat pipe) radiator study," National Aeronautics and Space Administration, NASA CR-1677, Washington, D.C., 1971.

[16] Perkins, L., and Buck, W., "Improvements in Devices for the Diffusion or Transference of Heat," UK Patent, 22, 1892.

[17] King, C., "Perkins' hermetic tube boilers," The Engineer, 152, pp. 405-406, 1931.

[18] Novotna, I., Nassler, J., and Zelko, M., "Compatibility of Steel-Water Heat Pipes," *Proc. Proceeding of the Third International Heat Pipe Symposium*, Tsukuba, Japan, pp. 89-95, 1988.

[19] Zhang, H., and Zhuang, J., "Research, development and industrial application of heat pipe technology in China," *Applied Thermal Engineering*, 23(9), pp. 1067-1083, 2003.

[20] Rassamakin, B. M., Gomelya, N. D., Khairnasov, N. D., and Rassamakina, N. V., "Choice of the effective inhibitors of corrosion and the results of the resources tests of steel and aluminum thermosyphon with water," *Proc. Proceedings of the 10th International Heat Pipes Conference*, Stuttgart, Germany, 1997.

[21] Bricard, A. et al. "Recent advances in heat pipes for hybrid heat pipe heat exchangers," *Proc. 7th International Heat Pipe Conference*, Minsk, Belarus, May 21-25, 1990.

[22] Wu, L.-K., Zhang, X.-F., and Hu, J.-M., "Corrosion protection of mild steel by one-step electrodeposition of superhydrophobic silica film," *Corrosion Science,* 85, pp. 482-487, 2014.

[23] Anderson, W. G., Hartenstine, J. R., Sarraf, D. B., and Tarau, C., "Intermediate temperature fluids for heat pipes and loop heat pipes," *Proceedings of the International Energy Conversion Engineering Conference*, St. Louis, MO, 2007.

[24] Anderson, W. G., Rosenfeld, J. H., Angirasa, D., and Mi, Y., "Evaluation of heat pipe working fluids in the temperature range 450 to 700 K," *Space Technology and Applications International Forum-STAIF 2004,* Albuquerque, NM, http://dx.doi.org/10.1063/1.1649553, p. 20, 2004.

[25] Anderson, W. G., Tamanna, S., Tarau, C., Hartenstine, J. R., and Ellis, D., "Intermediate Temperature Heat Pipe Life Tests and Analyses," *Proc. 43rd International Conference on Environmental Systems (ICES)*, Vail, CO, 2013.

[26] Stubblebine, M., Amouzegar, L., and Catton, I., "Passivation and Performance of Inorganic Aqueous Solutions in a Grooved, Aluminum Flat Heat Pipe," *International Mechanical Engineering Congress and Exposition*, ASME, San Diego, CA, 2013.

[27] Stubblebine, M., Reilly, S., Yao, Q., and Catton, I., "Use of an Inorganic Aqueous Solution to Prevent Non-Condensable Gas Formation in Aluminum Heat Pipes," *ASME Summer Heat Transfer Conference*, Minneapolis, MN, 2013.

[28] Kendig, M. W., and Buchheit, R. G., "Corrosion inhibition of aluminum and aluminum alloys by soluble chromates, chromate coatings, and chromate-free coatings," *Corrosion Science*, 59(5), pp. 379-400, 2003.

[29] Rocco, A., Nogueira, T., Simão, R. A., and Lima, W. C., "Evaluation of chromate passivation and chromate conversion coating on 55% Al–Zn coated steel," *Surface and Coatings Technology*, 179(2), pp. 135-144, 2004.

[30] Blackmon, J. B., and Entrekin, S. F., "Preliminary Results of an Experimental Investigation of the Qu Superconducting Heat Pipe," NASA Marshall, NNM05AA22A, NASA Grant NCC 8-200, 2006.

[31] Rao, P., "Thermal Characterization Tests of the Qu Tube Heat Pipe," Masters Report, University of Alabama, Huntsville, 2009.

[32] Reilly, S. W., and Catton, I., "Utilization of Advanced Working Fluids With Biporous Evaporators," Journal of Thermal Science and Engineering Applications, 3(2), 2011.

[33] Stubblebine, M. J., and Catton, I., "Passivation and Performance of Inorganic Aqueous Solutions in a Grooved Aluminum Flat Heat Pipe," J Heat Trans-T ASME, 137(5), pp. 052901-052901, 2015.

[34] Reilly, S., Amouzegar, L., Tao, H., and Catton, I., "Use of Inorganic Aqueous Solutions for Passivation of Heat Transfer Devices," *Proc. 10th International Heat Pipe Symposium*, Taipei, Taiwan, 2011.

[35] Yao, Q., "Investigation of the Use of an Inorganic Aqueous Solution (IAS) in Phase Change Heat Transfer Devices," Report, University of California, Los Angeles, CA, 2016, http://escholarship.org/uc/item/805215b9.

[36] Yao, Q., Stubblebine, M., Reilly, S., Amouzegar, L., and Catton, I., "Using an Inorganic Aqueous Solution (IAS) in Copper and Aluminum Phase Change Heat Transfer Devices," *International Mechanical Engineering Congress and Exposition*, ASME, San Diego, CA, 2013.

[37] Free, M. L., Hydrometallurgy: fundamentals and applications, John Wiley & Sons, 2013.

[38] Uhlig, H. H., and Revie, R. W., Uhlig's corrosion handbook, John Wiley & Sons, 2011.

[39] Helgeson, H. C., and Kirkham, D. H., "Theoretical prediction of the thermodynamic properties of aqueous electrolytes at high pressures and temperatures. III. Equation of state for aqueous species at infinite dilution," *American Journal of Science,* 276(2), pp. 97-240, 1976.

[40] Oelkers, E. H., Helgeson, H. C., Shock, E. L., Sverjensky, D. A., Johnson, J. W., and Pokrovskii, V. A., "Summary of the Apparent Standard Partial Molal Gibbs Free-Energies of Formation of Aqueous Species, Minerals, and Gases at Pressures 1 to 5000 Bars and

Temperatures 25 to 1000-Degrees-C," *Journal of Physical and Chemical Reference Data*, 24(4), pp. 1401-1560, 1995.

[41] Shock, E. L., and Helgeson, H. C., "Calculation of the thermodynamic and transport properties of aqueous species at high pressures and temperatures: Correlation algorithms for ionic species and equation of state predictions to 5 kb and 1000°C," *Geochimica et Cosmochimica Acta*, 52(8), pp. 2009-2036, 1988.

[42] Tanger, J. C., and Helgeson, H. C., "Calculation of the Thermodynamic and Transport-Properties of Aqueous Species at High-Pressures and Temperatures - Revised Equations of State for the Standard Partial Molal Properties of Ions and Electrolytes," *American Journal of Science*, 288(1), pp. 19-98, 1988.

[43] Shock, E. L., Sassani, D. C., Willis, M., and Sverjensky, D.A., "Inorganic species in geologic fluids: Correlations among standard molal thermodynamic properties of aqueous ions and hydroxide complexes," *Geochimica Et Cosmochimica Acta*, 61(5), pp. 907-950, 1997.

[44] Ghali, E., Corrosion resistance of aluminum and magnesium alloys: understanding, performance, and testing, John Wiley & Sons, 2010.

[45] Haynes, W. M., CRC handbook of chemistry and physics, CRC press, 2012.

[46] Bard, A. J., Parsons, R., and Jordan, J., Standard potentials in aqueous solution, CRC press, 1985.

[47] Chase, M. W., and Force, J. A. N. A., "NIST-JANAF thermochemical tables," 1998.

[48] Hemingway, B. S., and Robie, R. A., "The entropy and Gibbs free energy of formation of the aluminum ion," *Geochimica et Cosmochimica Acta*, 41(9), pp. 1402-1404, 1977.

[49] Hovey, J. K., and Tremaine, P. R., "Thermodynamics of aqueous aluminum: Standard partial molar heat capacities of Al3+ from 10 to 55°C," *Geochimica et Cosmochimica Acta,* 50(3), pp. 453-459, 1986.

[50] Bénézeth, P., Palmer, D. A., and Wesolowski, D. J., "Aqueous high-temperature solubility studies. II. The solubility of boehmite at 0.03 m ionic strength as a function of temperature and pH as determined by in situ measurements," *Geochimica et Cosmochimica Acta*, 65(13), pp. 2097-2111, 2001.

[51] Chen, Q., Xu, Y., and Hepler, L. G., "Calorimetric study of the digestion of gibbsite, Al(OH)3(cr), and thermodynamics of aqueous aluminate ion, Al(OH)4−(aq)," *Canadian Journal of Chemistry*, 69(11), pp. 1685-1690, 1991.

[52] Hovey, J. K., Hepler, L. G., and Tremaine, P. R., "Thermodynamics of aqueous aluminate ion: standard partial molar heat capacities and volumes of tetrahydroxyaluminate (1-)(aq) from 10 to 55. degree. C," *The Journal of Physical Chemistry*, 92(5), pp. 1323-1332, 1988.

[53] Novotna, I., Nassler, J., and Zelko, M., "Contribution to Compatibility of Steel-Water Heat Pipes," *Proc. 3rd International Heat Pipe Symposium*, Tsukukba, Japan, 1988.

[54] Beverskog, B., and Puigdomenech, I., "Revised pourbaix diagrams for chromium at 25–300 °C," *Corrosion Science*, 39(1), pp. 43-57, 1997.

[55] Dellien, I., Hall, F. M., and Hepler, L. G., "Chromium, Molybdenum, and Tungsten - Thermodynamic Properties, Chemical-Equilibria, and Standard Potentials," *Chemical Reviews,* 76(3), pp. 283-310, 1976.

[56] Holzheid, A., and O'Neill, H. S. C., "The Cr ・ Cr 2 O 3 oxygen buffer and the free energy of formation of Cr 2 O 3 from high-temperature electrochemical measurements," *Geochimica et Cosmochimica Acta,* 59(3), pp. 475-479, 1995.

[57] Klemme, S., O'Neill, H. S. C., Schnelle, W., and Gmelin, E., "The heat capacity of MgCr2O4, FeCr2O4, and Cr2O3 at low temperatures and derived thermodynamic properties," *American Mineralogist*, 85(11-12), pp. 1686-1693, 2000.

[58] Radhakrishnamurty, P., and Adaikkalam, P., "Ph Potential Diagrams at Elevated-Temperatures for the Chromium Water-System," *Corrosion Science*, 22(8), pp. 753-773, 1982.

[59] Marcus, P., and Protopopoff, E., "Thermodynamics of thiosulfate reduction on surfaces of iron, nickel and chromium in water at 25 and 300 °C," *Corrosion Science*, 39(9), pp. 1741-1752, 1997.

[60] Zordan, T. A., and Hepler, L. G., "Thermochemistry and Oxidation Potentials of Manganese and Its Compounds," *Chemical Reviews,* 68(6), pp. 737, 1968.

[61] Macdonald, D. D., "The thermodynamics and theoretical corrosion behavior of manganese in aqueous systems at elevated temperatures," *Corrosion Science,* 16(7), pp. 461-482, 1976.

[62] Robie, R. A., and Hemingway, B. S., "Low-temperature molar heat capacities and entropies of MnO_2(pyrolusite), Mn_3O_4(hausmanite), and Mn_2O_3(bixbyite)," *The Journal of Chemical Thermodynamics,* 17(2), pp. 165-181, 1985.

[63] Jacob, K. T., Kumar, A., Rajitha, G., and Waseda, Y., "Thermodynamic Data for Mn3O4, Mn2O3 and MnO2," *High Temperature Materials and Processes*, 30(4-5), pp. 459-472, 2011.

[64] Grundy, A. N., Hallstedt, B., and Gauckler, L. J., "Assessment of the Mn-O system," *Journal of Phase Equilibria*, 24(1), pp. 21-39, 2003.

[65] Brown, O. L., Smith, W. V., and Latimer, W. M., "The Heat Capacity and Entropy of Potassium Permanganate from 15 to 300° Absolute. The Entropy and Free Energy of Permanganate Ion," *Journal of the American Chemical Society*, 58(11), pp. 2144-2146, 1936.

[66] Bale, C. W., and Belisle, E., "FACT - Facility for the Analysis of Chemical Thermodynamics," http://www.crct.polymtl.ca/fact/index.php, 2016.

[67] Sengupta, A. K., and Clifford, D., "Important process variables in chromate ion exchange," *Environ Sci Technol*, 20(2), pp. 149-155, 1986.

[68] Pourbaix, M., Atlas of electrochemical equilibria in aqueous solutions, 2ed, Publisher: National Association of Corrosion Engineers, Houston, TX, 1974.

[69] Revie, R. W., <u>Corrosion and Corrosion Control</u>, John Wiley & Sons, 2008.

[70] Yao, Q., and Catton, I., "Chemical Analysis of an Inorganic Aqueous Solution (IAS) in Heat Transfer Devices," *Journal of Heat Transfer*, HT-14-1433, 2014.

[71] Mashud, M., Inam, M. I., Arani, Z. R., and Tanveer, A., "Experimental Investigation of Heat Transfer Characteristics of Cylindrical Fin with Different Grooves," *International Journal of Mechanical & Mechatronics Engineering IJMME*, 9(10).

Appendix A: Thermodynamic Property Review

Table A1. Thermodynamic properties of water and related species

Compound	[kJ/mol]		[J/mol*K]	T = 298.15 K, P = 1 bar
	$\Delta_f H°$	$\Delta_f G°$	$S°$	Reference
$H_2O_{(l)}$	-285.830	-237.141	69.950	CRC Handbook, 93rd Ed. (2012)
	-285.830		69.950	Revie (2011)
	-285.830	-237.178	69.91	Bard et al. (1985)
		-237.178	69.91	Macdonald (1976)
$H_{2\ (g)}$	0.0	0.0	130.680	CRC Handbook, 93rd Ed. (2012)
	0.0	0.0	130.571	Revie (2011)
	0.0	0.0	130.684	Bard et al. (1985)
	0.0	0.0	130.574	Macdonald (1976)
$O_{2\ (g)}$	0.0	0.0	205.148	CRC Handbook, 93rd Ed. (2012)
	0.0	0.0	205.038	Revie (2011)
	0.0	0.0	205.028	Bard et al. (1985)
	0.0	0.0	205.029	Macdonald (1976)
$H^+_{(aq)}$	0.0	0.0	0.0	CRC Handbook, 93rd Ed. (2012)
	0.0	0.0	0.0	Revie (2011)
	0.0	0.0	0.0	Bard et al. (1985)
	0.0	0.0	0.0	Macdonald (1976)
$OH^-_{(aq)}$	-230.0	-157.2	-10.8	CRC Handbook, 93rd Ed. (2012)
	-229.987		-10.878	Revie (2011)
	-230.025	-157.328	-10.71	Free (2013)
	-230.02	-157.30	-10.7	Shock et al. (1997)
	-229.994	-157.293	-10.75	Bard et al. (1985)

Approved for public release: distribution is unlimited.

Table A2: Thermodynamic properties of aluminum and related species

	Compound	[kJ/mol]		[J/mol*K]	T = 298.15 K, P = 1 bar
	Compound	$\Delta_fH°$	$\Delta_fG°$	S°	Reference
Aluminum	Al (s)	0.0	0.0	28.3	CRC Handbook, 93rd Ed. (2012)
		0.0	0.0	28.35	Bard et al. (1985)
		0.0	0.0	28.3	NIST-JANAF Tables
	Al$_2$O$_3$-α (s)	-1675.7	-1582.3	50.9	CRC Handbook, 93rd Ed. (2012)
		-1675.7	-1582.3	50.92	Bard et al. (1985)
		-1675.692		50.92	NIST-JANAF Tables
	Al^{3+} (aq)	-531.0	-485.0	-321.7	CRC Handbook, 93rd Ed. (2012)
		-531.0	-489.4	-308	Free (2013)
		-530.673	-483.708	-325	Shock et al. (1997)
		-531	-485	-322	Bard et al. (1985)
				-308	Hemingway and Robie (1977)
					Hovey and Tremaine (1986)
	AlO$_2^-$ (aq)	-930.9	-830.9	-36.8	CRC Handbook, 93rd Ed. (2012)
		-929.4	-831.3	-30.2	Shock et al. (1997)
		-918.8	-823.4	-20.9	Bard et al. (1985)
			-839.7		Free (2013)
	Al(OH)$_4^-$ (aq)	-1502.5	-1305.3	102.9	CRC Handbook, 93rd Ed. (2012)
				111.3	Benezeth et al. (2001)
		-1502.77	-1305.00	101.49	Chen et al. (1991)
		-1490.3	-1297.8	117	Bard et al. (1985)
			-1305.6	111.3	Hovey and Hepler (1988)

Table A3: Thermodynamic properties of manganese and related species

	Compound	[kJ/mol]		[J/mol*K]	T = 298.15 K, P = 1 bar
	Compound	$\Delta_fH°$	$\Delta_fG°$	S°	Reference
Manganese	Mn (s)	0.0	0.0	32.0	CRC Handbook, 93rd Ed. (2012)
		0.0	0.0	32.3	Zordan and Hepler (1968)
		0.0	0.0	32.0	Macdonald (1976)
	MnO_2 (s) (IV)	-520.0	-465.1	53.1	CRC Handbook, 93rd Ed. (2012)
			-465.14		Free (2013)
		-520.0	-466.17	52.75	Robie and Hemingway (1985)
		-520.5	-465.7	53.05	Zordan and Hepler (1968)
		-521.449	-466.405	52.75	Jacob et al. (2011)
			465.18	53.05	Macdonald (1976)
		-520.48		53.95	Grundy et al. (2003)
	Mn_2O_3 (s) (III)	-959.0	-881.1	110.5	CRC Handbook, 93rd Ed. (2012)
		-959.0	-882.06	113.7	Robie and Hemingway (1985)
		-956.9	-879.1	110.5	Zordan and Hepler (1968)
		-961.536	-884.475	113.70	Jacob et al. (2011)
			-881.2	110.5	Macdonald (1976)
		-962.59		112.1	Grundy et al. (2003)
	Mn_3O_4 (s) (II,III)	-1387.8	-1283.2	155.6	CRC Handbook, 93rd Ed. (2012)
		-1384.5	-1282.46	164.1	Robie and Hemingway (1985)
		-1386.2	-1281.1	154.0	Zordan and Hepler (1968)
		-1386.185	-1284.409	165.60	Jacob et al. (2011)
		-1382.74		167.10	Grundy et al. (2003)
			-1283.2	155.6	Macdonald (1976)
	Mn^{2+} (aq)	-220.8	-228.1	-73.6	CRC Handbook, 93rd Ed. (2012)
		-220.70	-228.00	-73.6	Free (2013)
		-222.6	-230.5	-71.1	Zordan and Hepler (1968)
		-221.3	230.5	-67.8	Shock et al. (1997)
			-228.0	-115.5	Macdonald (1976)
	MnO_4^- (aq)	-541.4	-447.2	191.2	CRC Handbook, 93rd Ed. (2012)
			-447.20		Free (2013)
				195.4	Brown (1936)
		-543.5	-450.2	194.6	Zordan and Hepler (1968)
		-543.5	-450.2	194.6	Shock et al. (1997)
			447.3	212.1	Macdonald (1976)

Table A4: Thermodynamic properties of chromium and related species

	Compound	[kJ/mol] $\Delta_f H°$	$\Delta_f G°$	[J/mol*K] S°	T = 298.15 K, P = 1 bar Reference
Chromium	Cr (s)	0.0	0.0	23.8	CRC Handbook, 93rd Ed. (2012)
		0.0	0.0	23.6	Beverskog et. al. (1997)
		0.0	0.0	23.8	Dellien et al. (1976)
		0.0	0.0	25.2	Chase et al. (1985)
		0.0	0.0	23.7	Bard et al. (1985)
	Cr$_2$O$_3$ (s) (III)	-1139.7	-1058.1	81.2	CRC Handbook, 93rd Ed. (2012)
			-1053.1	81.2	Beverskog et. al. (1997)
		-1139.7	-1058.1	81.2	Dellien et al. (1976)
		-1124.6		85.7	Holzheid and O'Neill (1995)
		-1128.2		82.3	Klemme et al. (2000)
			-1090.1	81.3	Radhakrishnamurty (1982)
		-1139.7	-1058.1	81.7	Bard et al. (1985)
	Cr^{2+} (aq)	-143.5			CRC Handbook, 93rd Ed. (2012)
			-174.0	-100.0	Beverskog et. al. (1997)
		-143.5	-146.4	-100.4	Dellien et al. (1976)
			-176.1	-77.1	Radhakrishnamurty (1982)
		-163.2	-164.8	-101.3	Shock et al. (1997)
		-172.0	-174.0	-100.0	Bard et al. (1985)
			-164.0		Marcus and Protopopoff (1997)
	Cr^{3+} (aq)	-251.0	-215.0	-293.0	Beverskog et. al. (1997)
		-238.5	-194.6	-318.0	Dellien et al. (1976)
			-215.5	-307.5	Radhakrishnamurty (1982)
		-251.0	-206.3	-322.2	Shock et al. (1997)
		-251.0	-215.0	-293.0	Bard et al. (1985)
			-203.0		Marcus and Protopopoff (1997)
	CrO$_4$$^{2-}$ (aq)	-881.2	-727.8	50.2	CRC Handbook, 93rd Ed. (2012)
			-727.8	50.2	Beverskog et. al. (1997)
		-881.2	-727.6	50.2	Dellien et al. (1976)
			-732.6	50.2	Radhakrishnamurty (1982)
		-882.5	-731.4	57.7	Shock et al. (1997)
		-881.2	-727.8	50.2	Bard et al. (1985)
			-727.8		Marcus and Protopopoff (1997)
	HCrO$_4$$^-$ (aq)		-765.1	195.2	Beverskog et. al. (1997)
		-878.2	-764.8	184.1	Dellien et al. (1976)
			-773.6	184.1	Radhakrishnamurty (1982)
		-878.6	-768.6	195.0	Shock et al. (1997)
		-878.2	-764.8	184.1	Bard et al. (1985)
			-764.8		Marcus and Protopopoff (1997)
	Cr(OH)$^{2+}$ (aq)		-431.8	-151.0	Beverskog et. al. (1997)
		-481.2	-410.0	-175.7	Dellien et al. (1976)
			-431.0	-146.4	Radhakrishnamurty (1982)
		-496.2	-420.5	-192.9	Shock et al. (1997)
		-495.0	-430.0	-156.0	Bard et al. (1985)
			-418.0		Marcus and Protopopoff (1997)

Appendix B: Additional Heater Block, Natural Convection

List of Figures in Appendix B

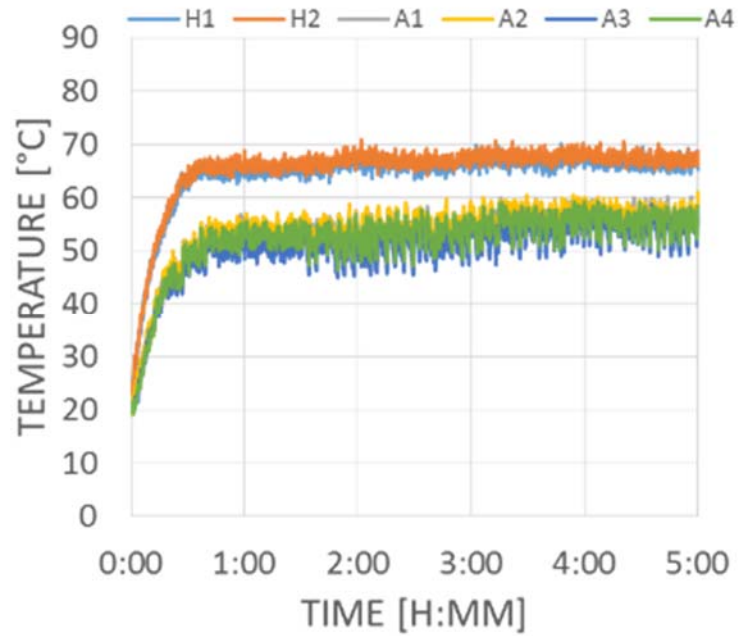**Thermo-syphon Data**

Copper/Water

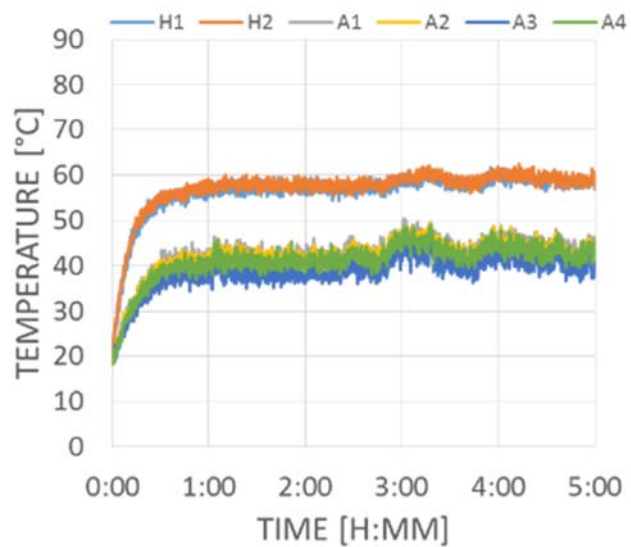**Figure B1: Copper/water #1, temperature vs. time**

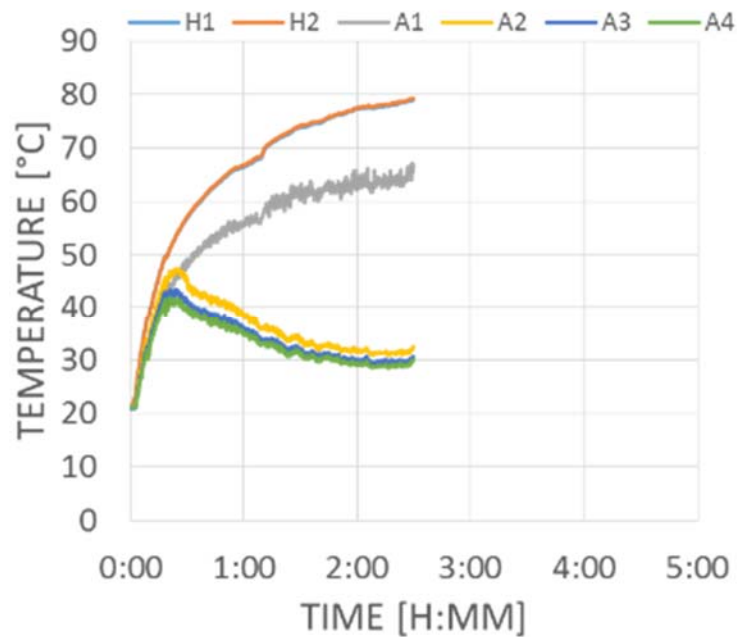**Figure B2: Copper/water #2, temperature vs. time**

Aluminum/Water

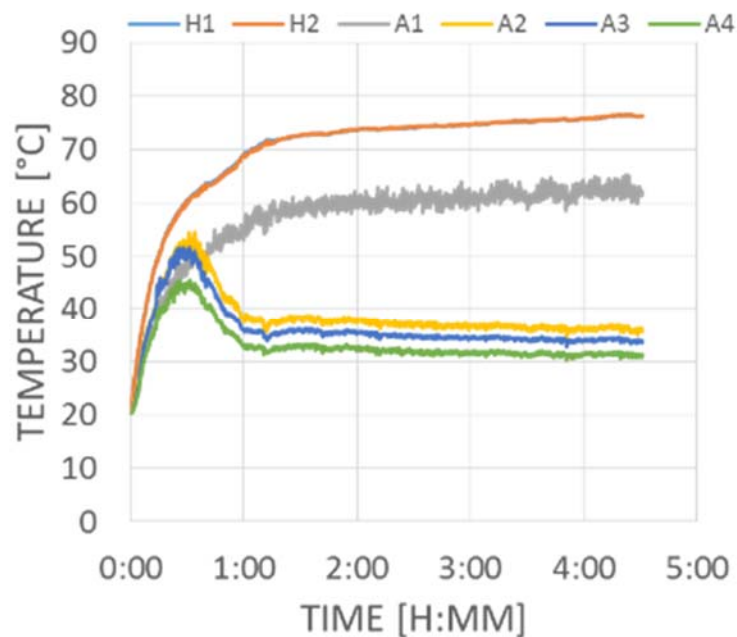**Figure B3: Aluminum - H_2O #1, temperature vs. time**

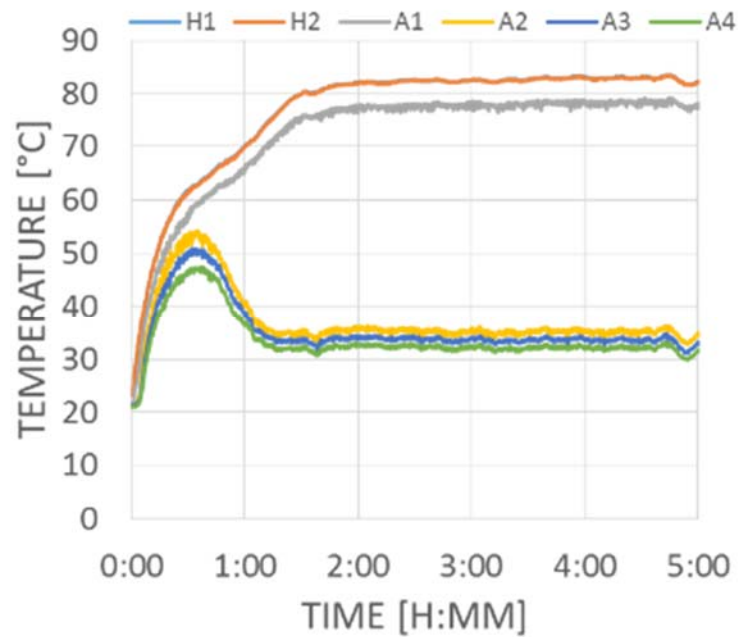**Figure B4: Aluminum - H_2O #2, temperature vs. time**

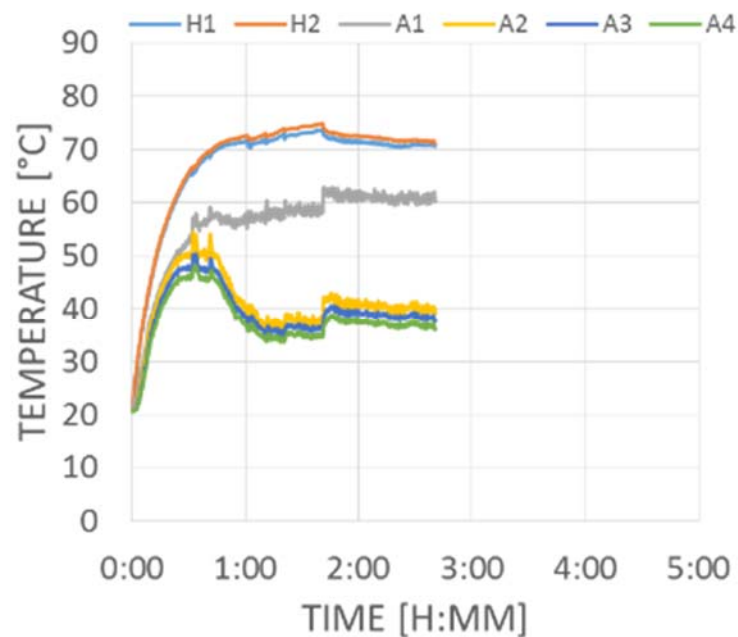**Aluminum/$Mn - 0$**

Figure B5: Aluminum/$Mn - 0$ #1, temperature vs. time

Figure B6: Aluminum/$Mn - 0$ #2, temperature vs. time
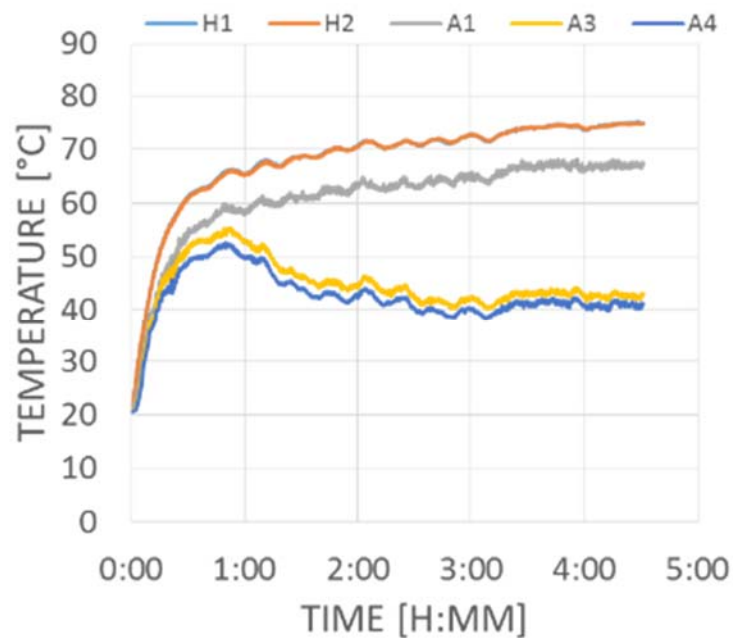
Figure B7: Aluminum/$Mn - 0$ #3, temperature vs. time
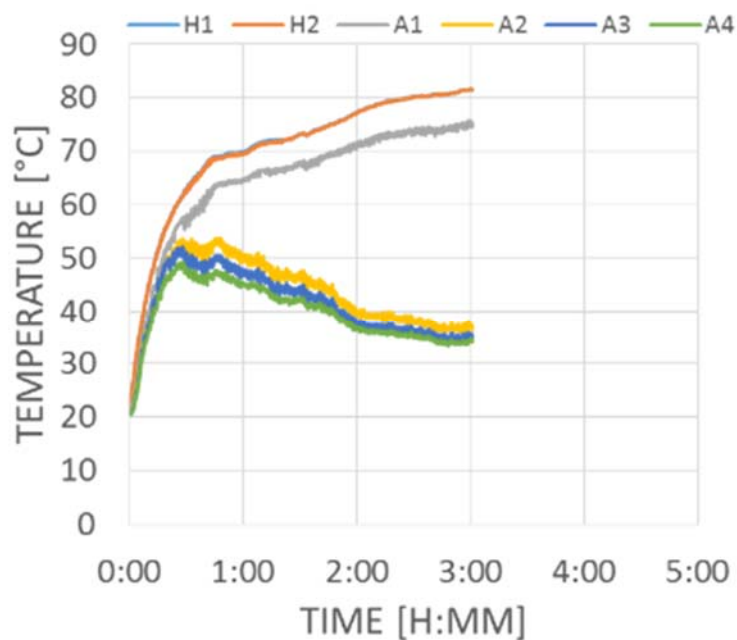
Figure B8: Aluminum/$Mn - 0$ #4, temperature vs. time

Approved for public release: distribution is unlimited.
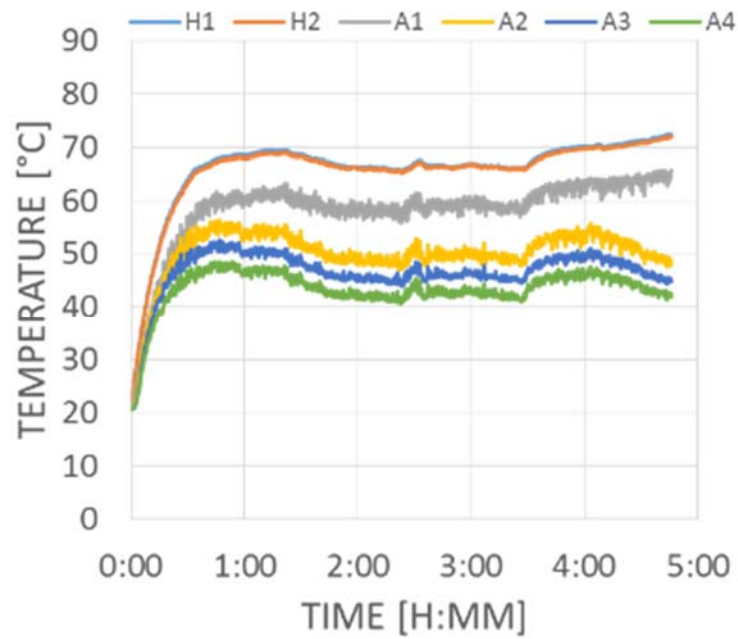
Aluminum/$Mn-1$

Figure B9: Aluminum/$Mn-1$ #1, temperature vs. time
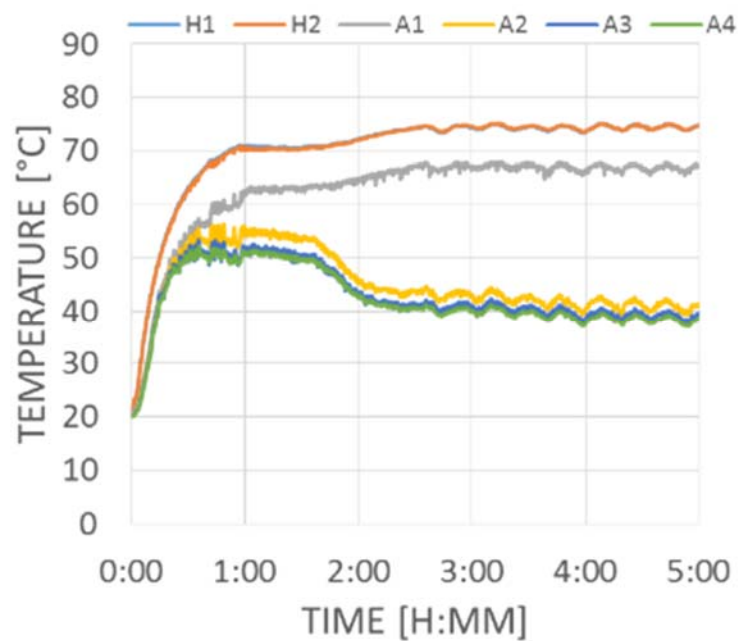
Figure B10: Aluminum/$Mn-1$ #2, temperature vs. time
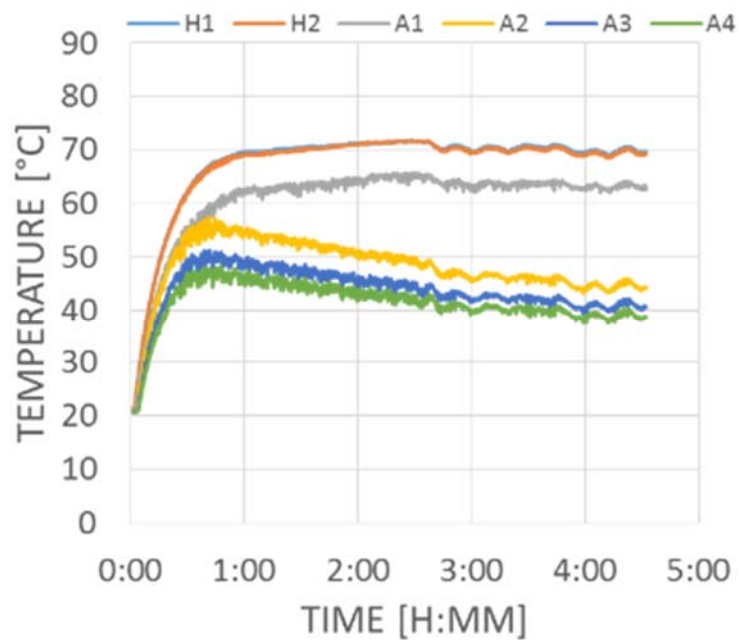
Figure B11: Aluminum/$Mn-1$ #3, temperature vs. time

Approved for public release: distribution is unlimited.
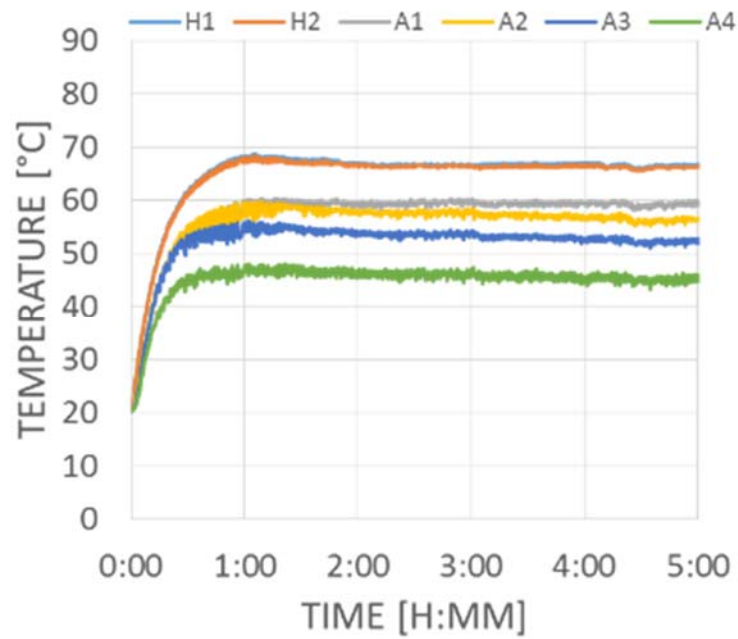
Aluminum/$Mn-2$

Figure B12: Aluminum/$Mn-2$ #1, temperature vs. time
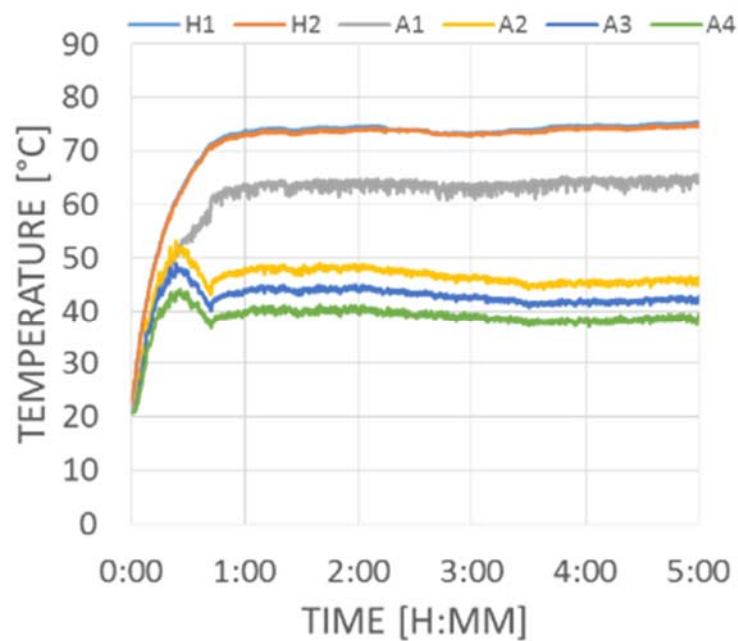
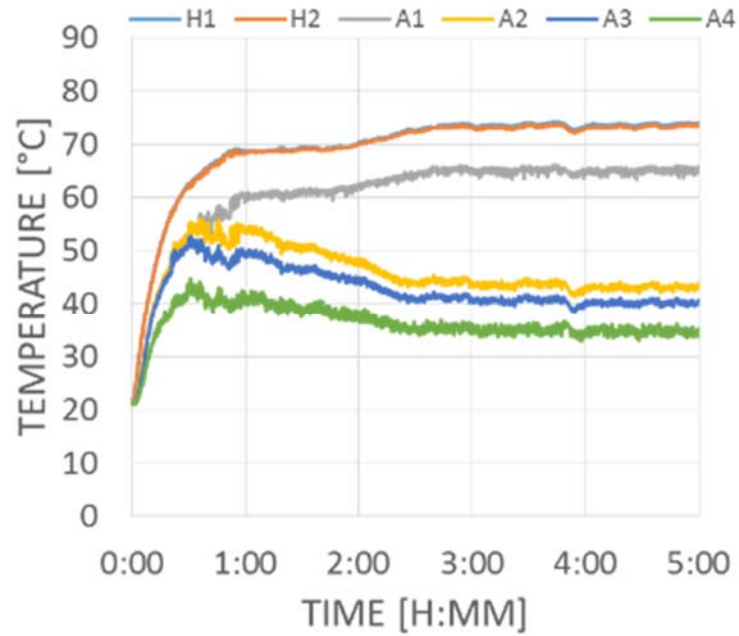**Figure B13: Aluminum/$Mn-2$ #2, temperature vs. time**

Figure B14: Aluminum/$Mn-2$ #3, temperature vs. time
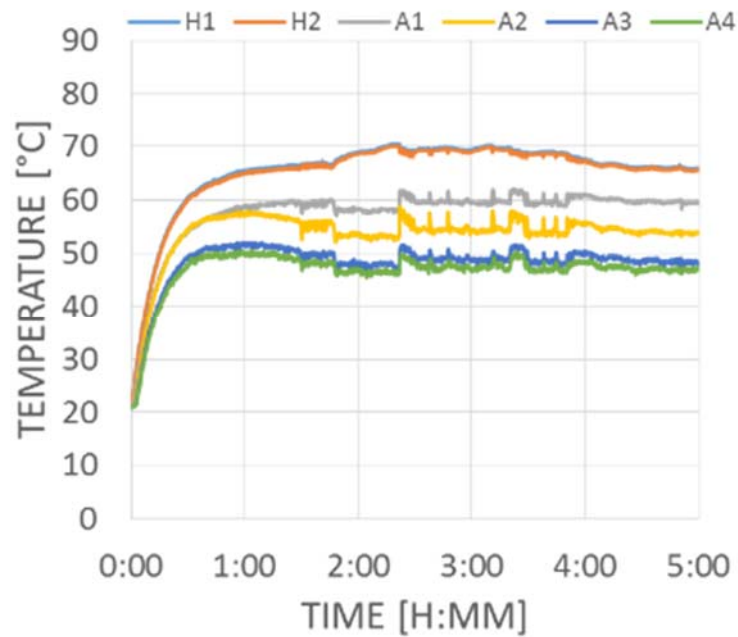
Aluminum/$Mn-4$

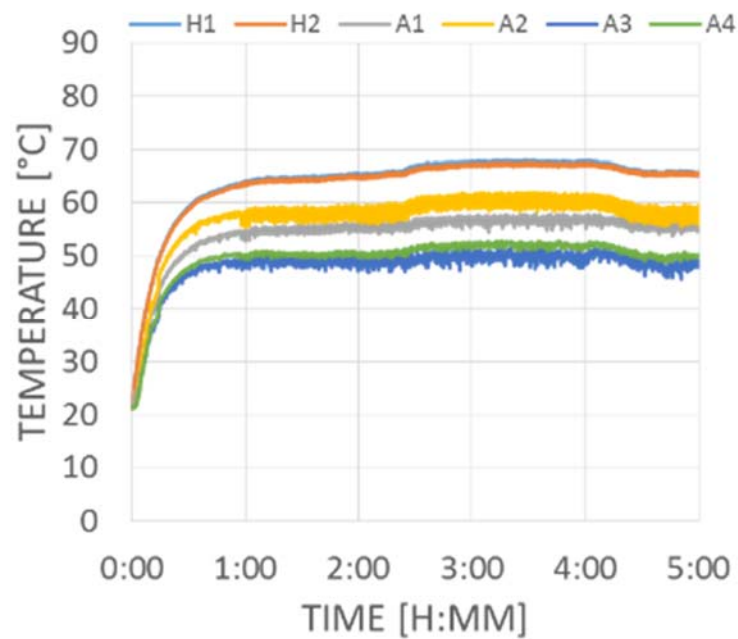**Figure B15: Aluminum/$Mn-4$ #1, temperature vs. time**

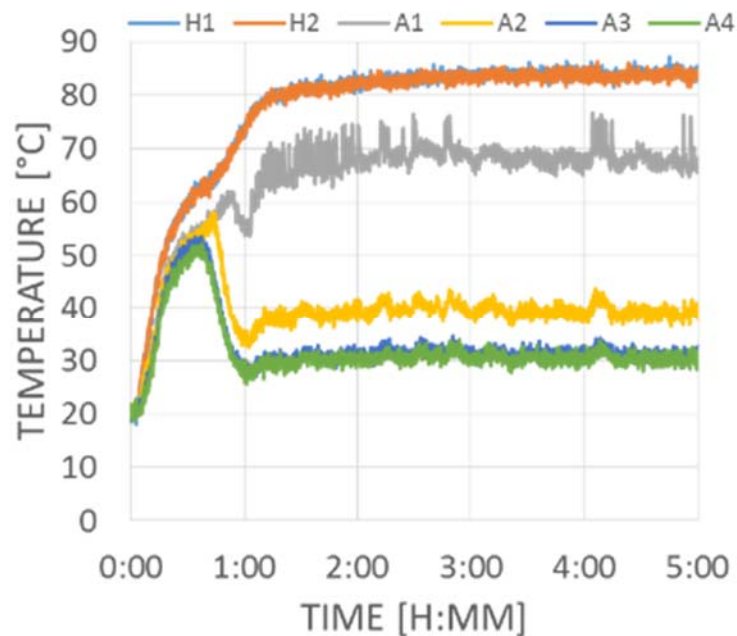**Figure B16: Aluminum/$Mn-4$ #2, temperature vs. time**

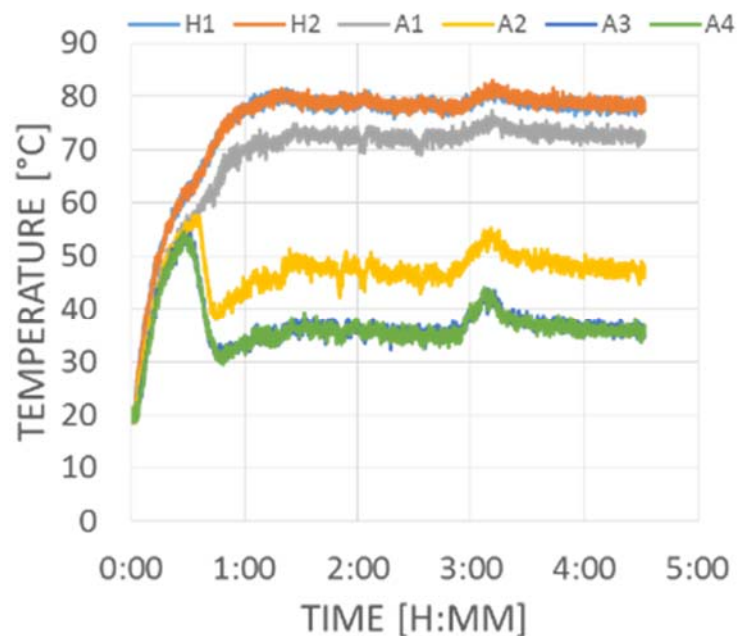**Figure B17: Aluminum/$Mn - 4$ #3 (pretreated), temperature vs. time**

Figure B18: Aluminum/$Mn - 4$ #4 (pretreated), temperature vs. time

List of Symbols, Abbreviations, and Acronyms

Variables

α – chemical activity

c – molarity or molar concentration [mol/L, M]

C_p – specific heat (constant pressure) [J/mol*K]

E – electrochemical reduction potential [V]

G – Gibbs energy [kJ/mol]

ΔG – change in Gibbs energy [kJ/mol]

ΔG_r – change in Gibbs energy for a reaction [kJ/mol]

H – enthalpy [kJ/mol]

ΔH – change in enthalpy [kJ/mol]

K – equilibrium constant

m – mass [kg]

M – molar mass [g/mol]

σ_l – liquid surface tension [N/m]

h_{fg} – latent heat of vaporization [kJ/kg]

ν_l – liquid kinematic viscosity [m²/s]

M_{wf} – heat pipe working fluid figure of merit

V_{charge} – heat pipe/thermo-syphon liquid fill volume (mL, charge amount)

Q_{in} – power into the device evaporator [W]

q_{in} – heat flux into the device evaporator [W/cm^2]

T_h – heat pipe evaporator temperature [°C]

T_c – heat pipe condenser temperature [°C]

ΔT – referred to in this paper as T_e-T_c [°C]

n – molar amount [moles]; number of transferred electrons in reaction

P – pressure [atm]

Q – reaction quotient

S – entropy [J/mol*K]

ΔS – change in entropy [J/mol*K]

T – temperature [K]

V – volume [m^3]

A_e – internal surface area of heat pipe evaporator section [cm^2]

A_t – internal surface area of entire heat pipe [cm^2]

L_e – evaporator length [in]

L_t – total device length [in]

OD – outer tube diameter [in]

ID – inner tube diameter [in]

Constants

F – Faraday's constant [96,485.3 C/mol]

R – universal ideal gas constant [8.314 J/mol*K]

Abbreviations

CCC – chromate conversion coatings

DI water – de-ionized water

EDS - energy dispersive spectroscopy

FLIR - forward looking infrared

HKF - Helgeson-Kirkham-Flowers

IAS – inorganic aqueous solution

IR - infrared

NCG – non-condensable gas

ORP – oxidation reduction potential

PCHT – phase change heat transfer

PDAQ - personal data acquisition

SEM – scanning electron microscope

SHE – standard hydrogen potential

S.L.E. - special limits of error

TGP - thermal ground planes

UCLA – University of California, Los Angeles

USB - universal serial bus

Subscripts

(aq) – aqueous phase

(g) – gaseous phase

(s) – solid phase

h – heater

c or cond – condenser

a – adiabatic

DISTRIBUTION LIST

DTIC/OCP
8725 John J. Kingman Rd, Suite 0944
Ft Belvoir, VA 22060-6218   1 cy

AFRL/RVIL
Kirtland AFB, NM 87117-5776   2 cys

Official Record Copy
AFRL/RVSV/Andrew Williams   1 cy

(This page intentionally left blank)